

Politecnico di Milano

Academic Year 2014-2015

Master's Degree in Space Engineering

Coupled Orbital-Attitude Dynamics of Large Structures in Non-Keplerian Orbits

Advisor:
Prof. Michèle Lavagna
Co-Advisor:
Davide Guzzetti

Master's Thesis of:
Lorenzo Bucci
817034

Abstract

Interest on Large Space Structures (LSS), orbiting in strategic and possibly long-term stable locations, is nowadays increasing in the space community. They can serve as strategic outpost to support a large variety of manned and unmanned mission, or may carry scientific payloads to broaden the knowledge of our Universe. The present work is devoted to the analysis of LSS in the Earth-Moon system, exploiting the peculiar dynamics offered by such multi-body gravitational environment. The coupling between attitude and orbital dynamics is investigated, with particular interest on the gravity gradient torque exerted by the two massive attractors. First, natural periodic orbit-attitude solutions are obtained; a LSS which exploits such solutions would benefit of a naturally periodic body rotation synchronous with the orbital motion, easing the effort of the attitude control system to satisfy pointing requirements. Then, the effect of Solar Radiation Pressure is investigated, eventually introducing it in the full dynamical model and finding novel periodic attitude solutions. Benefits of such behaviors are discussed throughout the work. Finally, the effects of flexible structures are introduced and examined, with a simple yet effective model. The coupling of structural vibrations and attitude motion is preliminarily explored, drawing conclusions on possible issues encountered by LSS.

Sommario

L'interesse verso Strutture Spaziali Estese (SSE), poste in posizioni strategiche e possibilmente stabili sul lungo periodo, è oggigiorno sempre più ampio nella comunità spaziale. Queste possono essere utilizzate come avamposti strategici per supportare varie missioni con e senza equipaggio, oppure trasportare strumenti scientifici avanzati per ampliare la conoscenza del nostro Universo. Il presente lavoro è dedicato all'analisi di SSE nel sistema Terra-Luna, sfruttando la dinamica peculiare che tale ambiente gravitazionale offre. L'accoppiamento fra moto di assetto e orbitale è indagato, focalizzando l'attenzione sulla coppia di gradiente gravitazionale esercitata dai due attrattori massivi. Inizialmente si ottengono soluzioni naturalmente periodiche del moto assetto-orbitale; una SSE potrebbe sfruttare una di tali soluzioni e trarre beneficio da un moto rotazionale di assetto periodico, sincrono con il moto orbitale, semplificando l'azione di un sistema di controllo d'assetto nel soddisfare alcuni requisiti di puntamento. Successivamente si indaga l'effetto della Pressione di Radiazione Solare, fino alla sua integrazione nel modello dinamico completo, trovando nuove soluzioni periodiche del moto d'assetto. Il lavoro discute e argomenta i possibili benefici di tali moti. Si introduce infine l'effetto della flessibilità, con un modello semplice ma efficace allo scopo. L'accoppiamento fra vibrazioni strutturali e moto d'assetto è indagato in maniera preliminare, traendo alcune conclusioni sui possibili fenomeni problematici a cui le SSE potrebbero andare incontro.

ESTRATTO IN LINGUA ITALIANA

Il Problema Circolare Ristretto dei Tre Corpi consiste nell'analisi del moto orbitale di un corpo, soggetto all'azione gravitazionale di altri due corpi massivi aventi massa molto superiore a quella del corpo in esame. I due attrattori orbitano l'uno attorno all'altro secondo le leggi della dinamica Kepleriana; è dunque conveniente studiare il moto del terzo corpo in un sistema di riferimento rotante, solidale col moto relativo dei due corpi massivi. Tale sistema ha una natura caotica, ovvero un'alta sensibilità alle condizioni iniziali, per cui piccoli cambiamenti di queste ultime portano a grandi variazioni della soluzione; le ampie possibilità operazionali fornite da tale ambiente lo rendono tuttavia interessante per diverse missioni spaziali che necessitano di posizioni e orbite strategiche.

La Tesi si pone l'obiettivo di analizzare la dinamica di Strutture Spaziali Estese nel sistema Terra-Luna, nell'ottica di fornire strumenti di indagine preliminare utili a future missioni spaziali. L'indagine si concentra sui moti accoppiati di orbita e di assetto, dove quest'ultimo è fortemente influenzato dalla traiettoria tramite la variazione delle coppie derivanti dall'ambiente.

DINAMICA ACCOPPIATA DI CORPO RIGIDO

L'analisi inizia con un esame approfondito della dinamica di corpo rigido accoppiata con il moto orbitale. Il termine di accoppiamento deriva dalla coppia di gradiente gravitazionale esercitata dai due attrattori, che dipende dalla posizione e dall'assetto istantanei. La Tesi indaga i moti planari, fornendo tuttavia gli strumenti per estendere l'analisi a orbite e dinamiche di assetto tridimensionali. Le Distant Retrograde Orbits (DRO) sono usate per l'indagine, grazie alle loro proprietà di stabilità e per l'interesse della comunità scientifica; la missione ARM (Asteroid Redirect Mission) della NASA, ad esempio, prevede l'utilizzo di una DRO lunare.

Il principale risultato è la creazione di mappe di periodicità, ovvero grafici che permettono di visualizzare, per ogni orbita, quali condizioni

iniziali sono necessarie per instaurare un moto di assetto periodico. Questa periodicità si sovrappone alla periodicità orbitale, in modo da ottenere nel complesso una soluzione assetto-orbitale periodica. Tali mappe sono parametrizzate rispetto a un coefficiente che riflette la topologia del satellite, tramite il rapporto fra i suoi momenti principali d'inerzia. In questo modo è possibile avere un'immediata idea di come un cambio di proprietà inerziali (es. aggancio/sgancio di un modulo di una stazione spaziale) vada a influenzare il moto di assetto e, quindi, quali misure debbano essere prese per garantire la periodicità desiderata. Il lavoro presenta anche una discussione dei possibili usi di soluzioni periodiche assetto-orbitali per missioni spaziali, contestualizzandone i vantaggi e le limitazioni.

DINAMICA ACCOPPIATA CON PRESSIONE DI RADIAZIONE SOLARE

Dopo l'analisi dei moti naturali assetto-orbitali, il lavoro prosegue con l'introduzione della Pressione di Radiazione Solare (SRP nella tradizionale nomenclatura anglosassone), analizzando in particolare la coppia esercitata sul veicolo spaziale. Questa coppia, rappresentata tramite due diversi modelli con diversi gradi di accuratezza, è in grado di influenzare fortemente il moto d'assetto, avendo un'ampiezza paragonabile o superiore a quella della coppia di gradiente gravitazionale. Le soluzioni trattate considerano un particolare insieme di orbite, il cui periodo è un sottomultiplo intero del periodo solare apparente, in maniera da mantenere la periodicità del moto d'assetto in sincronia col moto orbitale.

Il modello semplificato di SRP permette la creazione di mappe di periodicità analoghe alle precedenti, dando vita a soluzioni in cui la coppia di radiazione solare e di gradiente gravitazionale si combinano e instaurano moti di assetto periodici, paragonati a quelli ottenuti con sola azione gravitazionale. Il modello più raffinato di SRP permette ugualmente di ottenere moti periodici, ma la visualizzazione e rappresentazione dei risultati è meno immediata, dato il maggior numero di parametri in gioco. Infine, si forniscono indicazioni per raffinare il modello, considerando la perturbazione orbitale indotta dalla SRP e studiandone l'accoppiamento col moto d'assetto.

DINAMICA DI CORPO FLESSIBILE

L'ultimo capitolo presenta l'analisi della flessibilità del veicolo spaziale, accoppiata alla rotazione dello stesso. Usando un modello a parametri concentrati, con componenti linearmente elastici, si ricava l'eccitazione strutturale indotta dal moto d'assetto, e viceversa la perturbazione provocata dalle vibrazioni delle parti flessibili (es. pannelli solari, moduli strutturali).

L'analisi evidenzia come il risultato dipenda dal rapporto fra le frequenze naturali della struttura e quelle proprie dei moti orbitali e di assetto. Quando le prime sono largamente superiori alle seconde, i due moti possono essere disaccoppiati per ricavare i risultati, e si ottengono soluzioni approssimate in forma chiusa; questo caso è il più probabile, poiché anche strutture molto estese possiedono frequenze proprie di qualche ordine superiori a quelle assetto-orbitali. Nel caso gli ordini di grandezza siano paragonabili, si osserva un maggiore accoppiamento fra vibrazioni strutturali e moto rotazionale; questo caso è più astratto, poiché improbabile per strutture moderne, ma potrebbe risultare utile in future applicazioni con strutture estese e fortemente elastiche, con una cedevolezza tale da raggiungere frequenze proprie dell'ordine di grandezza delle frequenze orbitali e di assetto.

CONCLUSIONI

Il lavoro di tesi si colloca nell'innovativo contesto della dinamica accoppiata assetto-orbitale nel Problema Circolare Ristretto dei Tre Corpi. Si identificano soluzioni periodiche in ambiente puramente gravitazionale, per poi estendere l'analisi all'effetto della pressione di radiazione solare e agli effetti della flessibilità strutturale.

Il contributo principale è la classificazione dei risultati in famiglie di soluzioni e la definizione di mappe di periodicità, che offrono all'analista di missione uno strumento immediato e intuitivo per indagini preliminari. I risultati sono validati utilizzando soluzioni dalla letteratura contemporanea, che risultano essere parte delle famiglie di soluzioni ottenute nel presente lavoro. La pressione di radiazione solare viene introdotta non come perturbazione, ma come parte integrante del modello dinamico, consentendo una più profonda analisi dell'interazione con l'ambiente gravitazionale.

L'effetto della flessibilità del veicolo spaziale presenta aspetti interessanti se le frequenze proprie di quest'ultimo sono dell'ordine di grandezza di quelle relative ai moti orbitali; per i casi più pratici, le frequenze strutturali sono molto superiori a quelle orbitali, e la presente ricerca propone risultati analitici approssimati per trarre conclusioni preliminari sul comportamento strutturale.

ACKNOWLEDGMENTS

It is a warm spring afternoon in Milan, and I've just finished to write the last word of my Master's Thesis. It seems the right time to think back to this period of my life and acknowledge all the people that contributed to my path, up to this very moment.

First, I want to thank my family. My parents, who made me the person I am, supporting all of my decisions, even the wrong ones, allowing me to discover life on my own, while always being there with the capability to bring out the best in me; and my four grandparents, whose never ending love and affection accompanied me during my whole life.

Special thanks to Giulia, the most valuable resource I had in these years, always supportive, helpful and understanding. This and any other work wouldn't have been possible without her by my side.

A great acknowledgment goes to Davide, whose support and guide was essential during this work. I had the luck to cross paths with him, and he had the will to advise and follow me throughout these months despite the 7346 km between us. Many beers and pizzas will be necessary to repay the long Skype calls we had! I would also like to thank prof. Kathleen C. Howell for the interest she showed in my research, and for the nice chats we had on various topics. I thank her whole Research Group at Purdue University, and I hope we'll meet personally one day.

I am extremely grateful to my advisor, prof. Michèle Lavagna: she allowed me to pursue this Thesis, guiding me in difficult times while leaving me a freedom of choice that I never expected to deserve; she always valued and trusted my opinion, while teaching me how to improve with a constructive and positive attitude on every topic; and she allowed me to live some wonderful professional experiences, which I never thought I'd be part of, and yet there I was.

Finally, I want to thank the Spazzini group Andrea, Francesco, Lorenzo and Marco, for making my years at Politecnico an enjoyable time, and for the invaluably great moments that we shared (spritz, Martino, football, among the most notable); my friends Matteo and Stefano, for all the wonderful

things we did together and for having the patience to keep our friendship strong notwithstanding the long periods of my bad mood and absence; my fellows Alessandro, Andrea, Matteo and the others in sala calcolo, for helping me (not) to write and (not) to work in the long days together; my friend Giulio for standing me even when I knew nothing. An entire chapter would be necessary to thank all the friends that shared with me these years of my life, so I would like to address a large "thank you" to all of you.

CONTENTS

ESTRATTO IN LINGUA ITALIANA iii

ACKNOWLEDGMENTS vii

1 INTRODUCTION 1
- 1.1 Problem Definition 2
- 1.2 State of the Art and Previous Works 3
- 1.3 Contribution of the present work 4

2 BACKGROUND 7
- 2.1 Circular Restricted Three-Body Problem 7
  - 2.1.1 Equations of motion in the rotating frame 8
  - 2.1.2 Equilibrium solutions 10
  - 2.1.3 Jacobian constant and energy 11
- 2.2 Distant Retrograde Orbits 12
  - 2.2.1 Computation of the family 13
  - 2.2.2 Stability 15
  - 2.2.3 Period and resonant orbits 16
  - 2.2.4 Asymptotic behaviors 19

3 COUPLED ORBIT–ATTITUDE RIGID BODY DYNAMICS 24
- 3.1 Model 24
  - 3.1.1 Attitude dynamics and kinematics 25
  - 3.1.2 Orbital dynamics 27
- 3.2 Validation 28
  - 3.2.1 Two-body problem 28
  - 3.2.2 Three-body problem 29
- 3.3 Periodic orbit-attitude solutions 33
  - 3.3.1 Method and algorithm 33
  - 3.3.2 Solution space mapping 37
  - 3.3.3 Algorithm validation 38
  - 3.3.4 Sensitivity to spacecraft topology 39
- 3.4 Final remarks 42

4 COUPLED DYNAMICS WITH SOLAR RADIATION PRESSURE 45
4.1 Model 45
4.1.1 Solar radiation pressure 46
4.1.2 Sun motion 47
4.1.3 Sun-resonant orbits 48
4.1.4 General spacecraft model 49
4.1.5 Simplified spacecraft model 51
4.2 Modified periodic solutions 52
4.2.1 Method and algorithm 53
4.2.2 Solution space mapping 54
4.2.3 Algorithm validation 57
4.2.4 Results with general spacecraft model 58
4.3 Final remarks 60

5 SPACECRAFT FLEXIBILITY ANALYSIS 62
5.1 Model 62
5.1.1 Spacecraft model 62
5.1.2 Equations of motion 65
5.1.3 Extension to complex cases 68
5.2 High structural frequencies 68
5.2.1 Flexible parts response 69
5.2.2 Attitude motion perturbation 71
5.2.3 Highlights and wrap-up 73
5.3 Low structural frequencies 73
5.3.1 Flexible parts motion 74
5.3.2 Attitude motion 74
5.3.3 Analysis of the results 77
5.4 Final remarks 78

6 CONCLUSION 81
6.1 Orbit-attitude rigid body dynamics 81
6.2 Coupled dynamics with solar radiation pressure 82
6.3 Effects of spacecraft flexibility 83
6.4 Future works 83
6.4.1 Analysis of other families of orbits 83
6.4.2 Extension to spatial dynamics 84
6.4.3 Inclusion of Sun gravitational perturbation and Earth-Moon orbit eccentricity 84
6.4.4 Improvement of the elastic formulation 84

LIST OF FIGURES

Figure 1 CR3BP coordinate systems 9
Figure 2 Equilibrium points 11
Figure 3 DRO family in the Earth-Moon system 12
Figure 4 Differential correction procedure 15
Figure 5 DRO family eigenvalues 16
Figure 6 DRO period 17
Figure 7 1:1 resonant DRO 18
Figure 8 ECI orbital elements for 1:1 DRO 18
Figure 9 Detail of lunar encounters for 1:4 resonant DRO, ECI frame 19
Figure 10 Some resonant DROs in ECI frame 20
Figure 11 Some near-resonant DROs in ECI frame 21
Figure 12 Near-Earth DROs 22
Figure 13 Linear trend of osculating near-Earth eccentricity 23
Figure 14 Near-Moon DROs 23
Figure 15 Reference frames 25
Figure 16 Stable attitude response validation 30
Figure 17 DeBra-Delp region attitude response validation 30
Figure 18 Eccentricity resonance attitude response validation 30
Figure 19 Stability chart for a rigid body at L_1 31
Figure 20 L_1 small oscillations, stable region 32
Figure 21 L_1 small oscillations, "strip" stable region 32
Figure 22 JC variation with Fourier series expansion, DRO with $T = 19.92$ days 34
Figure 23 Angle and angular velocity variation, DRO period $= 12.66$ days 35
Figure 24 Attitude periodicity maps for DROs, $Kz = 0.8$ 38
Figure 25 Guzzetti's periodic orbit-attitude solution 39
Figure 26 Different inertia topology representations, rod-like spacecraft 39
Figure 27 Attitude periodicity family, $N = 1$ 40

Figure 28 Attitude periodicity family, $N = 0$ 41
Figure 29 Attitude periodicity family, $N = -1$ 41
Figure 30 Rotation angle for some periodic attitude motions, DRO period = 12.66 days 43
Figure 31 Angular velocity for some periodic attitude motions, DRO period = 12.66 days 44
Figure 32 Possible surface-light ray interactions 46
Figure 33 Apparent Sun motion in CR3BP 47
Figure 34 Sun-resonant set of DROs 48
Figure 35 SRP periodicity maps, 1:2 Sun-resonant DRO 55
Figure 36 SRP periodicity maps, 1:4 Sun-resonant DRO 55
Figure 37 Comparison of periodic solutions, small effect of SRP 56
Figure 38 Comparison of periodic solutions, large effect of SRP 56
Figure 39 Sun-pointing spacecraft angular accelerations 58
Figure 40 Periodicity map for $K_z = 0.6$, $C_d = 0$, $A/m = 0.016$, different values of C_s 59
Figure 41 Periodicity map for $C_s = 0.4$, $C_a = 0.5$, $A/m = 0.016$, different values of K_z 59
Figure 42 Spacecraft lumped parameter model 63
Figure 43 Schematic spacecraft model 64
Figure 44 Sample flexible coordinate analytical solution 71
Figure 45 Structural response with lowered frequencies Ω_i 75
Figure 46 Body angular velocity with lowered frequencies Ω_i 76
Figure 47 Free-free beam first natural frequency 78

LIST OF TABLES

Table 1 Near-1:1 DRO orbital parameters in ECI frame 17

Table 2 Perturbing non-dimensional accelerations in the Earth-Moon CR3BP 28

Table 3 Validation test cases 29

Table 4 Auxiliary k parameter 31

Table 5 Spacecraft model properties 65

1 INTRODUCTION

> [...] I seem to have been only like a boy playing on the sea-shore, [...], whilst the great ocean of truth lay all undiscovered before me.
>
> Isaac Newton
> Memoirs of the Life, Writings, and Discoveries of Sir Isaac Newton (1855)

The Circular Restricted Three-Body Problem has a chaotic nature, exhibiting large variations of the state variables for small changes in initial conditions. This complex dynamical space buries set of periodic and bounded solutions, towards which the interest of great scientists was directed during the last two centuries; when the three-body orbital dynamics is coupled with rotational rigid body, the complexity of the problem increases, and it is extended to a six degrees-of-freedom dynamical structure, thus making the search for periodic, exploitable solutions even more difficult for the investigator.

Nevertheless, such dynamical space is of great interest for future and near-future space mission. Many existing spacecraft (ISEE-3, SOHO, GAIA, LISA Pathfinder) exploited three-body dynamics, and it is not difficult to imagine large manned space stations in the Earth-Moon system, or refueling outpost to ease travel to Mars, or again a new generation of large telescopes to explore the depths of the Universe from a privileged position. As the need for fine pointing and control requirements increases, together with the mission's complexity, the usual point-mass approximation may no longer provide a suitable model for the analyses. Rigid body rotational behaviors, and subsequently flexible spacecraft model, are thus needed to be introduced in the mission design process, providing the analyst with new investigation tools and allowing missions otherwise infeasible.

The purpose of this work is the definition of a framework to investigate the coupled orbit-attitude problem in the CR3BP. Tools for preliminary analysis of Large Space Structures are presented and examined, in order to provide results for realistic mission scenarios.

1.1 PROBLEM DEFINITION

This Thesis aims at the examination of Large Space Structures (LSS) dynamics in the Circular Restricted Three-Body Problem (CR3BP). Interest in LSS is growing in the space field, and after the previous experiences (ISS, Skylab, MIR) the new possible goals for a space station are well beyond the so-far exploited low Earth orbits. It is then necessary a deeper analysis of the 6 degrees-of-freedom dynamical behavior (i.e. attitude and orbital components) of large structures in multi-body gravitational environments, where the single-attractor hypothesis must be dropped and the resulting motion is not Keplerian.

When investigating this challenging topic, one can find three main research fields:

A. Analysis of trajectories and rigid body dynamics, together with related attitude control strategies. The gravity gradient torque resulting from multiple attractors shows features strongly coupled with the orbital motion, and the classical literature techniques (passive stabilization, linearized motion in the local vertical-local horizontal frame) have to be adapted to the CR3BP. The coupling of the movement along the orbit and the variation of the gravity gradient torque might be exploited to obtain naturally stable, bounded attitude behaviors.

B. Perturbation and stability analysis, both for the orbital and the attitude motion. For restricted problems that do not include the Sun in the model, the latter's gravitational perturbation may actually prove to be quite significant (e.g. the Earth-Moon CR3BP); furthermore, solar radiation pressure (SRP) might be a strong source of perturbation for LSS which possess large surfaces. SRP perturbs both the orbital and the attitude motion; these two fields may be studied separately or jointly, according to the desired degree of complexity.

C. Examination of structural flexibility. Due to their large extension and poor structural damping, LSS present a high degree of flexibility which might couple with orbital and attitude motion; modal and finite element analyses provide results on such effects for Earth-orbiting spacecraft, but the effect of the peculiar multi-body gravitational environment on flexible structures is still an open field.

1.2 STATE OF THE ART AND PREVIOUS WORKS

The study of the interaction between orbital and attitude dynamics dates back to 1780, when Lagrange [1] first investigated the coupled dynamics of the Moon's libration and orbital motion. Such dynamical interaction regained attention, nearly two centuries later, with the launch of artificial satellites in Earth orbit. The effects of libration on the orbital motion were studied by Moran [2], using a dumbbell satellite model. The analysis was later extended to a body with arbitrary mass distribution [3, 4, 5], with a deeper understanding of the energy exchange between attitude and orbital motion. The effect of the body extension on its orbit, anyway, are of marginal interest for practical purposes; Kane [6] points out that for Earth satellites this perturbation may be neglected even for high accuracy propagator, since it is several orders of magnitude smaller than other orbital perturbations.

The Circular Restricted Three-Body Problem attracts nowadays great interest from the space community. Orbits in the CR3BP show peculiar non-linear behaviors which might be exploited for low-cost transfers [7], and the vast span of trajectories allows novel operational possibilities for mission design and analysis [8]. Such environment is thus an interesting field of investigation for large space structures; a space station located in the Earth-Moon system might serve as outpost for human missions to the lunar surface, or as support infrastructure for interplanetary travels. The attitude dynamics of a rigid body in the CR3BP was first approached by Kane and Marsh [9], who studied to attitude stability of an axisymmetric satellite located at one of the Lagrangian points. Few years later, Robinson [10, 11] extended the analysis to arbitrary rigid bodies and to the rigid dumbbell case. More recent studies [12, 13] continued this field of investigation, keeping the hypothesis of rigid body artificially fixed at one of the equilibrium points.

An analysis of the attitude behavior along an orbit in the vicinity of both collinear and equilateral Lagrangian points first appears in [14]. The authors consider the attitude dynamics of a rigid body along small, linearized Lyapunov orbits in the Sun-Earth system, providing stability charts analogous to [11], with the addition of the roll-yaw resonance curve, and pointing out the analogy with geocentric satellites attitude behavior. They also noted the existence of a critical inertia ratio, which delimits the regions of bounded and unbounded motion along the considered trajectories. Later investigations by Guzzetti, Knutson et al. [15, 16, 17, 18] are devoted to the study of attitude dynamics along large, nonlinear Lyapunov and halo orbits in the

Earth-Moon CR3BP, dropping the hypothesis of keeping the body fixed or in the vicinity of the Lagrangian points. Periodic orbit-attitude solutions are also identified [19, 20], deepening the knowledge and the exploration of the dynamical structures associated with attitude and orbital motion in the CR3BP. The search for periodic or bounded behaviors in a 3D formulation is a pristine field of exploration; bounded solutions are obtained and investigated by Knutson [15, 16], whereas a preliminary periodic solution is identified by the author in [21]. The fully coupled orbit-attitude motion is addressed in [22], with a study on the stabilizing effect exerted on the orbital dynamics by the fast rotation of the spacecraft, along three-dimensional orbits in the Hill's problem. Recently, Meng et al. [23] also investigated the dynamics of a dual-spin satellite in the CR3BP framework, identifying the frequency components of the attitude response using semi-analytical techniques to model the gravity gradient torques.

So far, the presented literature treats the spacecraft as a rigid body; when dealing with LSS, such assumption might not be completely suitable, since the flexible response of the vibrating structure may lead to non-negligible orbital and attitude perturbations. The early study of Misra and Modi [24] shows that a spacecraft with 230 meters-long appendages, in an orbit with $a = 12231$ km and $e = 0.001$, after one year undergoes a radial oscillatory perturbation of 4.87 m, due to the energy exchange between librational and orbital motion through elastic excitation. In the same years a variety of investigations, [25, 26, 27, 28] among the most relevant, was devoted to the orbital dynamics of multi-body spacecraft, considering the latter to be composed by a set of rigid and non-rigid interconnected bodies in various configurations. A continuum approach was instead used for other early studies [29, 30] to assess the dynamic behavior of large flexible bodies librating in orbit.

The analysis of flexible bodies in a multi-body gravitational environment is still a novel and pioneering topic. The recent works of Guzzetti [18] and Colagrossi et al. [31] preliminarily present and investigate flexible spacecraft dynamics in the CR3BP framework.

1.3 CONTRIBUTION OF THE PRESENT WORK

The scope of the present work is to further investigate the coupled orbit-attitude rigid body motion in the CR3BP framework. The Earth-Moon

system is considered throughout the analysis, identifying periodic orbit-attitude solutions both under gravity gradient torque and solar radiation pressure. A peculiar class of planar orbits is investigated, providing the motivations for such choice; extension of the results to other orbits is then briefly discussed. The flexibility of the spacecraft is eventually introduced as a perturbation to the orbital and attitude motion, assessing its effects on both dynamical behaviors. The work is organized as follows:

- Chapter 2 provides the mathematical background for the dynamical formulation of the problem. The CR3BP is briefly introduced (Section 2.1), providing the necessary fundamentals to the reader and describing the characteristics of the dynamical structure of the problem. Section 2.2 is devoted to the discussion of Distant Retrograde orbits, which are the main subject of the Thesis; their properties are described, together with methodologies for their identification and their relations with nearly-Keplerian orbits.
- Chapter 3 investigates the fully coupled orbit-attitude motion of a rigid body in the CR3BP. The equations of motion are presented, along with some validation test to assess the reliability and correctness of the author's numerical code. The core of the Chapter is Section 3.3, which presents periodic orbit-attitude solutions, i.e. dynamical behaviors where both the orbital and the attitude dynamics are periodic. Some recent studies investigated this kind of solutions and obtained notable results; the novelty offered by the Thesis is a classification of such solutions into families, providing tools for a systematic investigation of the dynamical space. Periodicity maps are provided, to visually identify the operational possibilities offered by a periodic behavior and serve as a tool for preliminary analyses.
- Chapter 4 further improves the analysis, introducing solar radiation pressure in the formulation. Two models are introduced to study the interaction between solar radiation and the surface of the spacecraft: a first, simplified one, suitable for preliminary assessments, and a more refined one, able to better represent the actual physical phenomenon. Periodic orbit-attitude behaviors are found with the introduction of SRP torque, showing novel solutions where such torque does not act as a perturbation but is an integral part of the dynamical system. The simplified spacecraft model allows to portray periodicity maps where the solution space is easily visualized, whereas the many parameters of the second model need for more case-specific maps.

- Chapter 5 analyzes the dynamical behavior of a flexible spacecraft, in the CR3BP framework. The coupling between attitude motion and the dynamics of the flexible parts of the spacecraft is investigated, using a lumped-parameters model to represent the flexible body. An analytical approximation is obtained when spacecraft structural frequencies are much higher than those of orbital and attitude dynamics, leading to an overall decoupling between the latter and the spacecraft flexibility. The cases where structural frequencies are much lower, and fall in the neighborhood of orbital frequency and attitude angular velocities, are the investigated, deepening the analysis of the coupling between attitude and flexible dynamics and showing results for a sample space station model.

- Chapter 6 draws the conclusions of the study, underlining its principal contributions and summarizing the results. Recommendations for future works are provided, drawn from the lessons learned during the investigation, together with some hints on possible fields of future interest.

2 BACKGROUND

> The beginning in every task is the chief thing.
>
> PLATO
> The Republic, Book II

This Chapter presents the background and the operational framework of the Thesis. Section 2.1 describes the mathematical model of the gravitational environment, briefly recalling equations of motion and standard analysis techniques. Section 2.2 is devoted to a more detailed description of the orbit family which is investigated in this work, in order to provide the reader with some details necessary to better understand the results of the research.

2.1 CIRCULAR RESTRICTED THREE-BODY PROBLEM

The classical two-body problem, considering the motion of two massive bodies subject to their mutual gravitational interaction, can be solved in closed form, having as solution the well-known elliptical orbit equation. Such problem is suitable for most analysis and possesses an outstanding value in physics and astrodynamics, but it is clearly limited when dealing with multi-body gravitational environments.

A simple, slight increase in complexity as the addition of a third massive body, however, is enough to transform the analytically integrable system into a complex problem with no closed-form solution. The Circular Restricted Three-Body Problem (CR3BP) overcomes some difficulties and provides a framework widely studied and adopted in real mission analysis. Consider three bodies of masses m_1, m_2, m_3, under the following assumptions:

- The mass of the third body is negligible compared to the other two.

- The mass distribution of the three bodies may be neglected, and they may be considered as point masses.
- The two larger bodies revolve around their center of mass in circular orbits.
- The smaller body is under the gravitational attraction of the two larger bodies, but does not affect their motion.

Many textbooks on orbital mechanics describe and treat the CR3BP, such as [32], [33], [34]. The work of Szebehely [35] is a fundamental reference for the topic.

2.1.1 Equations of motion in the rotating frame

The two larger bodies, m_1 and m_2, are called the primaries. The largest body m_1 is located on the left of the barycenter of the two primaries; Ω denotes the common angular velocity of the primaries' circular orbits. The problem is normalized as follows:

- The mass unit is the total system mass (recall that m_3 is negligible)

$$MU = m_1 + m_2 \tag{1}$$

- The time unit is taken in order to normalize the angular frequency Ω to 1

$$TU = \frac{1}{\Omega} \tag{2}$$

- The length is normalized in respect to the distance between the primaries

$$LU = d \tag{3}$$

- Using this set of units, the universal gravitational constant results naturally normalized

$$G = 1 \tag{4}$$

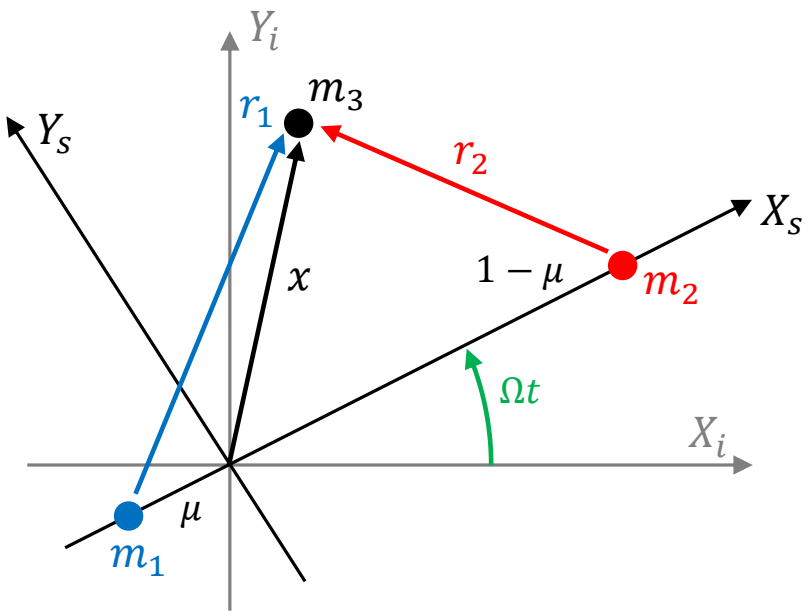


Figure 1: CR3BP coordinate systems

Through the presented normalization, the problem is fully defined by just one parameter, the so-called mass ratio

$$\mu = \frac{m_2}{m_1 + m_2} \tag{5}$$

which is the ratio between the mass of the smaller primary and the total mass of the system. This parameter may vary between 0 (unit mass placed at the origin) and 0.5 (two equal masses at equal distances from the barycenter).

Figure 1 depicts the geometry of the problem, representing the used reference frames. All coordinate systems are right-handed, thus the third axis is directed outside the paper. An inertial frame $X_iY_iZ_i$ is fixed in space, centered in the barycenter of the two primaries, is used as a basis; a rotating frame, called synodic, rotates with angular velocity Ω, its X_s axis directed from the larger towards the smaller primary, its Z_s axis directed outside the paper and Y_s that completes the right handed triad. The mass ratio defines the position of the primaries.

The aim of the CR3BP is to describe the motion of the smaller body in the synodic frame. The position of the point mass is $\mathbf{x}$; $\mathbf{r}_1$ and $\mathbf{r}_2$ are the

distances from the two primaries, fixed in the rotating frame. If one defines the effective potential

$$U(\mathbf{x}) = \frac{1}{2}(x^2 + y^2) + \frac{1-\mu}{r_1} + \frac{\mu}{r_2} \tag{6}$$

equations of motion of m_3 in the rotating frame, using normalized units, may be written as

$$\ddot{x} - 2\dot{y} = U_{/x} \tag{7}$$
$$\ddot{y} + 2\dot{x} = U_{/y} \tag{8}$$
$$\ddot{z} = U_{/z} \tag{9}$$

where $U_{/x}, U_{/y}, U_{/z}$ are the partial derivatives of U.

Throughout the Thesis, the Earth-Moon frame will be used, with a mass ratio of $\mu = 0.01215$. Most of the results may be generalized for any value of μ; for simplicity of notation, the two primaries will be always referred as Earth and Moon.

2.1.2 Equilibrium solutions

The CR3BP does not possess analytical closed-form solutions, although in some positions the centrifugal and the gravitational forces null each others, obtaining a local equilibrium. The coordinates of these points are obtained by nulling the gradient of U. Figure 2 depicts the position of such points in the synodic frame; they are divided in two classes:

- The collinear points L_1 (between Earth and Moon), L_2 (beyond the Moon), and L_3 (before the Earth), which lie on the x axis.
- The triangular, or equilateral, points L_4 and L_5, located at the vertexes of two equilateral triangles formed with the two primaries.

These equilibrium points are often called Lagrangian points [36]. While the position of the equilateral points may be computed straightforwardly, the x coordinate of the collinear points requires the solution of quintic polynomial, to be obtained numerically.

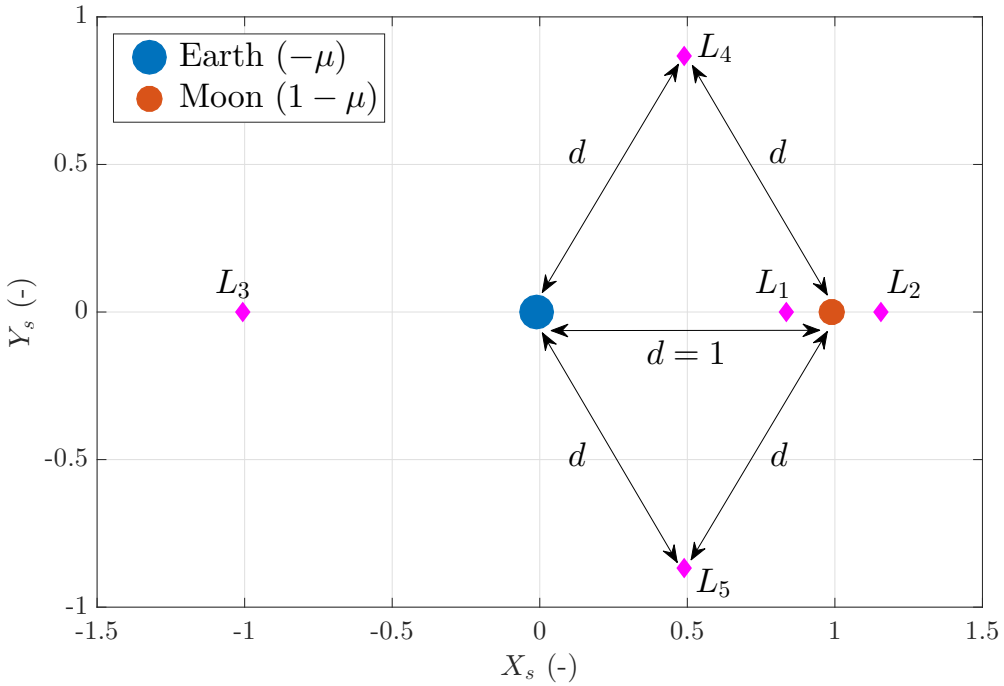


Figure 2: Equilibrium points

2.1.3 Jacobian constant and energy

The set of equations (7), (8), (9) possesses one integral of motion, the Jacobian constant JC, first introduced by Jacobi [37], although in a different formulation. In the synodic frame, it takes the form of equation (10)

$$JC(\mathbf{x}, \dot{\mathbf{x}}) = 2U - (\dot{x}^2 + \dot{y}^2 + \dot{z}^2) \tag{10}$$

recalling the definition of U from equation (6).

A direct relationship exists between the Jacobian constant and the total mechanical energy of the system

$$E(\mathbf{x}, \dot{\mathbf{x}}) = -U(\mathbf{x}) + \frac{1}{2}\dot{\mathbf{x}} \cdot \dot{\mathbf{x}} \tag{11}$$

being

$$JC = -2E \tag{12}$$

The Jacobian constant is the sole analytical integral of motion of the CR3BP [38].

2.2 DISTANT RETROGRADE ORBITS

The present work deals mainly with a particular family of periodic orbits, the Distant Retrograde Orbits (DRO) in the Earth-Moon rotating frame, depicted in Figure 3; the color scale corresponds to the Jacobian constant of each orbit.

This family was first studied by Broucke [39]; the numerical investigation of Hénon [40] classifies such orbits as family f, relative to the limiting Hill's case ($\mu \to 0$). Recently, these orbits were proposed for NASA's Jupiter Icy Moon Orbiter mission (canceled), with application in the Jupiter-Europa system [41], and for the Asteroid Redirect Mission [42]. Many studies further investigated the family [43, 44] and the possible transfer trajectories to and from such orbits [45, 46, 47, 48].

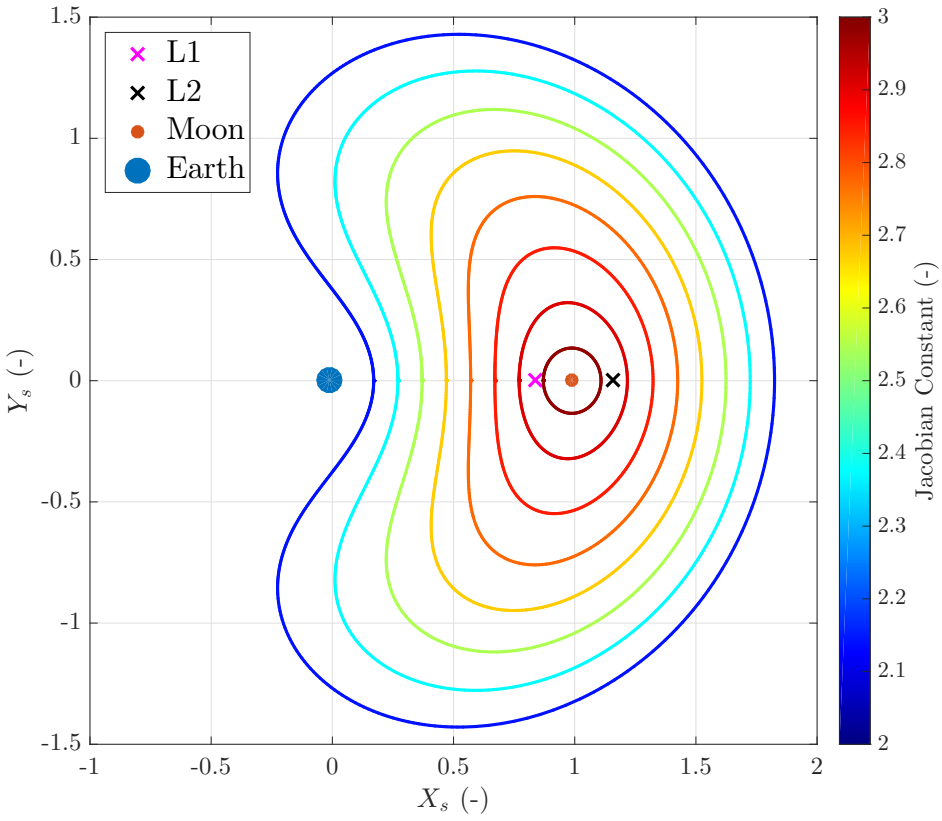


Figure 3: DRO family in the Earth-Moon system

2.2.1 Computation of the family

A differential correction scheme is used for the numerical computation of DROs, since no analytical solution exist. Once an orbit is obtained, it may be approximated through a truncated Fourier series [49], providing also a suitable guess for a continuation algorithm.

The set of equations (7), (8), (9), may be written as the first order variational form of (13)

$$\dot{\boldsymbol{\eta}} = [\tilde{A}](t)\boldsymbol{\eta} \tag{13}$$

where

$$\boldsymbol{\eta} = [x\ y\ z\ \dot{x}\ \dot{y}\ \dot{z}]^T \tag{14}$$

and

$$[\tilde{A}](t) = \begin{bmatrix} [0]_{3\times3} & [I]_{3\times3} \\ [U]_{\mathbf{xx}} & [\Omega] \end{bmatrix} \tag{15}$$

$[U]_{\mathbf{xx}}$ is the matrix of second derivatives of U with respect to the position vector, evaluated along the trajectory; $[\Omega]$ is a constant matrix which introduces the Coriolis acceleration terms

$$[\Omega] = \begin{bmatrix} 0 & 2 & 0 \\ -2 & 0 & 0 \\ 0 & 0 & 0 \end{bmatrix} \tag{16}$$

The State Transition Matrix $[\Phi]$ is the solution of the following matrix differential equation

$$[\dot{\Phi}](t, t_0) = [\tilde{A}](t)[\Phi](t, t_0) \tag{17}$$

which is a set of 36 scalar, first order differential equations. The STM is the basis of the differential correction algorithm, since it represents the partial derivative of the final state, at time instant t, in respect to a variation in the initial state at instant t_0. The first variation of the state at an instant t is, in fact,

$$\delta\mathbf{x} = \frac{\partial \mathbf{x}}{\partial \mathbf{x}_0}\delta\mathbf{x}_0 + \frac{\partial \mathbf{x}}{\partial t}\delta t = [\Phi](t, t_0)\delta\mathbf{x}_0 + \frac{\partial \mathbf{x}}{\partial t}\delta t \tag{18}$$

Exploiting the symmetry of the problem, DROs may be found starting from an initial state lying on the X_s axis with no horizontal velocity; being planar orbits, both z and $\dot{z}$ will always be zero. The numerical algorithm to generate a family of DROs, based on [50, 51], is set up as follows:

1. The initial abscissa is selected; throughout this work, DROs will be classified according to this coordinate, located between the Earth and the Moon, named x_0.

2. The vertical velocity $\dot{y}_0$ and the orbit period T are guessed; a convenient guess is to initialize the algorithm in the proximity of the Moon, providing as initial velocity and period the quantities relative to an equivalent low lunar orbit.

3. The orbit is integrated until the y coordinate changes sign.

4. At the crossing instant t_c, a periodic solution must possess null horizontal velocity, due again to the symmetry with respect to the x axis; a check is performed on $\dot{x}_c$, quitting the algorithm if $\dot{x}_c < 10^{-8}$.

5. If the crossing is not sufficiently orthogonal, the initial velocity is corrected using the STM at the instant t_c, through equation (18); being the problem planar and the correction on velocity only, this reduces to

$$\delta\dot{y}_0 = \left(\Phi_{45} - \frac{\ddot{x}_c}{\dot{y}_c}\Phi_{25}\right)^{-1} \delta\dot{x}_c \tag{19}$$

   where Φ_{ij} refers to the term of $[\Phi]$ in row i and column j.

6. The procedure is repeated until the crossing happens solely with vertical velocity (within the selected tolerance).

Figure 4 depicts how the differential correction works; the symmetry of the problem speeds up the computation, since only half orbit has to be computed.

Once a few close DROs are obtained (at least two), the family may be propagated through a numerical continuation scheme. Given two initial conditions $\mathbf{x}_0^{(1)}, \mathbf{x}_0^{(2)}$, a new initial guess for the differential correction scheme may be obtained as

$$\mathbf{x}_0^{guess} = \mathbf{x}_0^{(2)} + (\mathbf{x}_0^{(2)} - \mathbf{x}_0^{(1)}) = 2\mathbf{x}_0^{(2)} - \mathbf{x}_0^{(1)} \tag{20}$$

In the present work, the one-dimensionality of the problem is exploited, setting up a continuation method to provide initial guesses for $\dot{y}_0$ and T:

- The desired x_0 is fixed, with a prescribed shift Δx with respect to the previous DRO.

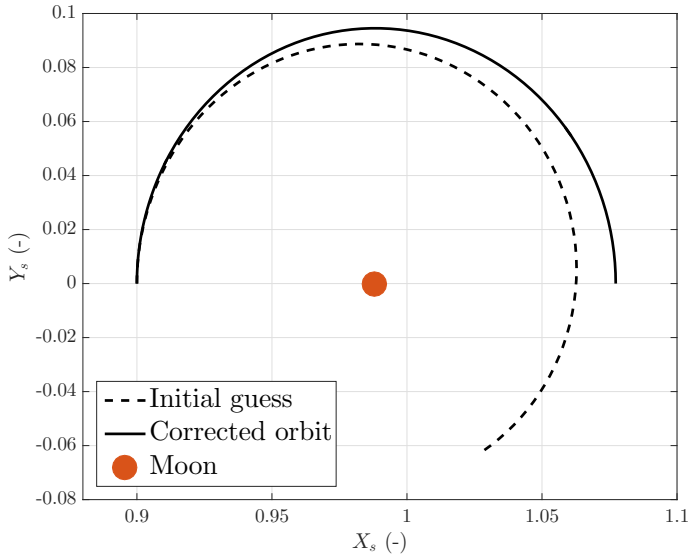


Figure 4: Differential correction procedure

- The derivatives of $\dot{y}_0$ and T, with respect to x_0, are computed; a first-order finite difference scheme is the most immediate to be used, but higher order approximations may be employed if a large span of DRO is available

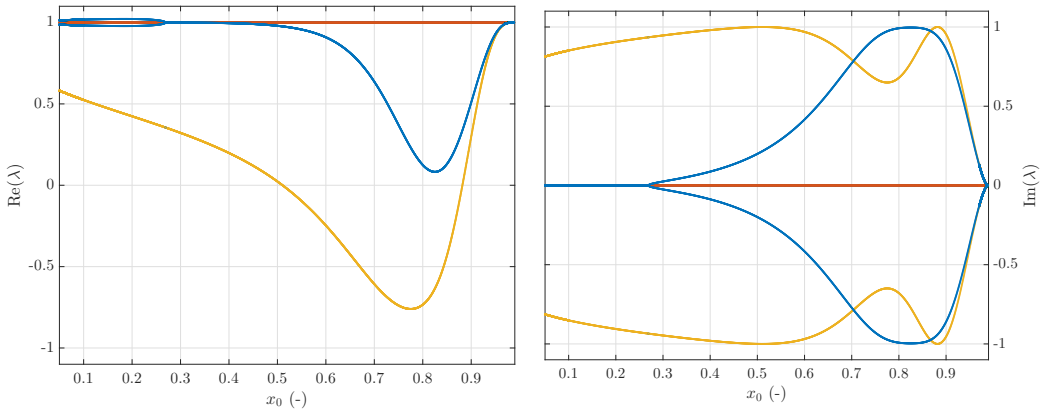
$$\frac{\partial \dot{y}_0}{\partial x_0} \simeq \frac{\dot{y}_0^{(i)} - \dot{y}_0^{(i-1)}}{x_0^{(i)} - x_0^{(i-1)}} \qquad \frac{\partial T}{\partial x_0} \simeq \frac{T^{(i)} - T^{(i-1)}}{x_0^{(i)} - x_0^{(i-1)}} \tag{21}$$

- The new guesses are obtain by linear extrapolation

$$\dot{y}_0^{(i+1)} = \frac{\partial \dot{y}_0}{\partial x_0} \Delta x + \dot{y}_0^{(i)} \qquad T^{(i+1)} = \frac{\partial T}{\partial x_0} \Delta x + T^{(i)} \tag{22}$$

2.2.2 Stability

The stability of DROs is among their most appealing features for practical applications. The orbits are stable up to a given amplitude, very far from the Moon. Figure 5 shows, as an index of stability, the eigenvalues of the monodromy matrix, computed along the family. At nearly 0.27 non-dimensional units, two of the four complex eigenvalues start moving along the real axis, with no imaginary part. One of the two consequently has a



(a) Real part **(b)** Imaginary part

Figure 5: DRO family eigenvalues

magnitude greater than the unity, and orbits from this point on towards Earth are unstable [47].

It is also noted that the DRO family shows a bifurcation with a family of three-dimensional DROs; the latter is not considered in this work, dealing only with planar motions.

2.2.3 Period and resonant orbits

In the Earth-Moon system, DROs have periods limited between 0 and approximately 27.45 days; these limits are discussed in Section 2.2.4. DRO useful for practical applications, such as ARM [42] or lunar outposts, are located in the neighborhood of the Lagrangian points L_1 and L_2; this location is appealing thanks to stability features and favorable position for mission to and from the lunar surface and to and from Earth. Figure 6 shows the period of DROs versus their left x coordinate, together with some resonances with the CR3BP synodic period.

A particular interest is devoted to the investigation of the DRO with a period 1:1 resonant with the lunar period (Figure 7); it shows no peculiar features in the synodic frame, while it appears as a non-keplerian (i.e. slightly perturbed) ellipse in the ECI frame. A more detailed analysis shows how the classical orbital parameters (the semi-major axis a, the eccentricity e and the perigee anomaly ω) present short-period oscillations (Figure 8). The

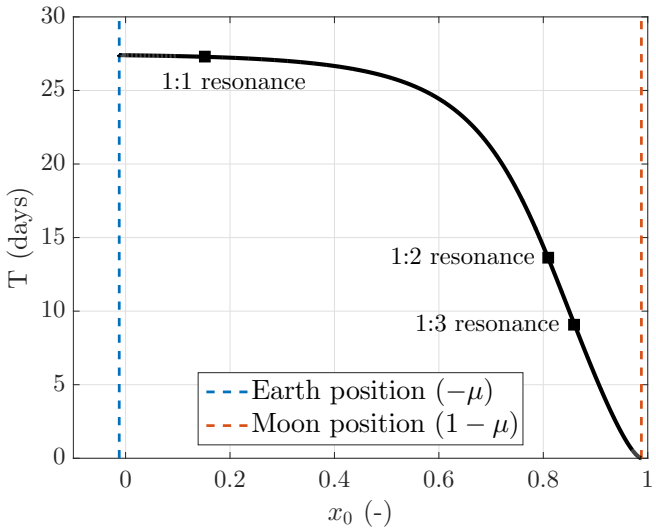


Figure 6: DRO period

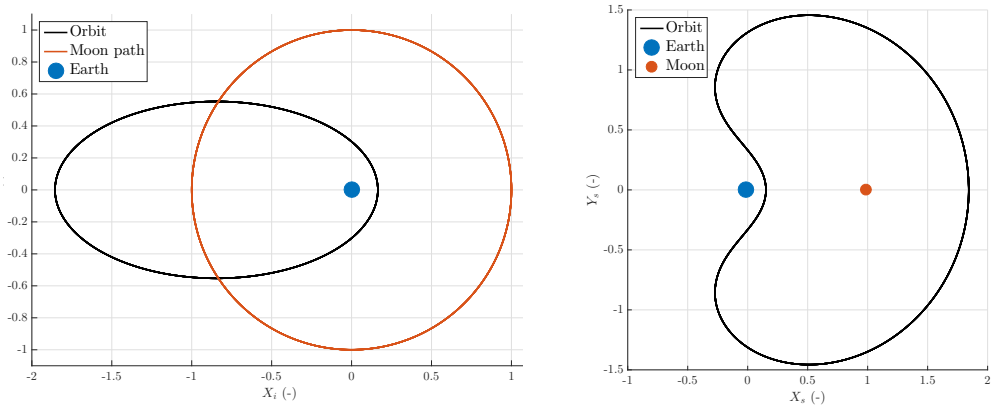
orbital period of the equivalent ECI ellipse do not actually coincide with 2π, since the perturbation due to the Moon actually confers the peculiar behavior to the orbit and allows the 1:1 resonance with the synodic frame; otherwise, the unperturbed Keplerian ellipse would not manifest periodicity in the synodic frame.

A further analysis may be conducted in the neighborhood of this 1:1 resonant orbit, looking at DROs in the ECI frame. These orbits too appear as perturbed ellipses, with the interesting feature of different direction of precession of the perigee, as summarized in Table 1; semi-major axis and eccentricity do not present secular variations (as expected from third-body perturbation theory). Such results might be useful in mission analysis for

$x_0\ (-)$	$\dot{\omega}\ (rad/T)$	$\bar{a}\ (km)$	$\bar{e}\ (-)$
0.1000	0.011	391,590	0.8830
0.1521	0	392,070	0.8312
0.2000	−0.014	392,500	0.7844

Table 1: Near-1:1 DRO orbital parameters in ECI frame

large DROs, since the ECI frame may ease operations and tracking; these orbits may be exploited for transfers towards the Moon or injection in smaller DROs [45].



(a) ECI frame **(b)** Synodic frame

Figure 7: 1:1 resonant DRO

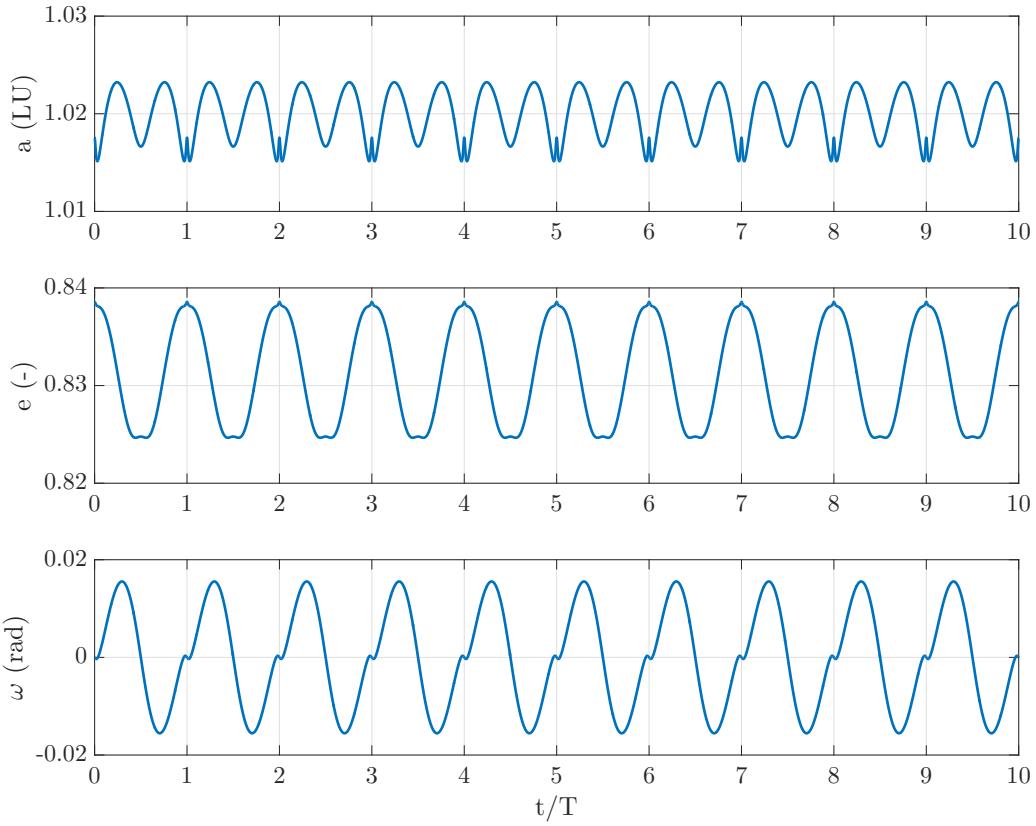


Figure 8: ECI orbital elements for 1:1 DRO

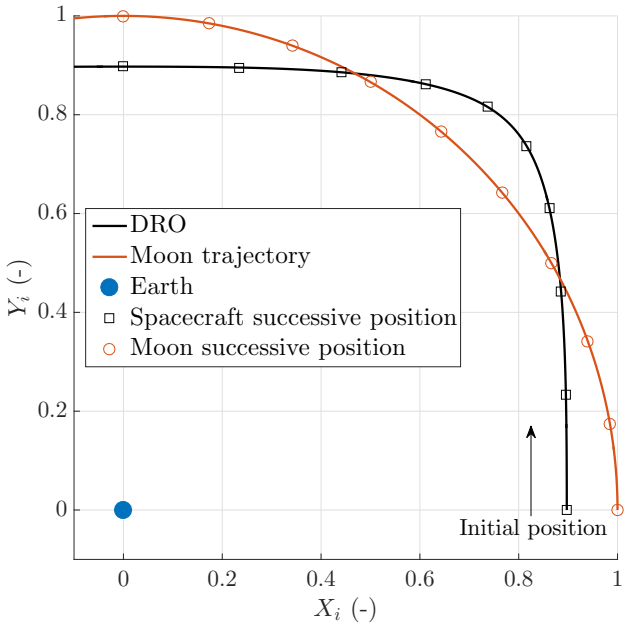
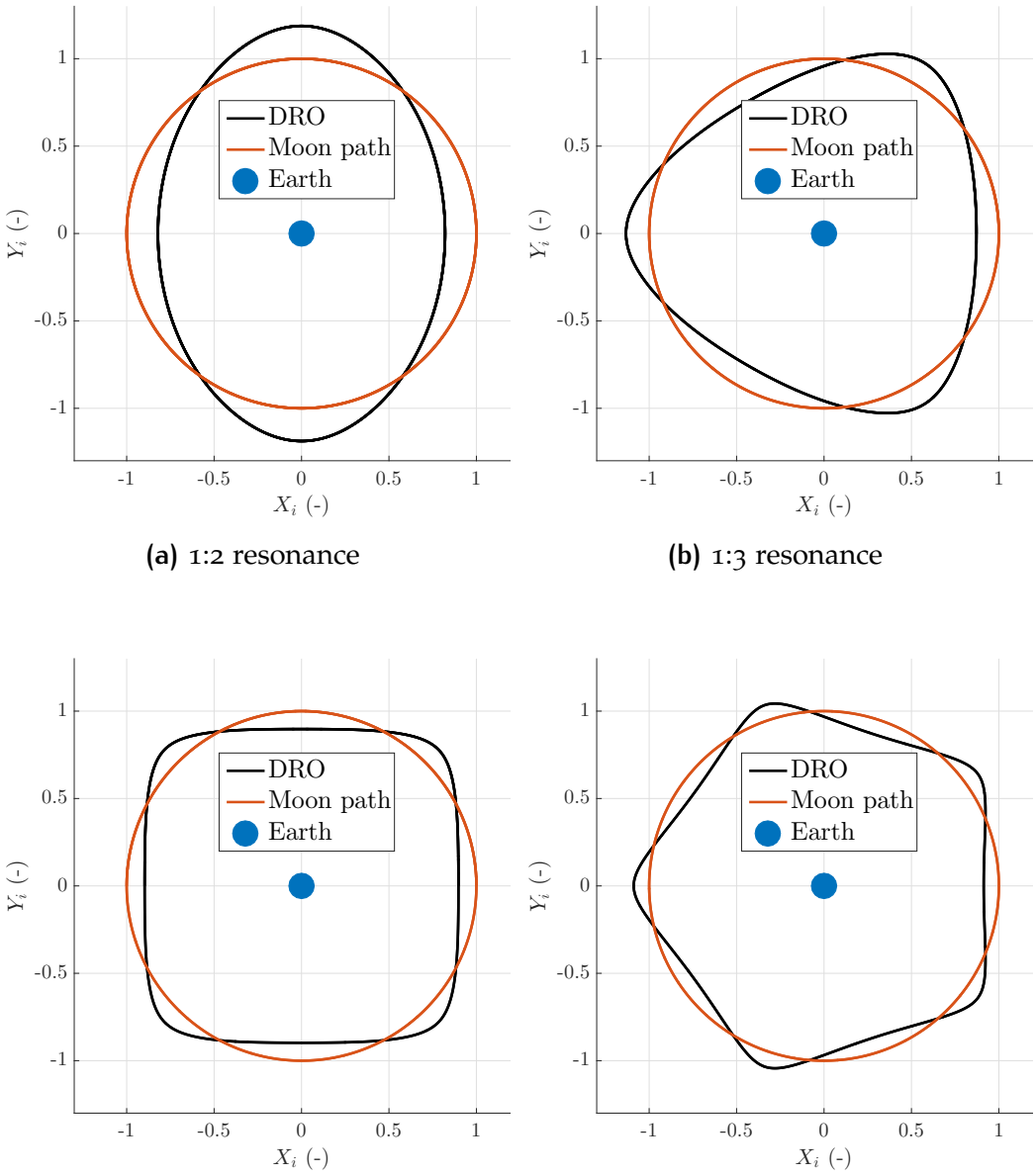


Figure 9: Detail of lunar encounters for 1:4 resonant DRO, ECI frame

Figure 10 shows other resonant DROs in the ECI frame. Their peculiar shape in this frame may be interpreted, for smaller resonances, as a series of close lunar encounters, as depicted in Figure 9; as the period decreases, they tend to become low lunar orbits. While the Keplerian representation may still be used for the 1:1 DRO, it is clear that it loses any validity as the orbit goes towards the Moon. Resonant orbits may be interesting since they maintain their shape both in the synodic and in the ECI frame, within the assumptions of the CR3BP; non-resonant DROs, while keeping their shape and periodicity in the synodic frame, appear as rotating in the ECI frame (this rotation may be compared, broadly speaking, to a perigee anomaly precession), as depicted in Figure 11.

2.2.4 Asymptotic behaviors

Two asymptotic cases may be investigated for the DRO, one in direction of the Earth and one towards the Moon. By looking at Figure 3, one notes that going towards the Moon DROs degenerate more and more into circular orbits around our natural satellite; on the opposite direction, DROs starting close to the Earth appear "beany" in the synodic frame, while they resemble



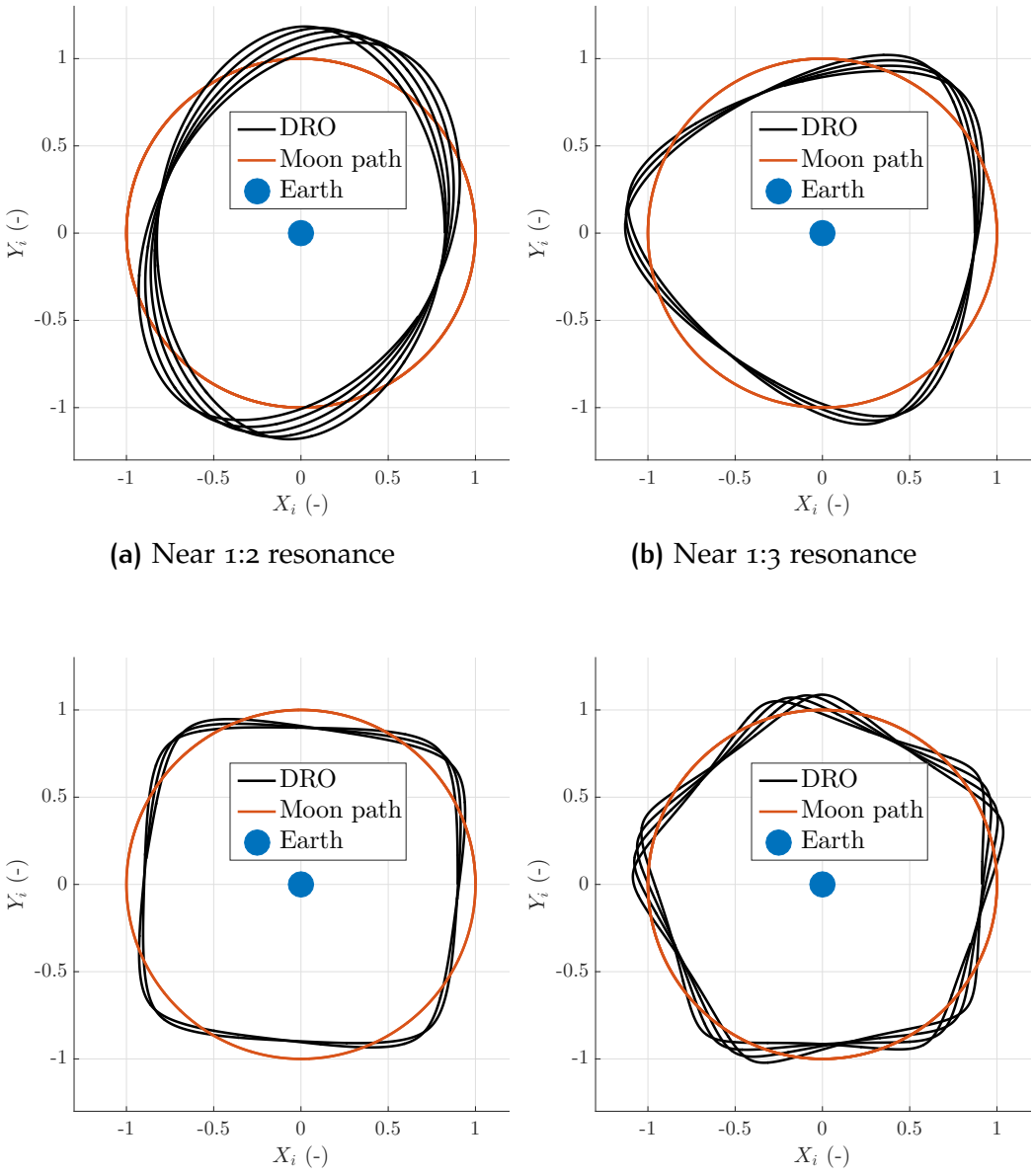
(a) 1:2 resonance

(b) 1:3 resonance

(c) 1:4 resonance

(d) 1:5 resonance

Figure 10: Some resonant DROs in ECI frame



(a) Near 1:2 resonance

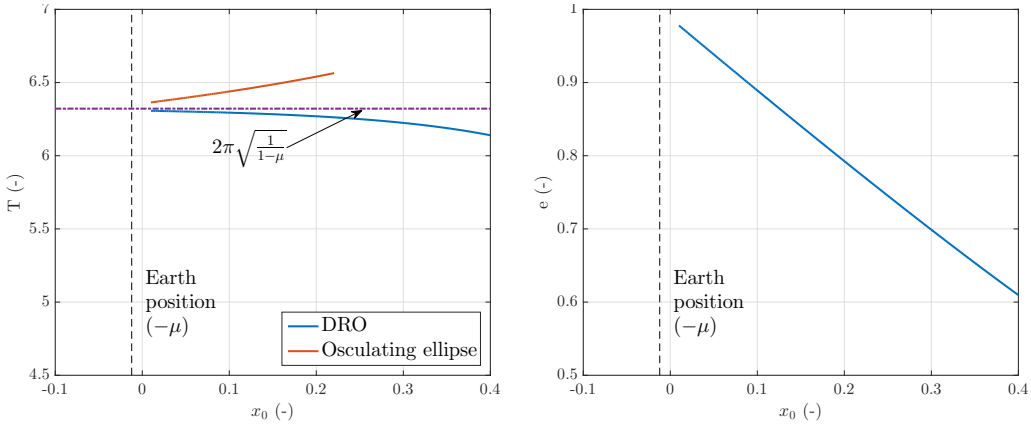
(b) Near 1:3 resonance

(c) Near 1:4 resonance

(d) Near 1:5 resonance

Figure 11: Some near-resonant DROs in ECI frame

to Keplerian ellipses in an Earth-centered inertial (ECI) frame (e.g. the 1:1 resonant DRO in Figure 7).



(a) Period **(b)** Eccentricity

Figure 12: Near-Earth DROs

Figure 12 shows the eccentricity and the period of the osculating ellipse in the ECI frame. The osculating ellipse is defined as the Keplerian orbit which results from the propagation of the initial state in ECI frame, where the effect of the Moon is neglected. The period of this orbit, if unperturbed, is computed as

$$T_{osc} = 2\pi\sqrt{\frac{a_{osc}^3}{1-\mu}} \tag{23}$$

When going towards the Earth, the osculating orbit's eccentricity tends linearly to 1, while the equivalent perigee distance approaches 0, considering ECI frame. The eccentricity may be assumed to follow the linear trend of equation (24), as depicted in Figure 13

$$e_{osc} = 1 - r_{p,osc} \tag{24}$$

In the limit case of collision DRO, one may obtain, analyzing the osculating ellipse,

$$\lim_{e_{osc}\to 1, r_{p,osc}\to 0} a_{osc} = \frac{1-e_{osc}}{1-e_{osc}} = 1 \tag{25}$$

which results in a period of

$$\lim_{x_0\to -\mu} T = 2\pi\sqrt{\frac{1}{1-\mu}} \tag{26}$$

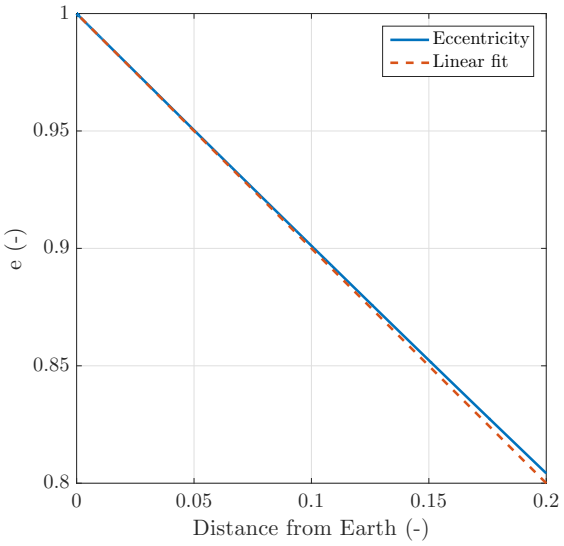
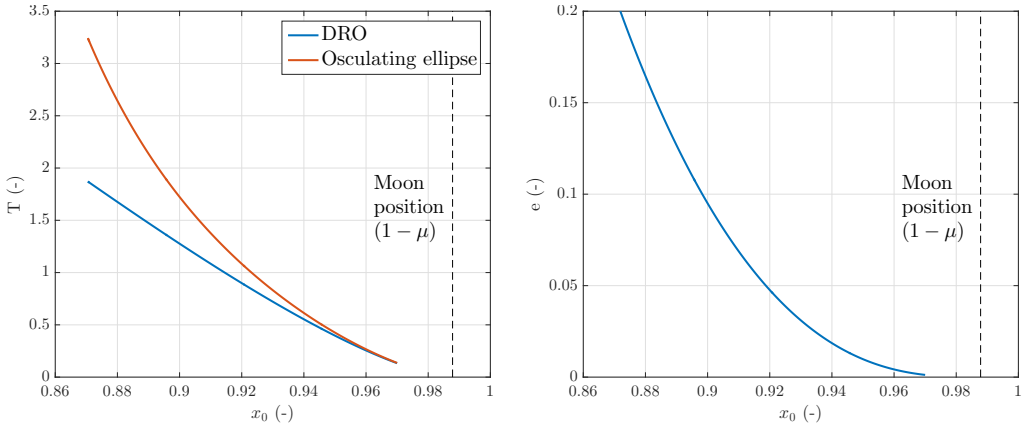


Figure 13: Linear trend of osculating near-Earth eccentricity

Equation (26) shows the asymptotic value of period for a DRO, traced in Figure 12a.

Figure 14 shows the DROs' period and osculating eccentricity in the opposite case, towards the Moon. In a Moon-centered inertial frame, the DROs tend to become circular orbits, with null eccentricity, up to degeneration into a singularity.



(a) Period **(b)** Eccentricity

Figure 14: Near-Moon DROs

3 COUPLED ORBIT-ATTITUDE RIGID BODY DYNAMICS

This Chapter presents the coupled orbit-attitude rigid body motion, describing the dynamical structure of the problem and identifying periodic solution. Such dynamical framework is the core of the research, treating the purely gravitational environment and introducing the gravity gradient torque exerted by both primaries. The solution and results obtained are the basis for the latter and future investigations.

The mathematical model is first presented in Section 3.1, underlining the coupling terms between orbital motion and attitude dynamics; the basic assumption are described and discussed, showing in Section 3.2 the validity of the algorithm with respect to other existing techniques and literature results. Section 3.3 presents the main results of the study, consisting in periodicity maps that visually portray the space of the coupled orbit-attitude solutions.

3.1 MODEL

The fully coupled orbital-attitude model aims at a description of the 6 degrees-of-freedom state of the spacecraft, considering the multi-body gravitational environment that acts both with force and torque components. The attitude motion is perturbed by the well-known gravity gradient torque, while the orbital dynamics requires the inclusion of higher-order gravitational term, to take into account the effect of the finite extension of the body with respect to the point-mass dynamics. The cross orbit-attitude terms depend both on the orientation and on the orbital position in a strongly non-linear fashion; the presence of multiple massive attractors further complicates the equations and increases the degree of non-linearity.

Figure 15 depicts the reference frames used for the analysis; recalling Figure 1, $X_sY_sZ_s$ is the rotating synodic frame, XYZ is an inertial frame, and $x_by_bz_b$ is a body-fixed principal inertia frame. The angle ϕ represents

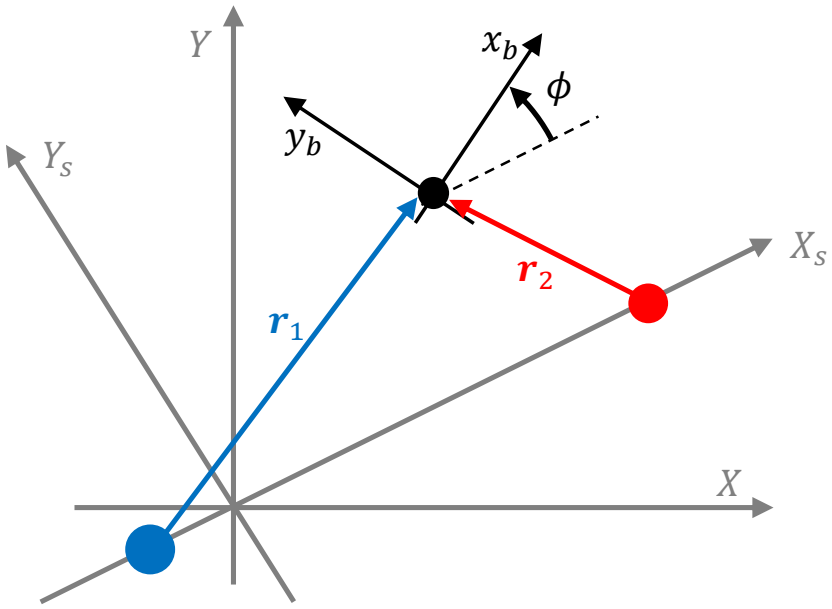


Figure 15: Reference frames

the rotation of the x_b axis with respect to the X_s axis. The inertia tensor $[I]$ of the spacecraft is assumed to be known in such principal frame, being

$$[I] = \begin{bmatrix} I_x & 0 & 0 \\ 0 & I_y & 0 \\ 0 & 0 & I_z \end{bmatrix} \tag{27}$$

The three-dimensional form of the equations will be derived and briefly discussed, but the present work will deal with planar orbits and rotational motions only.

3.1.1 Attitude dynamics and kinematics

Following [52], attitude dynamics is described by the set of Euler equations

$$[I]\dot{\boldsymbol{\omega}} + \boldsymbol{\omega} \times [I]\boldsymbol{\omega} = \mathbf{T}_{ext} \tag{28}$$

whose integration yields the time history of the angular velocity vector

$$\boldsymbol{\omega} = [\omega_x \ \omega_y \ \omega_z]^T \tag{29}$$

in body frame. $\mathbf{T}_{ext}$ is the external torque vector. The gravity gradient torque [52, 13] is computed through equation (30)

$$\mathbf{T}_{GG} = -3\frac{1-\mu}{r_1^5}[I]\mathbf{r}_1^b \times \mathbf{r}_1^b - 3\frac{\mu}{r_2^5}[I]\mathbf{r}_2^b \times \mathbf{r}_2^b \tag{30}$$

summing up the contribution of both primaries; $\mathbf{r}_1^b$ and $\mathbf{r}_2^b$ are the position vectors, in body axes, with respect to the Earth and the Moon respectively. All the quantities are to be expressed in non-dimensional units.

Considering planar orbital and attitude dynamics, i.e. the z_b axis is always parallel to the Z_s axis, and combining equations (28) and (30), one obtains equation (31)

$$\dot{\omega}_z = \frac{I_y - I_x}{I_z}\left(3\frac{1-\mu}{r_1^3}e_2e_1 + 3\frac{\mu}{r_2^3}l_2l_1\right) \tag{31}$$

describing the planar attitude dynamics of a spacecraft in the Earth-Moon CR3BP. e_1, e_2 denote the direction cosines of $\mathbf{r}_1^b$, whereas l_1, l_2 are the direction cosines of $\mathbf{r}_2^b$. Equation (31) leads to note that the spacecraft inertia topology, for the planar case, may be described through a single inertia coefficient

$$K_z = \frac{I_y - I_x}{I_z} \tag{32}$$

The kinematic state of the spacecraft, for the three-dimensional problem, is conveniently described by a quaternion parametrization [52]. Such formulation is convenient to avoid any singularity during the integration. In the hereby considered planar case, the rotation of the spacecraft may described by a single parameter, chosen to be the angle ϕ between the x_b and the X_s axes, counterclockwise. The derivative of this angle is the body angular velocity minus the rotational speed of the synodic frame; using non-dimensional units, this relationship reduces to

$$\dot{\phi} = \omega_z - 1 \tag{33}$$

Within the present work, quaternions are employed exclusively at numerical level, to perform integration and avoid undesired singularities that may arise with Euler angles. The kinematic state of the spacecraft is described by the angle ϕ, and the numerical algorithms as well are based on this angle. For the planar case, the components q_1, q_2, q_3 and q_4 of the quaternion (the

latter being the scalar part) are linked to the rotation angle through equation (34)

$$q_1 = 0 \qquad q_2 = 0 \qquad q_3 = \sin\frac{\phi}{2} \qquad q_4 = \cos\frac{\phi}{2} \tag{34}$$

The rotation between two reference frames may be performed using the rotation matrix $[A]$; in the considered planar case, the rotation matrix between the synodic and the body frame takes the simple form

$$[A] = \begin{bmatrix} \cos\phi & \sin\phi \\ -\sin\phi & \cos\phi \end{bmatrix} \tag{35}$$

so that

$$\mathbf{r}_i^b = [A]\mathbf{r}_i^s \tag{36}$$

Unless specified, throughout the work the 2×2 matrix $[A]$ will denote the rotation between synodic and body frames.

3.1.2 Orbital dynamics

Equations (7),(8), (9) describe the motion a point mass in the CR3BP. If the spacecraft is considered as an extended body, the gravitational force acting on it assumes a different expression, and becomes explicitly depending on the body's attitude and inertia properties. Considering a second-order gravitational potential (higher order might be included in a further model refinement), Kane [6] proves the following expression for the acceleration acting on an extended body, due to an attracting body of mass m, at a distance r

$$\mathbf{a}^{(2)} = -\frac{Gm}{r^4}\left[\frac{3}{2}\left(tr([I]) - 5\mathbf{r}^T[A]^T[I][A]\mathbf{r}\right)\mathbf{r} + 3[A]^T[I][A]\mathbf{r}\right] \tag{37}$$

where $\mathbf{r}$ is the unit vector of the line that joins the attracting body and the spacecraft. Equation (37) is referred to the synodic reference frame, so the principal inertia tensor $[I]$ must be rotated through a rotation matrix $[A]$, indicating the transformation between synodic and body frame.

It is noted that the inclusion of $\mathbf{a}^{(2)}$ in the model leads to perturbing accelerations which are several orders of magnitude smaller than other perturbations (e.g. solar radiation pressure, Sun's gravity, etc.) even for very large and massive spacecraft, as summarized in Table 2 using 10 times the dimensions of the International Space Station. Thus, the addition of

the second-order gravitational accelerations due to the Earth and the Moon does not produce any significant effect on the orbit. This coupling term might be considered in future studies concerning different gravitational environments, where it may play a significant, or at least non-negligible, role on the orbital dynamics.

Source	$\mathcal{O}$ (-)
Sun gravity	10^{-3}
Solar radiation pressure	10^{-5}
Body finite extension	10^{-13}

Table 2: Perturbing non-dimensional accelerations in the Earth-Moon CR3BP

3.2 VALIDATION

The numerical code shall be validated, testing its accuracy and reliability by comparison with known solutions. The validation is first performed in a two-body orbital framework, then extended to the Lagrangian points of the CR3BP up to a direct comparison with a literature periodic solution.

3.2.1 Two-body problem

The gravity gradient torque in the two-body problem has been widely studied in literature. Books such as [52], [6] and [53] provide the main results, here recalled. Given a rigid body in a nearly-circular Earth orbit, with an initial angular velocity equal to the orbital mean motion (often called a simple spin satellite), its attitude motion is stable when

$$I_{pitch} > I_{roll} > I_{yaw} \tag{38}$$

In the present framework, the following correspondence holds

$$I_{pitch} = I_z \qquad I_{roll} = I_y \qquad I_{yaw} = I_x \tag{39}$$

considering an orbit lying in the XY plane and the x_b direction to be aligned with the local vertical.

Figures 16, 17 and 18 depict the attitude response for a body in a low-Earth orbit, with semimajor axis $a = 10050$ km, eccentricity $e = 0.005$, for different inertia ratios; the inertia moment about the z_b axis is $I_z = 96.95 \times 10^6$ kgm^2. The pericenter lies on the X_s axis at the initial instant. Attitude dynamics is integrated both in the CR3BP framework (the code to be validated) and in a two-body inertial reference frame, considering the sole gravitational action of the Earth. The gravity gradient torque exerted by the Moon is expected to be negligible.

Condition	Figure	I_x (10^6 kgm^2)	I_y (10^6 kgm^2)
Canonical stability	16	12.12	89.68
DeBra-Delp stability	17	109.07	118.76
Stable eccentricity resonance	18	40.39	72.71

Table 3: Validation test cases

Table 3 summarizes the different test cases used to validate the author's code. The canonical stability condition is defined by equation (38); the DeBra-Delp region [54, 55], where a linearly stable condition is achieved with

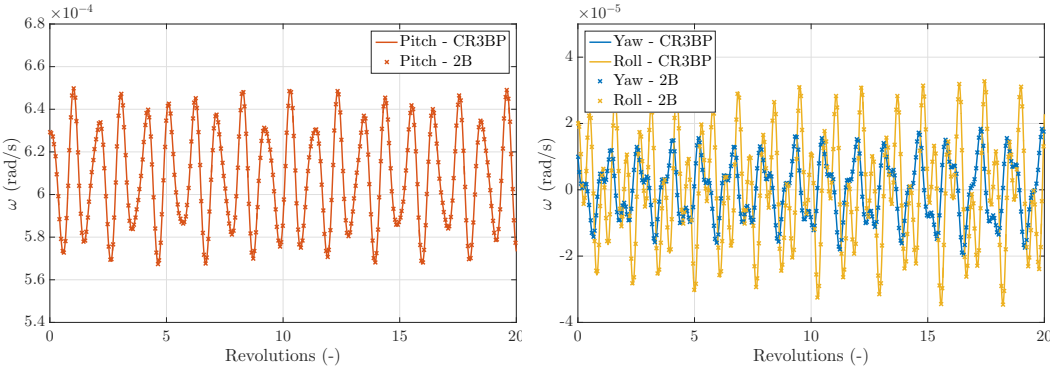
$$I_{roll} > I_{yaw} > I_{pitch} \tag{40}$$

is tested too. Finally, the eccentricity resonance condition ($K_z = 1/3$) is verified to be in accordance with the literature, noting beats phenomena in the pitch response.

3.2.2 Three-body problem

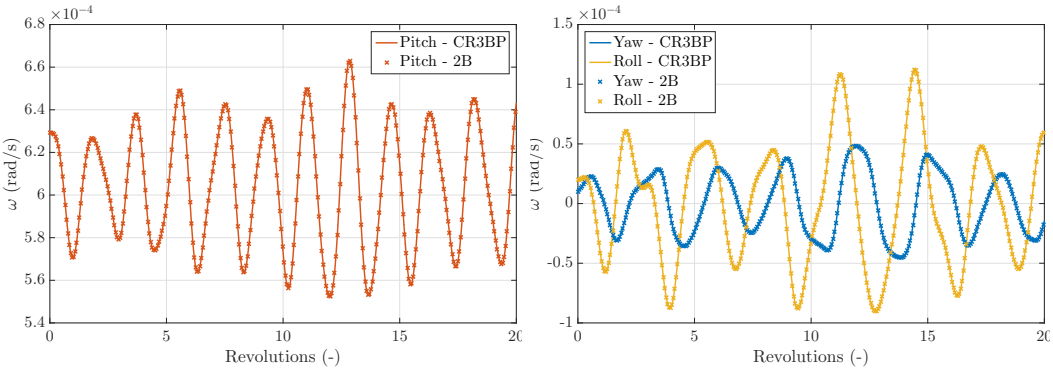
Once the code's results are assessed and verified in the simple two-body framework, one can proceed to validate some test cases in the CR3BP, with combined gravity gradient torque of both primaries.

Robinson [11] provides stability charts for a rigid satellite artificially kept at a Lagrangian point; Figure 19 portrays such stability map for the collinear L_1 point of the Earth-Moon system. The stability regions (red) are a function of two parameters depending on the inertia properties of the spacecraft, following the original author's nomenclature. Robinson's



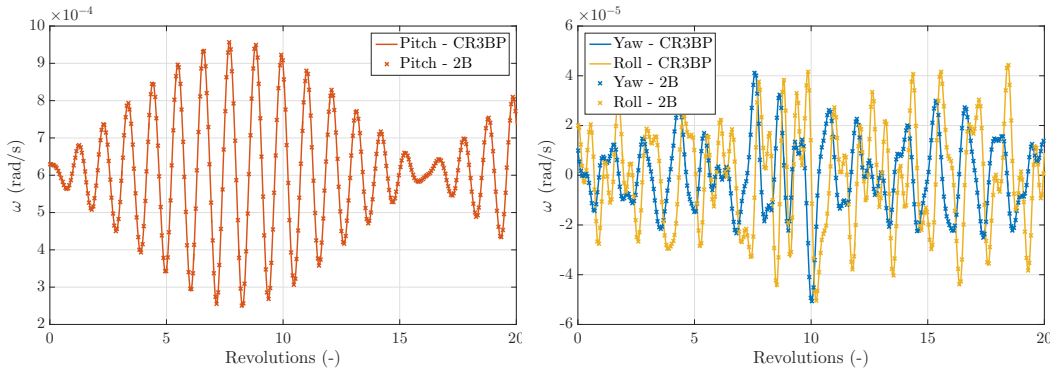
(a) Pitch oscillations **(b)** Yaw-roll oscillations

Figure 16: Stable attitude response validation



(a) Pitch oscillations **(b)** Yaw-roll oscillations

Figure 17: DeBra-Delp region attitude response validation



(a) Pitch oscillations **(b)** Yaw-roll oscillations

Figure 18: Eccentricity resonance attitude response validation

linearized equations, describing small oscillations at one of the collinear Lagrangian points, are reported in equations (41), (42), (43)

$$\ddot{\phi} = \frac{I_y - I_z}{I_x}\phi + \left(\frac{I_y - I_z}{I_x} + 1\right)\dot{\theta} \tag{41}$$

$$\ddot{\theta} = \frac{I_x - I_z}{I_y}(h+1)\theta - \left(\frac{I_x - I_z}{I_y} + 1\right)\dot{\phi} \tag{42}$$

$$\ddot{\psi} = h\frac{I_y - I_x}{I_z}\psi \tag{43}$$

The parameter h is an auxiliary coefficient; for the Earth-Moon system, it takes the values reported in Table 4. The angles ϕ, θ, ψ are a set of 123 Euler angles, and correspond to the first order small rotations about X_s, Y_s, Z_s respectively.

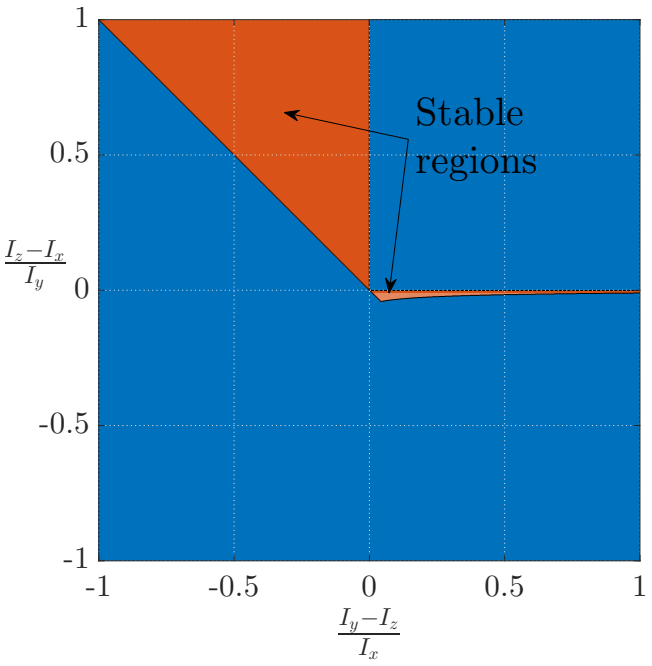
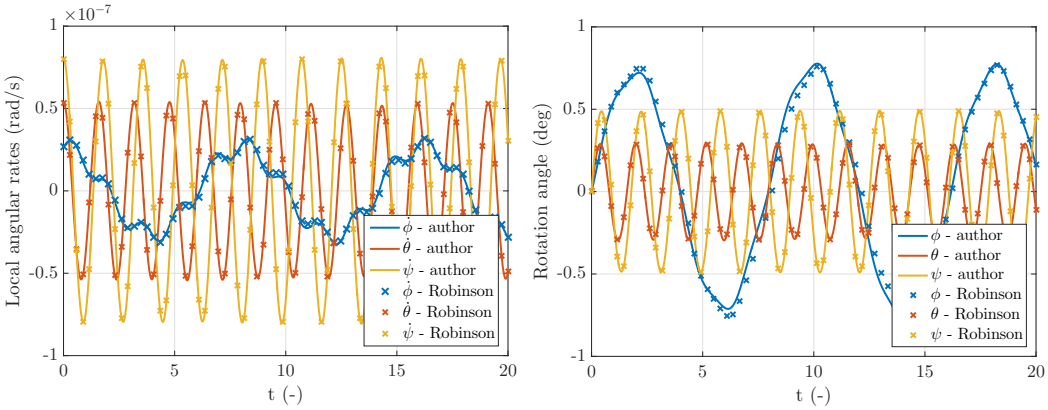


Figure 19: Stability chart for a rigid body at L_1

	L_1	L_2	L_3
$h(-)$	15.44	9.57	3.03

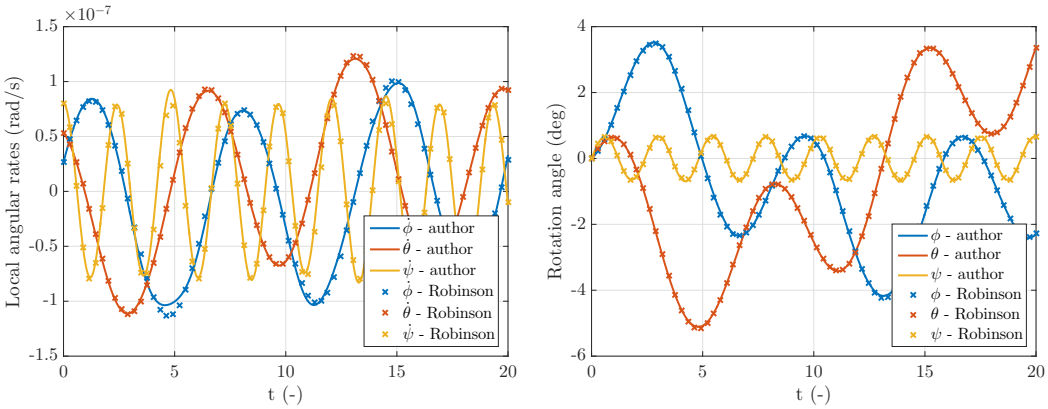
Table 4: Auxiliary k parameter

The comparisons between the author's code and Robinson's set of linear equations are portrayed in Figures 20 and 21. Figure 20 is referred to the larger stability region, using $I_x = 12.12 \times 10^6$ kgm^2, $I_y = 89.68 \times 10^6$ kgm^2; the results of Figure 21 are obtained with $I_x = 97.77 \times 10^6$ kgm^2, $I_y = 140.13 \times 10^6$ kgm^2, which belong to the smaller "strip" region of Figure 19.



(a) Angular rates **(b)** Euler angles

Figure 20: L_1 small oscillations, stable region



(a) Angular rates **(b)** Euler angles

Figure 21: L_1 small oscillations, "strip" stable region

3.3 PERIODIC ORBIT–ATTITUDE SOLUTIONS

The coupling between orbital and attitude dynamics is mainly manifested in the gravity gradient torque; this in fact is strongly orbit-dependent, and may lead to attitude instabilities and natural drifts from a desired attitude. While an attitude control system (ACS) may be designed to counteract such torque, the present study aims at searching natural periodic attitude solutions, i.e. dynamical structures where both the orbit and the attitude motion are periodic. These solutions might be exploited to relieve the ACS from the gravity gradient control, and to benefit from the natural stability to fulfill coarse pointing requirements [17, 19, 20].

3.3.1 Method and algorithm

The procedure to obtain a periodic orbit-attitude solution is presented using distant retrograde obits, which are the core of the present work, but it may in general be extended to other families of periodic planar orbits. It is underlined that the coupling between attitude and orbital motions is, in practice, a one-way coupling: the orbital path influences the attitude dynamics through the gravity gradient torque which varies along the orbit, whereas the perturbing acceleration due to the attitude motion does not influences the orbital dynamics, which might then be integrated using the point mass approximation, i.e. equations (7), (8) and (9). Section 3.1.2 supports this working assumption; in order to preserve the generality of the algorithm, equation (37) is introduced anyway into the numerical code, even though no significant effect is observed.

The algorithm is set up as follows:

1. A DRO with period T is obtained, using the differential correction technique presented in Section 2.2;
2. The orbit is reduced to an analytical formulation using a high fidelity Fourier series expansion [49], in order to preserve periodicity (avoiding numerical dissipation) even for long integration periods, and to lighten the numerical code

$$x(t) = a_0 + \sum_{n=1}^{N_f} a_n \cos\left(2n\pi\frac{t}{T}\right) \tag{44}$$

$$y(t) = \sum_{n=1}^{N_f} b_n \sin\left(2n\pi\frac{t}{T}\right) \tag{45}$$

The order N_f of the expansion is chosen according to the conservation of the Jacobian constant; Figure 22 portrays a sample variation of such integral of motion, computed with the Fourier series approximation, with respect to the initial value. For DROs, low orders (less than 10) are in general sufficient for a very good approximation, while other families of orbits may need a higher number of terms;

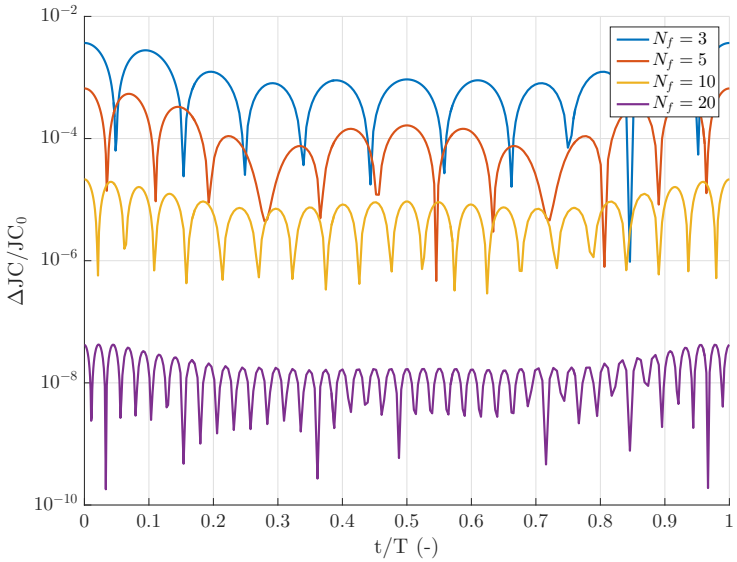


Figure 22: JC variation with Fourier series expansion, DRO with $T = 19.92$ days

3. The spacecraft topology is selected, fixing the K_z parameter;

4. The planar attitude motion is integrated along the selected DRO, using equation (31), for a large span of initial angular velocity $\omega_z(0)$, and starting from an initial condition with the x_b axis aligned with the X_s axis, namely $\phi(0) = 0$;

5. The final values of angular velocity $\omega_z(T)$ and rotation angle $\phi(T)$ are retrieved after one orbital period, computing their variations with respect to the initial value

$$\Delta\omega_z = \omega_z(T) - \omega_z(0) \qquad \Delta\phi = \phi(T) \quad -\pi < \phi \leq \pi \tag{46}$$

Figure 23 plots such variations along the span of $\omega_z(0)$, in non-dimensional units;

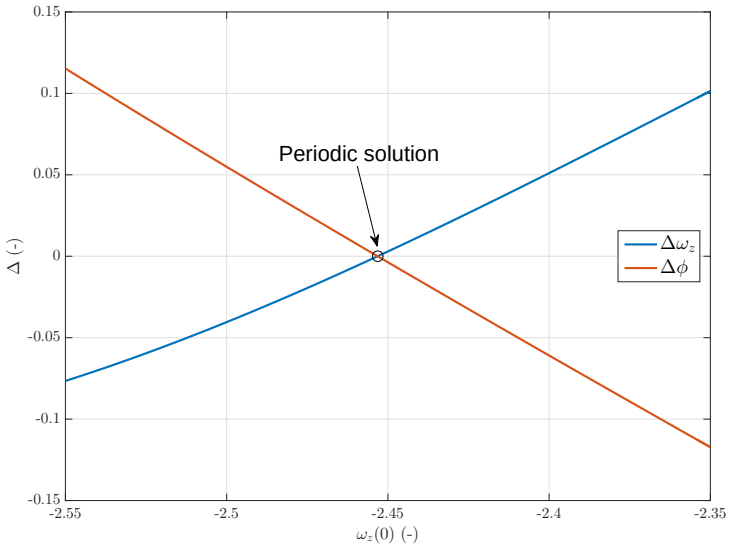


Figure 23: Angle and angular velocity variation, DRO period = 12.66 days

6. The value of $\omega_z(0)$ that yields a periodic solution, highlighted in Figure 23, is identified when both $\Delta\omega_z$ and $\Delta\phi$ are null, within a tolerance of 10^{-5} non-dimensional units.

The presented algorithm is able to identify a periodic attitude motion superposed to a given orbit, resulting in a periodic orbit-attitude behavior. The method is based on the residuals of angular velocity and rotation angle after an orbital period, and thus depends on the selected tolerance for such residuals; it is anyway very robust, since it is able to identify solutions, if they exist, for virtually any type of planar orbit, as long as the considered span of initial angular velocities is wide enough to comprise a solutions, if it exists.

In order to refine a given solution, a differential correction technique is also implemented, which might be used in parallel or in place of the presented algorithm. The differential correction scheme works as follows:

1. A DRO is obtained and its Fourier series expansion is computed;
2. Starting from an initial guess $\omega_z(0)$, the attitude motion is integrated for one orbital period, obtaining the final values of angular velocity

$\omega_z(T)$, angle $\phi(T)$, and the 2×2 state transition matrix $[\Phi](T,0)$, defined as

$$[\Phi](T,0) = \frac{\partial \boldsymbol{\eta}(T)}{\partial \boldsymbol{\eta}(0)} \tag{47}$$

where in this case the state is

$$\boldsymbol{\eta} = [\omega_z \ \phi]^T \tag{48}$$

The first variation of the final state may be written as

$$\delta\boldsymbol{\eta} = [\Phi](T,0)\delta\boldsymbol{\eta}(0) + \frac{\partial \boldsymbol{\eta}}{\partial t}\delta t \tag{49}$$

3. A first simplification arises, since the final time is constrained to coincide with the period of the orbital motion and in not free to vary, i.e. $\delta t = 0$, reducing equation (49) to

$$\begin{bmatrix} \omega_z(0) - \omega_z(T) \\ -\phi(T) \end{bmatrix} = \begin{bmatrix} \Phi_{11} & \Phi_{12} \\ \Phi_{21} & \Phi_{22} \end{bmatrix} \begin{bmatrix} \delta\omega_z(0) \\ \delta\phi(0) \end{bmatrix} = \begin{bmatrix} \Phi_{11}\delta\omega_z(0) + \Phi_{12}\delta\phi(0) \\ \Phi_{21}\delta\omega_z(0) + \Phi_{22}\delta\phi(0) \end{bmatrix} \tag{50}$$

4. The second step is to eliminate the correction on the initial angle $\delta\phi(0)$, since the initial attitude, for the present work, is always considered to be $\phi(0) = 0$. From the second equation of (49) one obtains

$$\delta\phi(0) = -\frac{\Phi_{21}\delta\omega_z(0) + \phi(T)}{\Phi_{22}} \tag{51}$$

which can be put into the first

$$\omega_z(0) - \omega_z(T) = \left(\Phi_{11} - \frac{\Phi_{12}\Phi_{21}}{\Phi_{22}}\right)\delta\omega_z(0) - \frac{\Phi_{12}}{\Phi_{22}}\phi(T) \tag{52}$$

obtaining the correction to be applied to the initial angular velocity

$$\delta\omega_z(0) = \frac{\omega_z(0) - \omega_z(T) + \dfrac{\Phi_{12}}{\Phi_{22}}\phi(T)}{\Phi_{11} - \dfrac{\Phi_{12}\Phi_{21}}{\Phi_{22}}} \tag{53}$$

5. The initial angular velocity is corrected using equation (53), iterating until convergence.

The differential correction algorithm allows to achieve more stringent tolerances (e.g. 10^{-9}) on the final values of ω_z and ϕ, with a reduced computational time, since the correction is always applied in a locally tangent direction indicated by the STM $[\Phi]$. On the contrary, the previously presented "shooting" algorithm is computationally intensive, requiring a full integration of the attitude along all the span of angular velocities; the larger this span, the more flexible is the algorithm, allowing to find solutions even from bad initial guesses, at the expense of increased computational time. Both algorithm might be used, or a combination of the two in a predictor-corrector fashion, to obtain periodic orbit-attitude solutions.

3.3.2 Solution space mapping

A planar orbit-attitude solution is fully defined when, given a periodic 2D orbit (DRO in the present work), the value of initial angular velocity $\omega_z(0)$ that guarantees a periodic attitude motion is found. In the present investigation, the initial attitude is constrained to the alignment of the body frame with the synodic frame, leading to a null initial gravity gradient torque. Non-trivial solutions, considering a three-dimensional attitude motion superposed to a planar orbit, might be object of future investigations.

Recalling Section 2.2, DROs are classified according to their initial abscissa x_0, located between the Earth and the Moon. For each DRO, multiple values of $\omega_z(0)$ yield a periodic attitude behavior along the orbit, with a different number of body rotation per orbital revolution. These solutions are grouped into families.

A family of periodic orbit-attitude solution is defined as the set of initial angular velocities that, for the class of considered orbits, leads to a periodic attitude behavior with a given number N of body rotations per orbital revolution. Note that the number N indicates the overall number of rotations, even if they are carried out with a non-uniform angular velocity; this number may be positive (i.e. the rigid body revolves N times about its z_b axis along one orbit), zero (the spacecraft oscillates, but the net number of body revolution per orbit is null), or negative (the rigid body carries out N revolutions per orbit with negative angular velocity). At the end of the Chapter, Figures 30 and 31 depict and further clarify the multiple possible solutions for a fixed DRO, belonging to different families.

The families may be visually portrayed, creating maps such as Figure 24. The horizontal axis denotes the DRO, classified through their initial

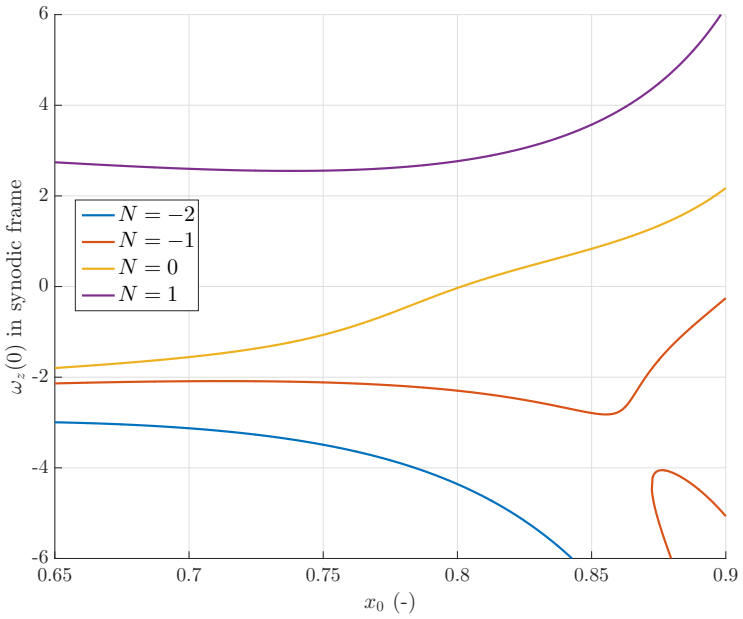


Figure 24: Attitude periodicity maps for DROs, $Kz = 0.8$

abscissa, whereas the vertical axis indicates the initial angular velocity which establishes a periodic attitude behavior. Different colors highlight the different families of solutions; it is interesting to note the double ramification of the $N = -1$ family for DROs closer to the Moon.

3.3.3 Algorithm validation

A comparison with a literature result is performed, as further validation of both the numerical code and the solution search algorithm. Guzzetti and Howell [20] identify a periodic orbit-attitude behavior for a rigid body with $K_z = 0.8$, in a DRO with $T = 13.22$ days. Starting with an angular velocity $\omega_z(0) = -3.75$ non-dimensional unit, the spacecraft performs two body rotations per orbit.

This solution is portrayed in Figure 25, showing the angle profile obtained with the author's code; a periodic attitude behavior is observed, matching the literature results and providing a verification of the code correctness.

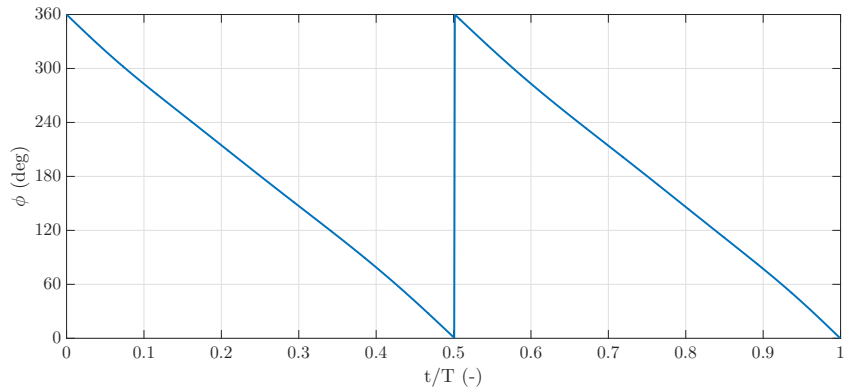
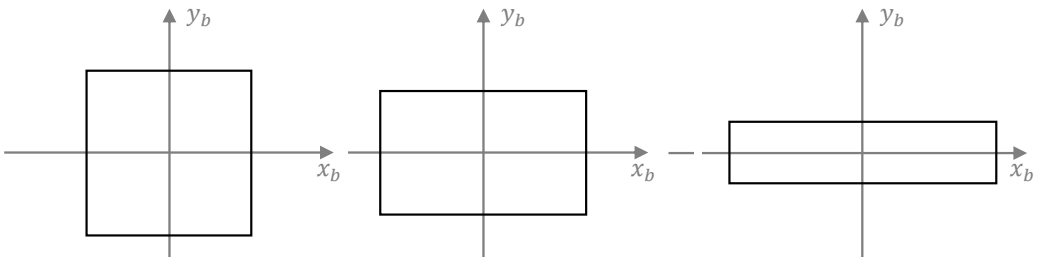


Figure 25: Guzzetti's periodic orbit-attitude solution

3.3.4 Sensitivity to spacecraft topology

The maps presented in Figure 24 might be generated for any other value of inertia ratio K_z, between the values 0 and 1. The zero value represents a rigid body symmetric about the z_b axis, whereas $K_z = 1$ denotes a rod-like body with mass distributed only on the x_b axis (i.e. no inertia moment about such axis). Any value in-between may be considered as an elongation parameter, providing information on the inertia and mass distribution. Negative values of K_z are characteristic of bodies with $I_x > I_y$, and might be reduced to positive values through a $\pi/2$ rotation of the body-fixed reference frame. For the present framework, this case may be treated as a different initial attitude (i.e. $\phi(0) = \pi/2$), and left for future analyses. Figure 26 depicts some rod-like structures, which represent a given inertia ratio.



(a) $K_z = 0$ **(b)** $K_z = 0.4$ **(c)** $K_z = 0.9$

Figure 26: Different inertia topology representations, rod-like spacecraft

Let's consider the $N = 1$ family as reference for the investigation of the different spacecraft topologies. Recalling equation (31), the case $K_z = 0$

corresponds to a torque-free motion (considering gravity gradient only), since the right-hand term is nulled. In order to obtain a periodic attitude motion, and revolve once about the z_b axis along one orbital revolution, the spacecraft must start with an angular velocity that equals the angular frequency of the DRO; such angular velocity will be conserved during all the path, as a consequence of the axisymmetricity of the body.

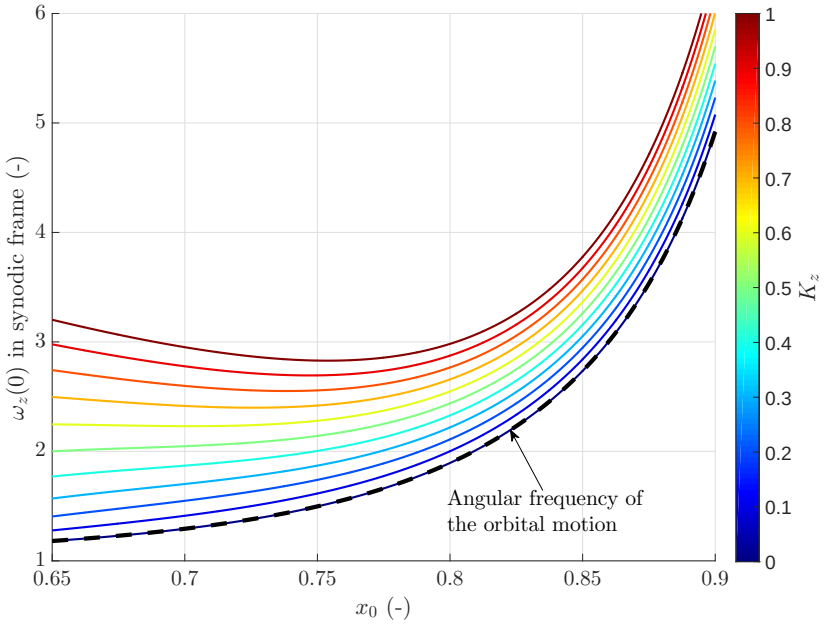


Figure 27: Attitude periodicity family, $N = 1$

Figure 27 depicts the whole family, along the considered span of DROs, for all the possible inertia ratios K_z. Note how the $K_z = 0$ curve coincides with the aforementioned angular frequency, i.e. $2\pi/T$. This feature may be exploited for a more efficient numerical search of the family, starting with low values of K_z and providing the orbit's frequency as initial guess, and then use numerical continuation to propagate the family up to $K_z = 1$. The two curves $K_z = 1$ and $K_z = 0$ act as boundaries, delimiting a region in the solution space which contains all the $N = 1$ family.

Figures 28 and 29 portray two other families, $N = 0$ and $N = -1$ respectively. In the $N = 0$ family, the curve with null inertia coefficient corresponds to a null initial angular velocity in the synodic frame; in the present framework with gravity gradient only, this condition leads to a null rotation, in the present framework with gravity gradient only. The $N = -1$ family in Figure 29 deserves a deeper investigation. As noted previously, a

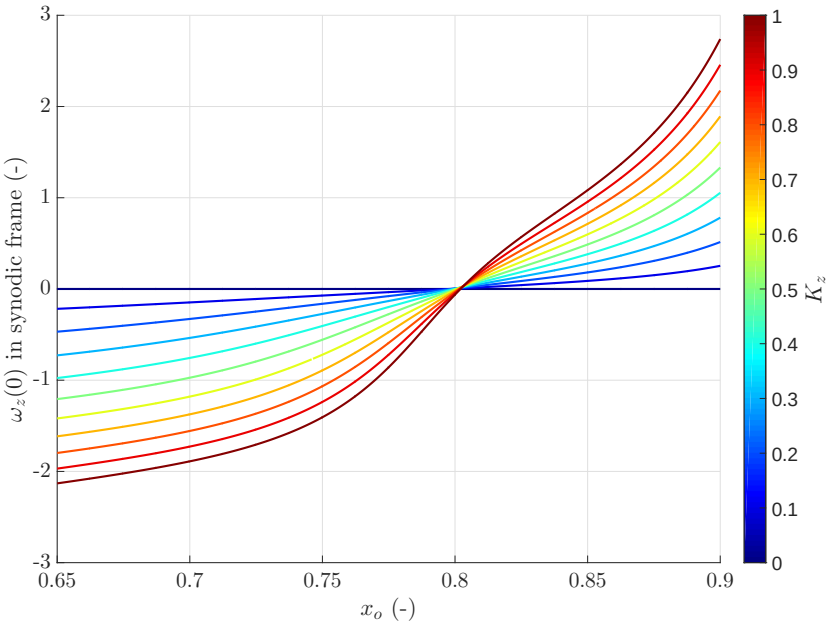


Figure 28: Attitude periodicity family, $N = 0$

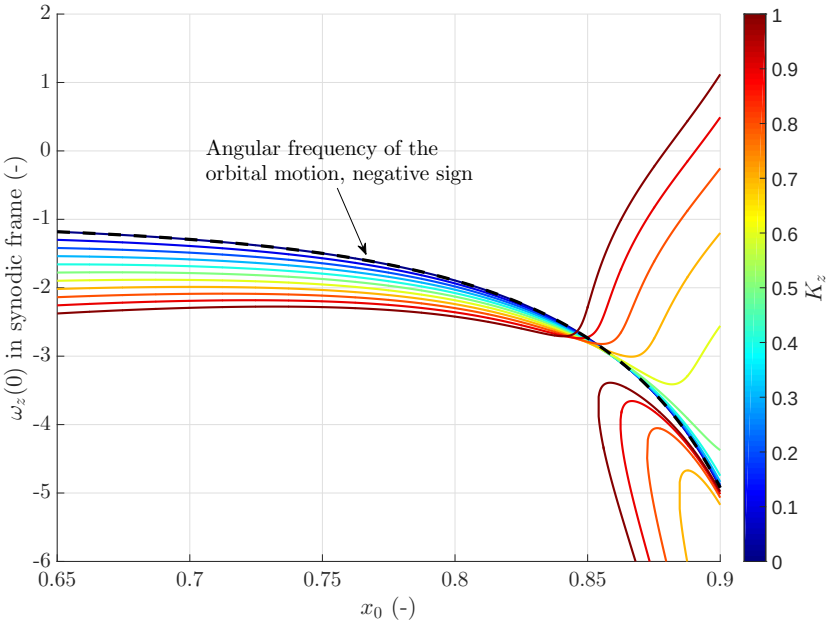


Figure 29: Attitude periodicity family, $N = -1$

bifurcation is observed, leading to the presence of three possible solutions for near-Moon DROs, up to $x_0 \simeq 0.86$. This ramification shows up for a value of K_z between 0.4 and 0.5; the exact value depends on the span considered for the DRO family. Recalling that the period of a DRO tends to infinity while $x_0 \to 1 - \mu$ (Figure 6), one might expect the presence of the bifurcation up to the asymptotic region, where practical purposes lose significance.

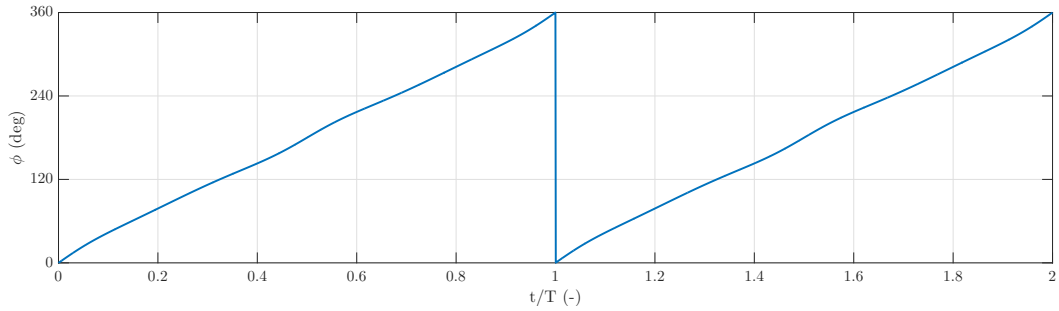
It is interesting to underline that the families may overlap in some parts of the solution space, but some regions do not include any periodic solution. The solution space is then made up by regions where an infinite number of solutions exist (i.e. the families), regions with multiple infinity of solutions (i.e. where two or more families overlap) and regions where no solution are found within the current definition and framework.

3.4 FINAL REMARKS

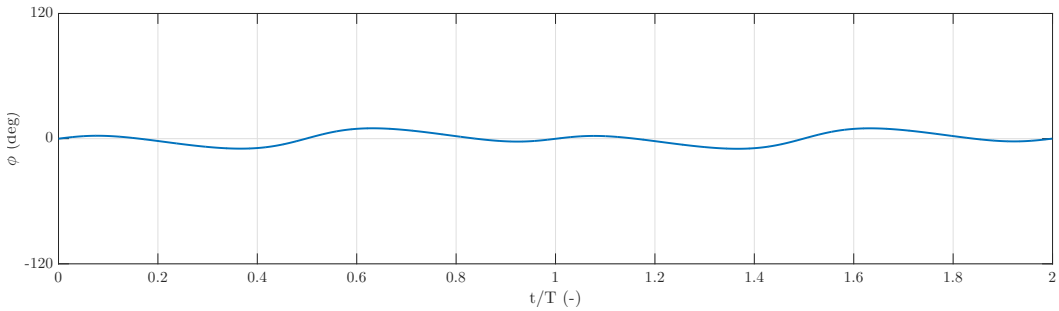
The Chapter has presented techniques and methods to identify, classify and investigate periodic orbit-attitude solutions, with the sole action of the gravity gradient torque and assuming the orbit to be unperturbed.

The numerical tools are validated with literature solutions, increasing their reliability and verifying their validity. The hypothesis of fixed orbit is reasonably valid in the presented framework, since the investigation of the perturbation due to the extension of the spacecraft led to the conclusion that it may be neglected. For large space structures, anyway, the rigid body assumption might not be totally suitable, since flexible appendages and structural vibrations may perturb both the orbit and the attitude dynamics. Furthermore, the large surfaces exposed to solar rays are likely to develop a non-negligible amount of acceleration due to solar radiation pressure, perturbing the attitude and the orbital motion.

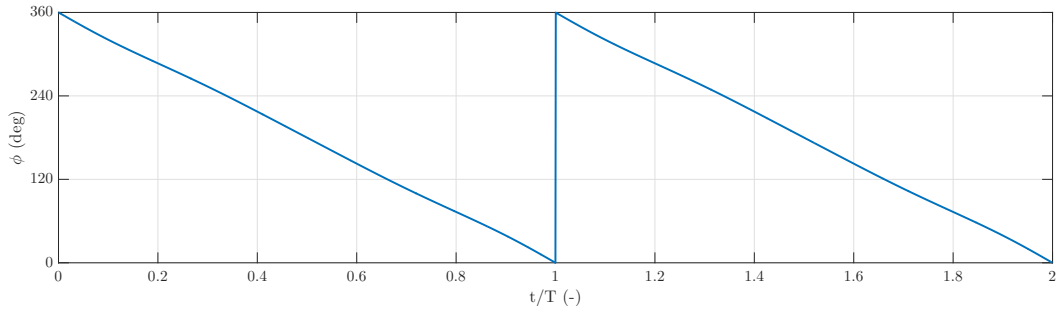
These two issues will be addressed and treated in the following Chapters, using techniques that are similar to those presented, with an increased accuracy of the model.



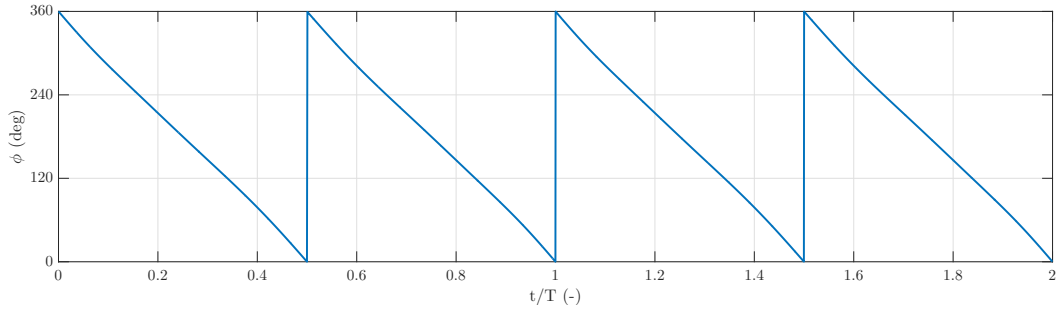
(a) 1 rotation per orbit, counterclockwise



(b) No net rotation per orbit

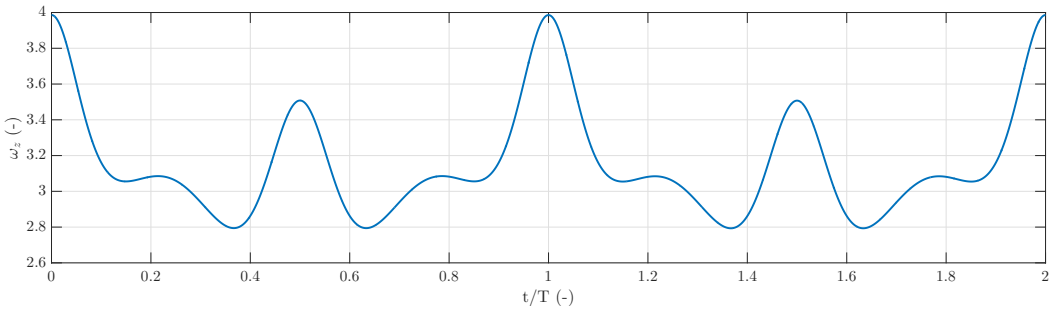


(c) 1 rotation per orbit, clockwise

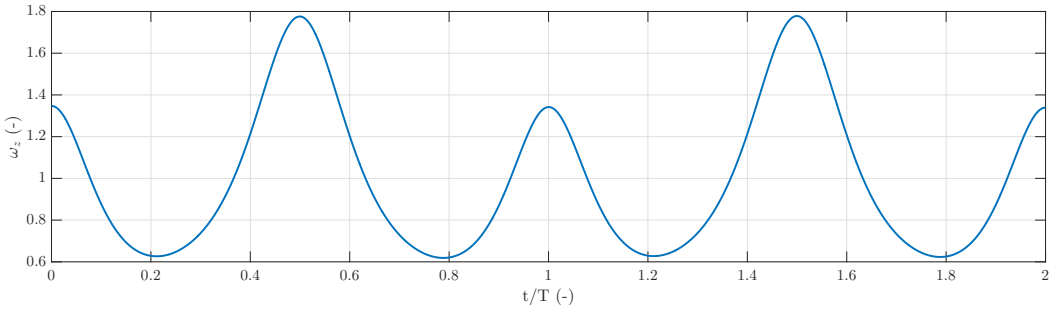


(d) 2 rotations per orbit, clockwise

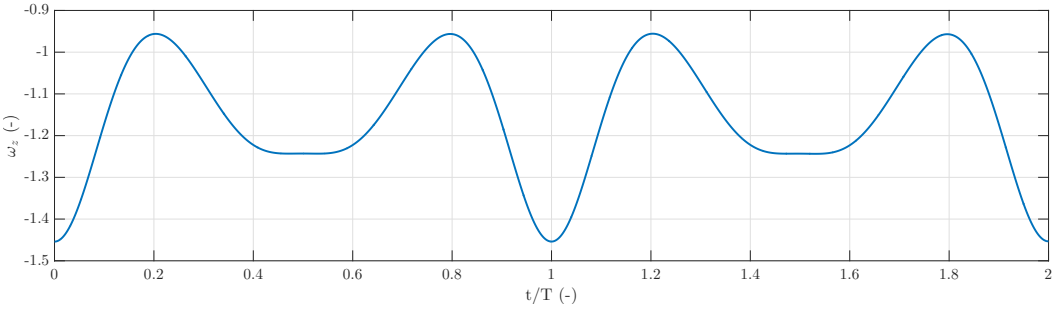
Figure 30: Rotation angle for some periodic attitude motions, DRO period = 12.66 days



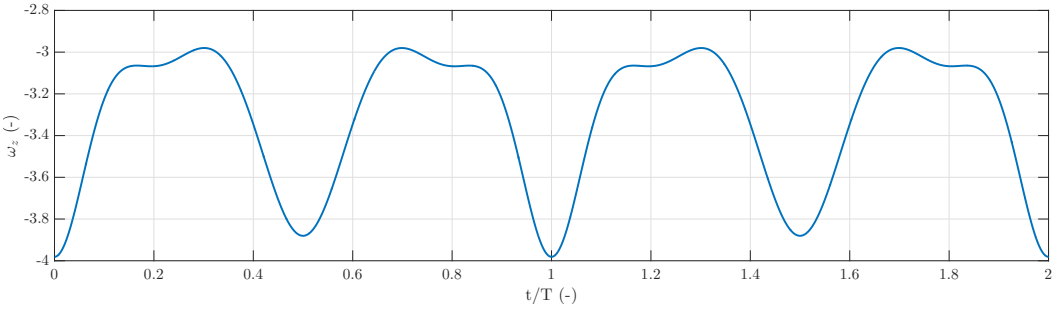
(a) 1 rotation per orbit, counterclockwise



(b) No net rotation per orbit



(c) 1 rotation per orbit, clockwise



(d) 2 rotations per orbit, clockwise

Figure 31: Angular velocity for some periodic attitude motions, DRO period = 12.66 days

4 COUPLED DYNAMICS WITH SOLAR RADIATION PRESSURE

The gravity gradient torque is the principal torque (even if not the largest in magnitude) in any gravitational environment, since its presence is inherent in the system. The sole existence of a massive attractor generates such torque; the resulting angular acceleration depends on some ratios between the inertia moments of the spacecraft, and not on its extensive properties (mass, dimension). The resulting coupled orbital-attitude gravitational environment is a conservative system, autonomous in respect to the synodic frame.

The introduction of an external, time-dependent acceleration causes the system to be no longer autonomous, and the time variable appears explicitly in the equations of motion. The Chapter investigates Solar Radiation Pressure (SRP) acceleration, i.e. the acceleration issued to the spacecraft from impinging photons. Large space structures will likely possess large surfaces (e.g. solar arrays) exposed to solar radiation, and thus the magnitude of the perturbation might be high enough to hinder the orbital trajectory; furthermore, any asymmetry of the illuminated surfaces with respect to the center of mass will also yield a net torque, perturbing the rotational motion too. The analysis aims at refining the dynamical system with the inclusion of SRP torque, in order to incorporate its effect in the model and no longer treat it as a perturbation of the attitude motion.

4.1 MODEL

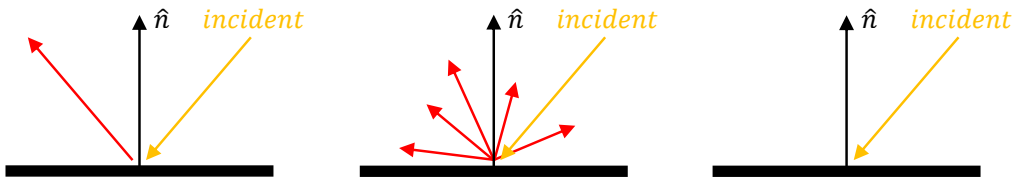
The acceleration due to SRP is strongly dependent on the spacecraft's properties. In order to provide a tool capable of yielding preliminary but meaningful results, two spacecraft models are employed: a first simplified one, which allows to modify the periodic orbit-attitude solutions ensuring periodicity under the effect of SRP, and a more refined one, which more realistically represents the spacecraft but complicates the visualization and interpretation of the results.

4.1.1 Solar radiation pressure

When a light ray impinges an opaque surface three type of interaction may appear [52, 56]:

- The light is specularly reflected, i.e. the angle of the outgoing ray with respect to the surface's normal is identical to the impinging ray's angle;
- The radiation is absorbed, retaining the photon's energy into the surface;
- The incoming ray is diffusively reflected, scattering light in all directions.

If the surface is semi-opaque, part of the radiation might also be transmitted with no interaction; for the purpose of the present work, this latter type of interaction is not considered and only opaque surfaces are taken into account. Figure 32 depicts the mentioned types of interplay between solar radiation and opaque surfaces.



(a) Specular reflection **(b)** Diffuse reflection **(c)** Absorption

Figure 32: Possible surface-light ray interactions

The magnitude of the pressure exerted by SRP depends on the solar radiation flux, which in turn varies with an inverse-square law with respect to the distance from the Sun. In the present work, the amount of radiation flux will be assumed to be constant within the considered system; the formulation, thus, will not be applicable to any Sun-planet CR3BP.

4.1.2 Sun motion

A simplified model is adopted to represent the interaction of the Sun with the CR3BP Earth-Moon system, analogous to the treatise reported in [34]. Referring to Figure 33:

- The Sun apparent angular motion θ_s is an explicit linear function of time, having constant angular velocity

$$\Omega_s = \frac{2\pi}{1\ year} - \Omega \simeq -0.9252\ (1/TU) \tag{54}$$

  and period

$$T_{sun} = \frac{2\pi}{|\Omega_s|} = 6.79\ TU \tag{55}$$

- The initial position of the Sun $\theta_s(0)$ depends on the starting epoch of the mission;
- The Sun light rays direction is assumed to be equal within the synodic frame, at a given time instant; this is reasonably true for the Earth-Moon system, as well as for any other planet-satellite couple of our solar system where the Sun distance is much greater than the characteristic length of the system.

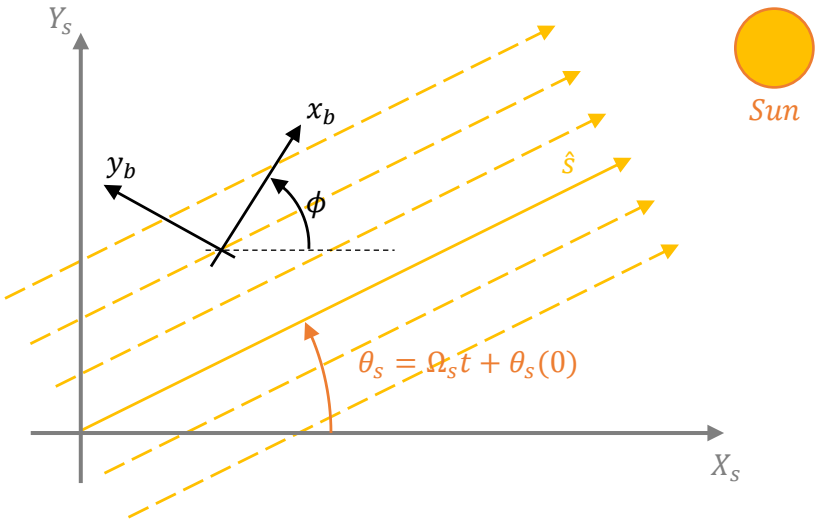


Figure 33: Apparent Sun motion in CR3BP

The presented model fits within the context of the Thesis, where only planar dynamics are considered. Furthermore, the inclination of the true apparent solar motion with respect to the Earth-Moon system is $\simeq 5°$; the planar approximation is thus a reasonable model for preliminary analyses.

4.1.3 Sun-resonant orbits

Since the principal objective is to investigate periodic orbit-attitude solution, one might deduce that the inclusion of SRP will generate a periodic excitation, whose period will depend on the relationship between the orbital period and that of the apparent Sun motion. If an integer ratio exists between such quantities, a periodic solution should be simpler to obtain, since its periodicity would be directly linked with the orbital period. On the contrary, any non-integer ratio between the two periods will likely lead to a possible periodic orbit-attitude solution, where the periodicity of the attitude motion might be observed only after a large number of orbital revolutions, i.e. after the relative period between the orbit and the apparent solar motion.

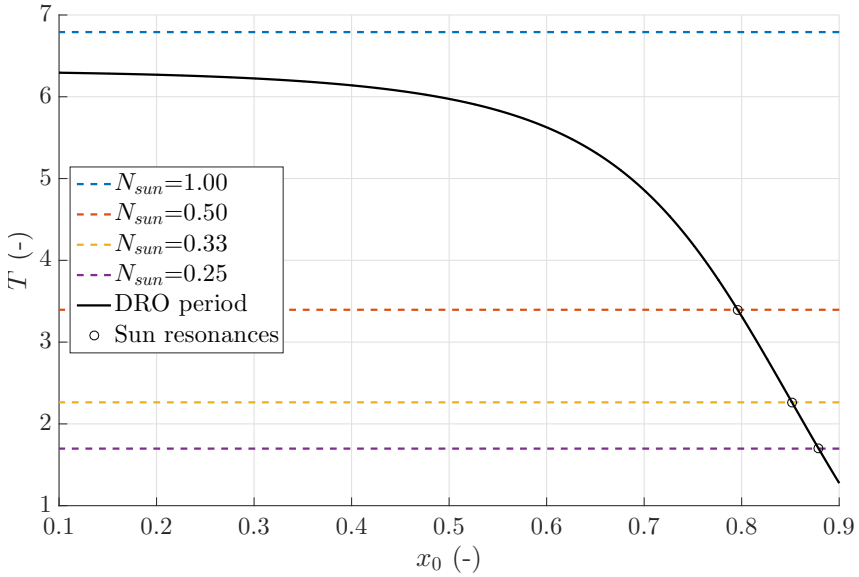


Figure 34: Sun-resonant set of DROs

Figure 34 depicts the set of DROs whose period possesses an integer ratio with the period of the apparent Sun. These are called Sun-resonant DROs. The auxiliary quantity

$$N_{sun} = \frac{T}{T_{sun}} \tag{56}$$

describes the relationship between the two periods. The 1:1 resonance does not exist within the Earth-Moon DRO family. Note how these Sun-resonant orbits tend to show up closer to the Moon as N_{sun} decreases, shifting towards simple low lunar orbits. Figure 34 indicates only resonances up to 1:4 for simplicity's sake.

Within this work most of the attention is devoted to the 1:2 Sun-resonant DRO, i.e. the orbit where the spacecraft carries out two orbital revolutions while the Sun revolves once relatively to the synodic frame. This condition eases the interpretation of the results and shows peculiar dynamical structures once SRP is introduced into the model, and will thus serve as basis for the present Chapter. The results might in general be extended to any other Sun-resonant DRO.

4.1.4 General spacecraft model

The impingement of solar radiation on an opaque surface generates a pressure on the latter, which is translated into a force exerted on the body. In the most general case, recalling Figure 32, each of the three type of interaction yields a component of acceleration.

Consider an infinitesimal surface dA, with normal $\hat{n}$, and let $\hat{s}$ indicate the Sun direction using the spacecraft as basepoint. Let also W_0 be the solar constant at 1 astronomical unit, i.e. in the Earth-Moon system, and denote with c_0 the speed of light in vacuum. The infinitesimal force dF acting on dA may be divided into its three contributions, due to specularly reflected (subscript s), diffusively reflected (subscript d) and absorbed (subscript a) radiation, respectively

$$d\mathbf{F}_s = -2\frac{W_0}{c_0} C_s (\hat{s}\cdot\hat{n})^2 \hat{n}\, dA \tag{57}$$

$$d\mathbf{F}_d = -\frac{W_0}{c_0} C_d \left(\frac{2}{3}(\hat{s}\cdot\hat{n})\hat{n} + (\hat{s}\cdot\hat{n})\hat{s}\right) dA \tag{58}$$

$$d\mathbf{F}_a = -\frac{W_0}{c_0} C_a (\hat{s}\cdot\hat{n})\hat{s}\, dA \tag{59}$$

The three coefficients C_s, C_d, C_a denote the amount of radiation involved in the considered phenomenon; each coefficient may range between 0 and 1. Furthermore, for an opaque surface the following relationship holds

$$0 \leq C_s + C_d + C_a \leq 1 \tag{60}$$

taking into account that some radiation might in general be transmitted if the surface is semi-opaque.

The dot product $\hat{s} \cdot \hat{n}$ indicates the cosine of the angle α between the Sun direction and the surface normal

$$\alpha = \arccos(\hat{s} \cdot \hat{n}) \tag{61}$$

Using the presented formulation, SRP acceleration acts on the surface only if the latter is illuminated, i.e. if $-90° < \alpha < 90°$.

The total force acting on the spacecraft may be evaluated through integration on all the external surface

$$\mathbf{F}_{SRP} = \int_{S/C} d\mathbf{F}_s + d\mathbf{F}_d + d\mathbf{F}_a \tag{62}$$

whereas the torque may be computed knowing the arm $\mathbf{d}$ between each surface and the barycenter

$$\mathbf{T}_{SRP} = \int_{S/C} \mathbf{d} \times (d\mathbf{F}_s + d\mathbf{F}_d + d\mathbf{F}_a) \tag{63}$$

For the present analysis, the whole external area of the spacecraft is assumed to be lumped into a single surface A, whose orientation $\hat{n}$ is known in a body-fixed principal inertia frame. Such surface is exposed to radiation on both sides, so that equation (62) may be reduced to

$$\mathbf{F}_{SRP} = -\frac{W_0}{c_0} A(\hat{s} \cdot \hat{n}) \left[C_a \hat{s} + C_d \left(\frac{2}{3} \hat{n} + \hat{s} \right) + 2C_s |\hat{s} \cdot \hat{n}| \hat{n} \right] \tag{64}$$

Equation (64) may be further simplified if the surface is assumed to be completely opaque, i.e. if

$$C_a + C_s + C_d = 1 \tag{65}$$

reducing equation (64) to

$$\mathbf{F}_{SRP} = -\frac{W_0}{c_0} A(\hat{s} \cdot \hat{n}) \left[(1 - C_s)\hat{s} + \left(\frac{2}{3}(1 - C_s - C_a) + 2C_s |\hat{s} \cdot \hat{n}| \right) \hat{n} \right] \tag{66}$$

Under this lumped-area approach, the torque may be modeled through the knowledge of the position $\mathbf{d}_c$ of the center of pressure, assumed to be fixed in the body principal frame. The total torque due to SRP results then

$$\mathbf{T}_{SRP} = \mathbf{d}_c \times \mathbf{F}_{SRP} \tag{67}$$

4.1.5 Simplified spacecraft model

A simpler model may be introduced at preliminary stage, in order to ease the parametrization of the results and assess the effect of SRP while maintaining a general framework. The presented model is usually adopted whenever a fast estimate of SRP acceleration is needed in early design phases [57]. The surface of the spacecraft is again lumped into a single surface A. The reflectance of such surface is modeled using a single coefficient C_r, so that the SRP acceleration may be written as

$$\mathbf{F}_{SRP} = -\frac{W_0}{c_0} A C_r (\hat{s} \cdot \hat{n}) \hat{n} \tag{68}$$

with no distinction between the different types of interaction with the incoming radiation. The torque is computed as in the previous model, using equation (67).

The introduction of this simplified model is made clear if one analyzes the scalar SRP torque component about the z_b axis, which is the sole of interest for the present planar case. The three quantities $\mathbf{d}_c$, $\hat{n}$, $\hat{s}$ lay in fact on the $x_b y_b$ plane, and the resulting cross product between $\mathbf{d}_c$ and $\mathbf{F}_{SRP}$ will yield a z_b-directed torque vector. Such torque will read

$$T_{z,SRP} = -\frac{W_0}{c_0} A C_r (\hat{s} \cdot \hat{n}) |\mathbf{d}_c \times \hat{n}| \tag{69}$$

Two more step are necessary to understand the advantage of the simplified formulation of equation (68):

1. First, the torque is divided by the inertia of the spacecraft, in order to obtain the angular acceleration about the z_b axis

$$\dot{\omega}_{z,SRP} = -\frac{W_0}{c_0} \frac{A C_r}{I_z} (\hat{s} \cdot \hat{n}) |\mathbf{d}_c \times \hat{n}| \tag{70}$$

   This allows having a term easily compared with the other perturbation, which may be directly put in equation (31) together with the gravity gradient torque.

2. Then, recalling that the cross product $\mathbf{d}_c \times \hat{n}$ results solely in a component on z_b, such scalar part is called d_z

$$d_z = (\mathbf{d}_c \times \hat{n}) \cdot z_b \tag{71}$$

These steps allow to write the angular acceleration, due to SRP, as

$$\dot{\omega}_{z,SRP} = -\frac{W_0}{c_0}\frac{AC_r}{I_z}d_z(\hat{s}\cdot\hat{n}) \tag{72}$$

and finally to collect some terms into a single coefficient

$$\Lambda_z = \frac{W_0}{c_0}\frac{AC_r}{I_z}d_z \tag{73}$$

The use of the coefficient Λ_z allows an easier parametrization of the results. All the properties of the spacecraft are grouped into a single parameter, with no need to run many analyses for different configurations. Furthermore, this coefficient contains also informations on the three-body environment under consideration, since the solar constant W_0 may be corrected according to the distance of the CR3BP system from the Sun. Recall that for any three-body system where the Sun is one of the primaries the whole formulation loses validity and shall be modified.

The introduction of Λ_z permits to visualize the results in maps, analogous to those presented for gravity gradient periodic solutions. Λ_z possess a direct physical meaning too, representing the maximum magnitude of angular acceleration induced to the spacecraft by SRP, since $-1 \leq \hat{s}\cdot\hat{n} \leq 1$.

4.2 MODIFIED PERIODIC SOLUTIONS

The effect of SRP on large space structures yields considerable torques, whose magnitude is comparable or greater than that of the gravity gradient torque. The so far presented periodic solutions will consequently be greatly affected by the presence of SRP; for a realistic and practical analysis, aimed at providing requirements for LSS design, the inclusion of such component in the dynamical model is then envisaged.

Thus, the search for periodic attitude solution is here extended to the SRP-perturbed environment. If a periodic behavior is obtained, the spacecraft may exploit again passive stabilization thanks to the coupled effects of both gravity gradient and SRP torques. A further relief on attitude control systems is obtained. Virtually, the SRP-induced torque might not be compensated at all; more realistically, ACS will have to control all the perturbations

not included in the model, primarily the out-of-plane component of SRP and those due to the actual motion of the Earth-Moon system with respect to the Sun.

The investigation methodology largely exploits the simplified spacecraft model of Section 4.1.5, thanks to the easier visualization of the results that it allows, even though remaining a theoretical framework. At the end of the Section, some results obtained with the general model (described in Section 4.1.4) will be shown too, in order to demonstrate the operational possibilities of a realistic spacecraft.

4.2.1 Method and algorithm

The algorithm is widely similar to the one presented in Section 3.3.1. The main difference is the independent variable; as described in Section 4.1.3, this Chapter deals only with Sun-resonant DROs, where a periodicity in the attitude motion might be found with a more direct relationship with the orbital motion (i.e. an integer ratio). The angular velocity needed to establish a periodic motion will then be mapped over the span of Λ_z, for a given Sun-resonant orbit. The algorithm steps are here briefly reported:

1. A Sun-resonant DRO is selected and its Fourier series expansion obtained;
2. The spacecraft topology is fixed thorough the inertia ratio K_z;
3. The SRP coefficient Λ_z is selected;
4. The attitude motion with both gravity gradient and SRP torque is integrated, for a large span of initial angular velocity $\omega_z(0)$;
5. The value of $\omega_z(0)$ that establishes a periodic attitude behavior is identified, as portrayed previously in Figure 23.

Two important remarks concern this analysis:

A. The epoch of the mission dictates the initial Sun angle $\theta_s(0)$; the analysis may be run for different values of such angle, taking into account different operational possibilities according to the desired, or needed, mission epoch.

B. The surface normal $\hat{n}$ is assumed to be known and fixed in the spacecraft principal body frame; since the body is assumed to start with $\phi(0) = 0$, i.e. with the x_b axis initially aligned with the X_s axis, the orientation of $\hat{n}$ in body frame might be a further degree of freedom of the analysis.

It is observed that these latter two quantities are actually linked. A periodic attitude solution is obtained only if the surface exposed to solar radiation is initially parallel to the Sun rays, i.e. if

$$\hat{n} \cdot \hat{s} = 0 \qquad \text{at} \qquad t = 0 \tag{74}$$

This leads to a behavior where both SRP and gravity gradient torques are null at the initial instant. The dependence on $\theta_s(0)$ and $\hat{n}$ thus disappears, since, for any solution, it is implicit that these quantities must be chosen so to satisfy equation 74.

4.2.2 Solution space mapping

The inclusion of SRP into the model allows again the existence of periodic-orbit attitude solutions. These are related to those obtained with gravity gradient only; note that the latter condition trivially corresponds to the case $\Lambda_z = 0$. Due to the increased numerical difficulty of the problem, the periodicity maps exhibit a discontinuous behavior, with gaps and scattered lines. In these cases, the algorithm did not converge with the desired tolerance; such solutions might correspond to bounded behaviors, where a quasi-periodic time history is manifested but attitude periodicity is not guaranteed. Further analyses will clarify the distinction between bounded and periodic solutions and investigate discontinuous regions of the solution space.

Thanks to the reduction of the spacecraft properties to a single coefficient, the results may be depicted in planar periodicity maps, portrayed in Figures 35 and 36 for two different Sun-resonant DROs. The horizontal axis represents the Λ_z parameter, in non-dimensional units. The vertical axis, in analogy with the results of Chapter 3, denotes the initial angular velocity needed to establish a periodic solution. Note that the periodicity of the attitude behavior is obtained, in accordance with the expected result, after a number of orbital periods corresponding to a full revolution of the apparent Sun in the synodic frame.

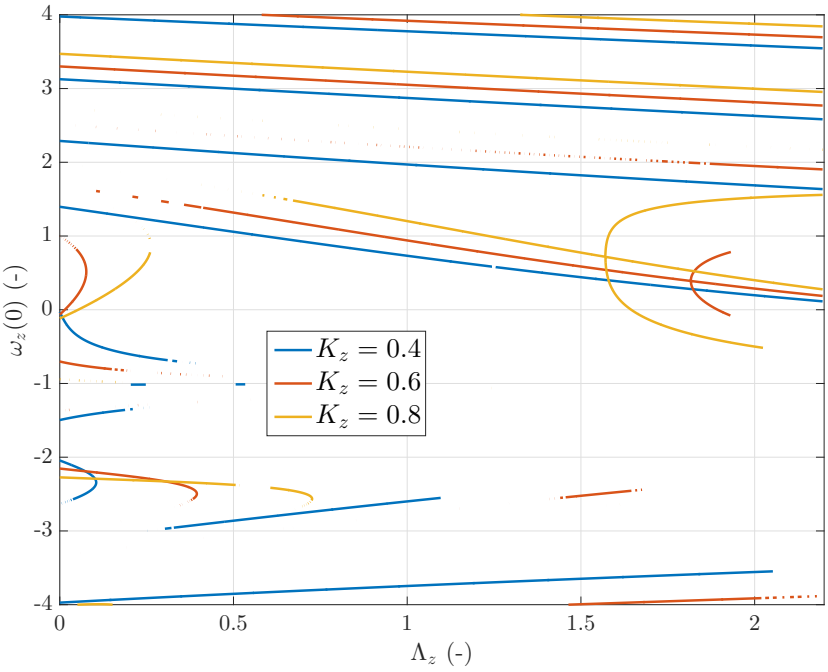


Figure 35: SRP periodicity maps, 1:2 Sun-resonant DRO

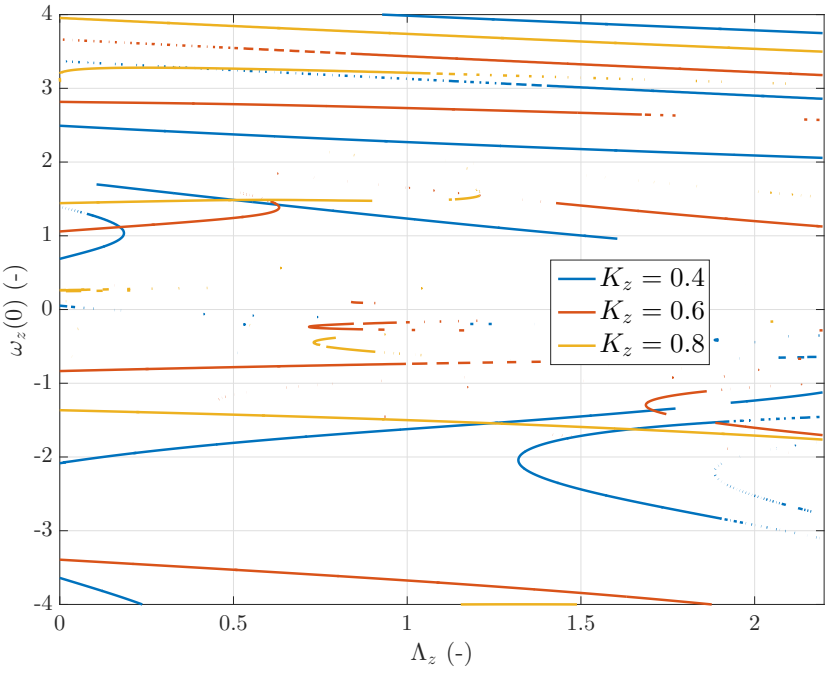
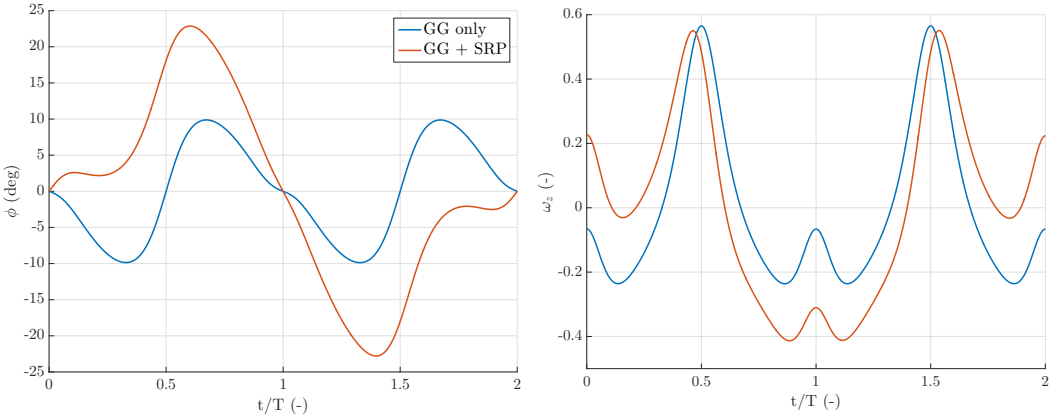


Figure 36: SRP periodicity maps, 1:4 Sun-resonant DRO

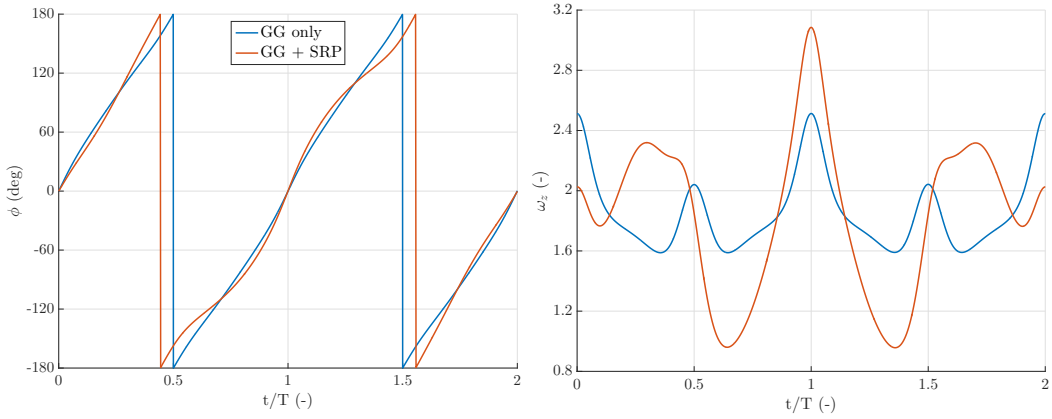
Figure 37 portrays a sample behavior. The gravity gradient solution belongs to the $N = 0$ family, with $K_z = 0.6$, along a 1:2 Sun-resonant DRO. The introduction of SRP torque modifies the value of $\omega_z(0)$ needed to ensure periodicity; in this case only a small change of nearly 0.2 non-dimensional units is necessary, since the SRP parameter is quite small ($\Lambda_z = 0.055$).



(a) Rotation angle **(b)** Angular velocity

Figure 37: Comparison of periodic solutions, small effect of SRP

Another sample solution is depicted in Figure 38, belonging to the $N = 1$ family. A large effect of SRP is considered in this case, with $\Lambda_z = 1.689$. The angular velocity profile, in fact, manifests large deviations from the behavior obtained with the sole gravity gradient torque, and the initial value $\omega_z(0)$ shall be consistently modified.



(a) Rotation angle **(b)** Angular velocity

Figure 38: Comparison of periodic solutions, large effect of SRP

Note how the presence of SRP modifies the time history of the coordinates:

A. With gravity gradient only, the periodicity of the attitude behavior is synced with the orbital periodicity; this is inherent in the definition of periodic orbit-attitude behavior presented in Chapter 3.

B. When SRP is introduced, the periodicity of the rotational coordinates synchronizes with the period of the apparent Sun motion, thus clarifying the choice of the discrete subset of Sun-resonant DROs. For any other DRO, periodic orbit-attitude behavior might exist, but a non-integer ratio between orbital and attitude periodicity would be encountered.

4.2.3 Algorithm validation

In order to check the correctness and consistency of the numerical code, a fictitious model is employed, with a spacecraft assumed to be divided into two sections:

- The actual spacecraft body, aligned with the principal body frame, subjected only to gravity gradient torque;
- The solar array (or, more generally, the sun-pointing surface), with $\hat{n}$ always directed towards the Sun, subjected only to SRP torque.

The SRP torque is assumed to be transmitted to the spacecraft by the large surface exposed to radiation, affecting its attitude motion, with an univocal relationship. This model represents a structure where a Sun-pointing section is irradiated and transmits torque to the whole body, without in turn being affected by gravity gradient; it clearly lacks of a practical physical meaning. This fictitious model is useful to check the validity of the code. A Sun-pointing spacecraft would undergo a constant SRP torque, since the magnitude of the force exerted on the surface would be constant.

Figure 39 portrays the angular accelerations in the 1:2 Sun-resonant DRO, using $K_z = 0.6$ and $\Lambda_z = 1.689$. The SRP torque is constant, as expected, and the angular acceleration it induces is equal to Λ_z. Due to the constant torque, the spacecraft starts spinning faster and faster; the gravity gradient

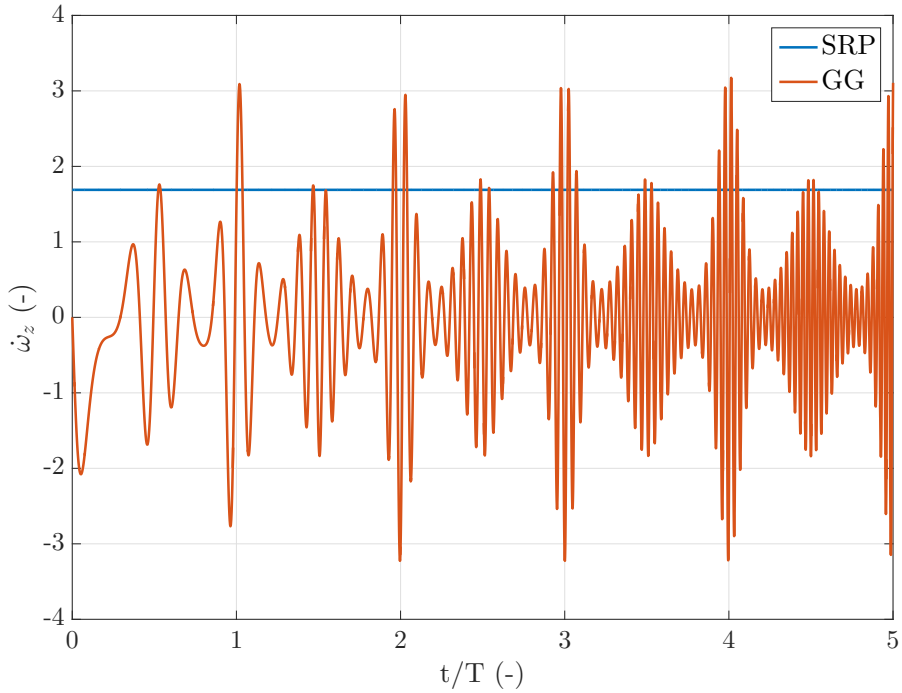


Figure 39: Sun-pointing spacecraft angular accelerations

torque exhibits then beats phenomena between long-period oscillations (along one orbital period) and short-period ones, whose frequency increases due to the increase in angular velocity.

No significant interest is sought in this solution. It is useful to validate the numerical code, checking that the SRP torque has a constant value if the surface is kept Sun-pointing, i.e. if equation (75) is enforced

$$\hat{s} \cdot \hat{n} \qquad \forall t \tag{75}$$

4.2.4 Results with general spacecraft model

The results presented so far refer to the simplified model to represent the interaction of the spacecraft surface with the Sun radiation. As explained throughout the Section, the advantage of such formulation is an easy parametrization of the result, providing a tool for fast preliminary analyses and assessments. The presented algorithm is suitable in any case

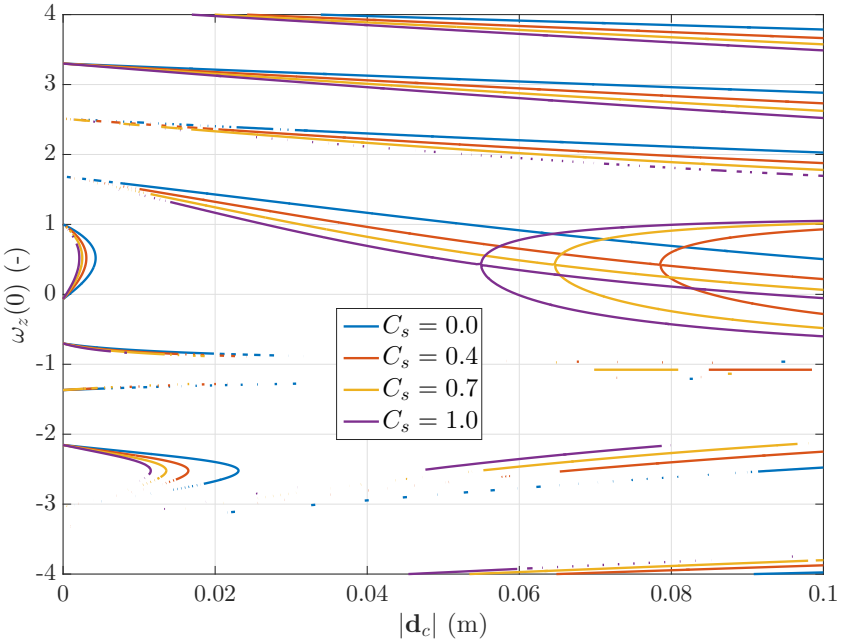


Figure 40: Periodicity map for $K_z = 0.6$, $C_d = 0$, $A/m = 0.016$, different values of C_s

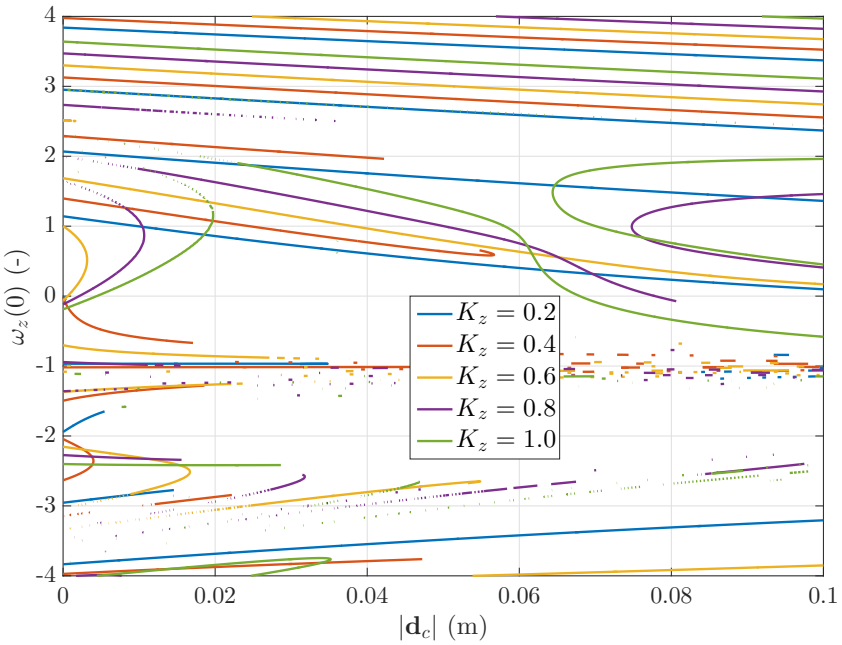


Figure 41: Periodicity map for $C_s = 0.4$, $C_a = 0.5$, $A/m = 0.016$, different values of K_z

for a more realistic analysis, based on the model presented in Section 4.1.4, namely equation (66). Periodic orbit-attitude solutions may again be obtained, but the parametrization of the results is not so straightforward.

This Section presents some possibilities of analysis with the general spacecraft model. Any combination of parameters might be employed; the reported results are just a hint of the multi-dimensional space of solutions that may be obtained varying any of the spacecraft properties.

Figure 40 portrays the values of $\omega_z(0)$ needed for a spacecraft with $K_z = 0.6$, $A/m = 0.016$ in a 1:2 Sun-resonant DRO, for different values of specular reflection coefficient. The diffuse reflection coefficient C_d is assumed to be null, thus the remaining parameter may be found using equation (65). Figure 41 depicts a similar map, where the reflectivity coefficients are fixed and various inertia ratios are spanned. The horizontal axis represents different distances of the center of pressure from the barycenter, whose direction is assumed to be orthogonal to the normal $\hat{n}$.

Figures 40 and 41 represent two examples of possible applications of the presented framework. According to the desired property to be investigated (e.g. reflectivity coefficients, inertia ratio...), similar maps may be created, allowing for a parametric analysis suitable according to the needs of the specific case.

4.3 FINAL REMARKS

In this Chapter, an analysis of the torque due to solar radiation pressure has been performed. The inclusion of such torque in the dynamical model allows to find periodic attitude behaviors superposed to a peculiar set of DROs, in order to ensure orbit-attitude coupled periodicity.

New periodicity maps may be created using different parameters and spacecraft models, including both gravity gradient and SRP torques. These novel orbit-attitude behaviors may be employed to further relieve ACS effort; gravity gradient and SRP produce a beneficial effect and ensure a periodic motion, so that the control system needs to compensate only other external disturbances. The analysis is run with a planar representation of the apparent Sun motion in the CR3BP; the effect of the out-of-plane motion may be treated as a perturbation, and thus neglected in preliminary assessments.

The perturbation induced on the orbit by SRP acceleration was not thoroughly investigated; its effect on the trajectory may be neglected for this preliminary analysis, for the following main reasons:

- As recalled in Table 2, the most important source of orbital perturbation in the Earth-Moon system is the gravity of the Sun, which should be investigated prior to the introduction of other perturbations such as SRP;
- The high stability of DROs guarantees that the trajectory remains close to the nominal one at least for a few (4-5) periods, thus allowing to search and obtain periodic orbit-attitude solutions without its inclusion in the model;
- An orbital station-keeping system may also be assumed to be present on board, fortifying the hypothesis of non-perturbed trajectory.

It is in any case suggested that later investigations are devoted to the analysis of SRP acceleration, looking for periodic or bounded solutions in orbital dynamics. Such analyses may be further coupled with the attitude dynamics problem, taking into account the rotation of the Sun-exposed surface with the presented formulation.

5 SPACECRAFT FLEXIBILITY ANALYSIS

This Chapter addresses the dynamics of a flexible spacecraft in the CR3BP environment. Large space structures may possess very low structural frequencies, due to their large extension, and poor structural damping as far as present and near-future materials and technologies are concerned. Some low natural modes might then be excited by the orbital and rotational motion; the latter in particular will be investigated in this work, while the former is left aside for future researches, since in general orbital motion is dominated by the position of the center of mass and its short-period vibration should not affect it largely.

5.1 MODEL

In order to provide results on a physical basis, a lumped-parameters approach is employed to describe the flexible parts of the spacecraft. Such approach is described in its general form, showing how to build a model of the spacecraft according to its structural configuration.

The limitation lays in the discretization of the flexible components; lumped-parameters models are in general not able to capture the full dynamical spectrum of a flexible structure, while they might be suitable enough to approximate the first fundamental natural modes. The present study aims at a preliminary description of the effects of flexibility on attitude motion, thus the use of such simple model is preferred.

5.1.1 Spacecraft model

Let us consider a spacecraft composed by a rigid part and some flexible components, with no out-of-plane dynamics. This treatise was first presented in [58].

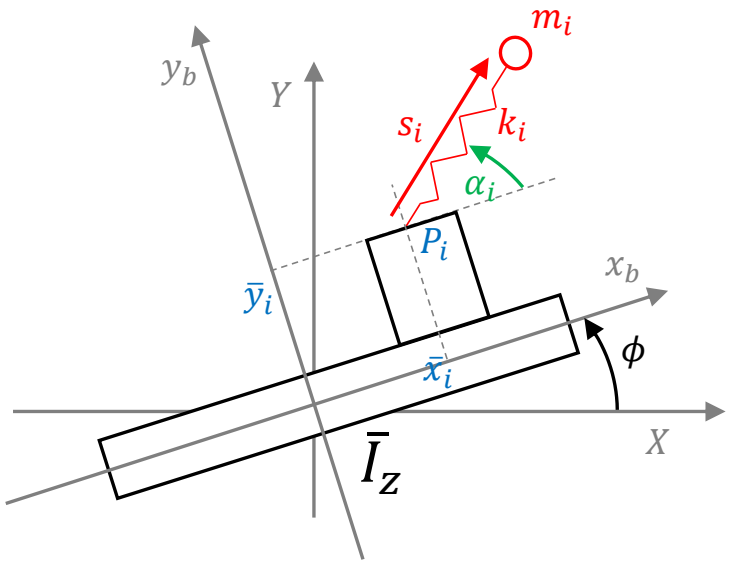


Figure 42: Spacecraft lumped parameter model

Referring to Figure 42, the rigid part is described through its inertia moment $\bar{I}_z$ about the z_b principal body axis; the flexible appendages are modeled as single-degree-of-freedom (SDOF) systems, where:

- The lumped mass m_i represents the equivalent mass of the single system, i.e. the mass that represents the vibrational motion, taking into account the dynamical constraints;
- The linear spring models the equivalent stiffness k_i of the flexible component;
- The natural frequency of each SDOF system is denoted with

$$\Omega_i = \sqrt{\frac{k_i}{m_i}} \tag{76}$$

- The point P_i, with coordinates $(\bar{x}_i, \bar{y}_i)$, is the origin of the SDOF system, and is assumed to be fixed and known in the principal body frame, representing the position of each appendage;
- The elongation of each spring is denoted by the coordinate s_i;
- The angle α_i describes the direction of vibration of each component, depending on the physical constraints of each part; for the present

analysis it is assumed to be known and fixed, while the investigation might be extended considering it as a further DOF of the problem.

The rotational and vibrational motion of the spacecraft are constrained to belong to the XY plane. The XYZ frame denotes a reference frame aligned with the synodic frame and centered in the barycenter of the spacecraft; since the orbital motion is not analyzed, the spacecraft is free to rotate in this frame, but the motion of its center of mass does not appear in the presented framework. In analogy with the previous Chapters, the rotation of the spacecraft is denoted with the angle ϕ, and its angular velocity about the z_b axis with $\omega_z = \dot{\phi}$.

In the following Sections, a lumped-parameters reference spacecraft model will be used to present and discuss the results. Such model is depicted in Figure 43, representing an ISS-like large space station with some flexible components. The inertia of the rigid section is 911.266×10^6 kgm^2; other properties are summarized in Table 5.

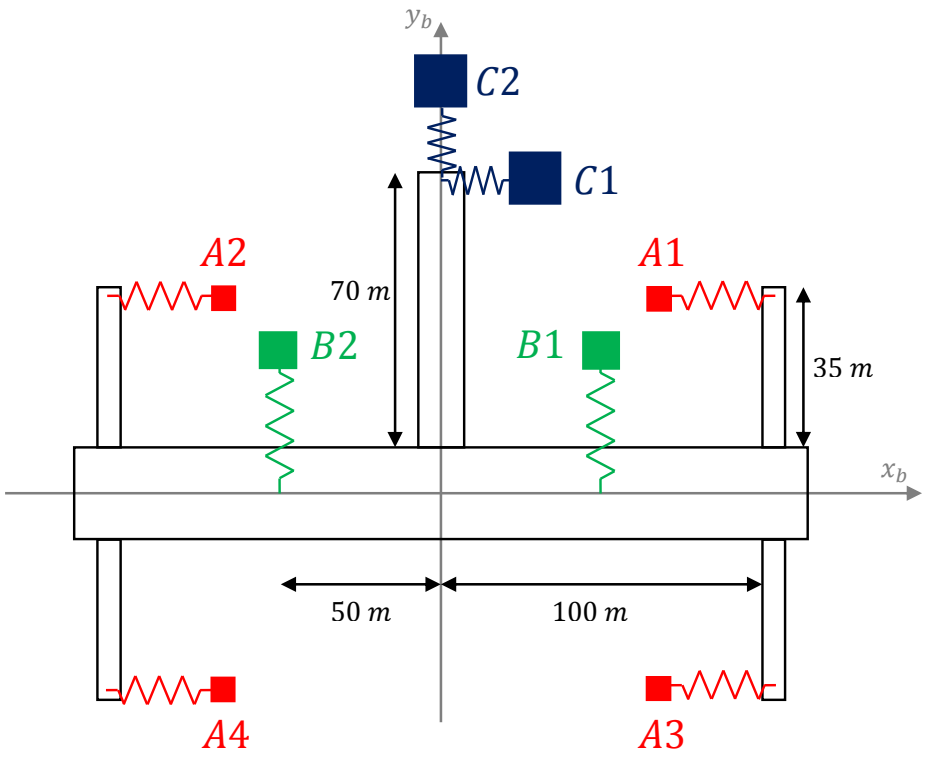


Figure 43: Schematic spacecraft model

Part	m (kg)	Ω (Hz)
A	150	0.06
B	500	0.10
C	5000	0.05

Table 5: Spacecraft model properties

5.1.2 Equations of motion

The equations of motion are written using a Lagrangian formalism, referring to the XYZ frame. Note how they do not include the gravitational action of the primaries, since the translational motion is not under consideration. As a consequence, the gravity gradient torque too will not directly appear in such equations, but will have to be inserted as an external torque.

The present development may seem cumbersome at first sight, but the Lagrangian formalism is, in the author's opinion, the most direct way to preserve a physical insight on the problem while deriving equations of motion. Other formulations allow a more compact and somewhat simpler notation, but might not be easy for an unfamiliar reader. Due to the novelty of the treatise and the peculiarity of the approach, it is preferred to explicit each step of the derivation.

Let us write the kinetic energy of a spacecraft with M flexible parts as

$$E_k = \frac{1}{2}\bar{I}_z\dot{\phi} + \frac{1}{2}\sum_{i=1}^{M} m_i(\dot{\mathbf{x}}_i \cdot \dot{\mathbf{x}}_i) \tag{77}$$

where $\dot{\mathbf{x}}_i$ denotes the velocity of the i-th mass in the XYZ frame. The position $\mathbf{x}_i$ may be written in Cartesian coordinates as

$$\mathbf{x}_i = \begin{bmatrix} s_i\cos(\alpha_i+\phi) + \bar{x}_i\cos\phi - \bar{y}_i\sin\phi \\ s_i\sin(\alpha_i+\phi) + \bar{y}_i\cos\phi + \bar{x}_i\sin\phi \\ 0 \end{bmatrix} \tag{78}$$

whereas the velocity reads

$$\dot{\mathbf{x}}_i = \begin{bmatrix} \dot{s}_i\cos(\alpha_i+\phi) - \sin\phi\dot{\phi}(\bar{x}_i + s_i\cos\alpha_i) - \cos\phi\dot{\phi}(\bar{y}_i + s_i\sin\alpha_i) \\ \dot{s}_i\sin(\alpha_i+\phi) + \cos\phi\dot{\phi}(\bar{x}_i + s_i\cos\alpha_i) - \sin\phi\dot{\phi}(\bar{y}_i + s_i\sin\alpha_i) \\ 0 \end{bmatrix} \tag{79}$$

The potential energy contribution comes exclusively from the linear springs, since the gravitational component is not considered (it will be later introduced as external torque)

$$E_p = \sum_{i=1}^{M} \frac{1}{2} k_i s_i^2 \tag{80}$$

The Lagrangian function of the system, defined as $\mathcal{L} = E_k - E_p$, may be adopted to write the equations of motion. The rotational motion is governed by equation (81)

$$\frac{d}{dt}\left(\frac{\partial \mathcal{L}}{\partial \dot{\phi}}\right) - \frac{\partial \mathcal{L}}{\partial \phi} = T_z \tag{81}$$

where T_z is the generalized component of the external torque. The flexible vibrations are described by a set of M equations (82)

$$\frac{d}{dt}\left(\frac{\partial \mathcal{L}}{\partial \dot{s}_i}\right) - \frac{\partial \mathcal{L}}{\partial s_i} = 0 \tag{82}$$

In the present work, no external force is assumed to act on the masses m_i. The gravitational pull of the Earth and the Moon is assumed to act only on the barycenter, governing the orbital motion but with no effect on the structural dynamics; this assumption is reasonable for a preliminary analysis as the present one, and will be further clarified in Section 5.2.

Let us explicit equations (81) and (82), in order to grasp the physical coupling between angular motion and structural vibrations. Recalling that $\dot{\phi} = \omega_z$, equation (81) results in

$$\dot{\omega}_z \left[\bar{I}_z + \sum_{i=1}^{M} m_i \left(s_i^2 + \bar{x}_i^2 + \bar{y}_i^2 + 2 s_i L_i \right) \right] + \omega_z \sum_{i=1}^{M} 2 m_i \left(s_i \dot{s}_i + \dot{s}_i L_i \right) = \\ = T_z - \sum_{i=1}^{M} m_i \ddot{s}_i A_i \tag{83}$$

whereas equation (82) may be written as

$$m_i \ddot{s}_i + (k_i - m_i \omega_z^2) s_i = m_i \omega_z^2 L_i - m_i \dot{\omega}_z A_i \tag{84}$$

where two auxiliary coefficients have been defined

$$L_i = (\bar{x}_i \cos \alpha_i + \bar{y}_i \sin \alpha_i) \qquad A_i = (\bar{x}_i \sin \alpha_i - \bar{y}_i \cos \alpha_i) \tag{85}$$

The set of equations (84) may be conveniently rewritten in matrix form, grouping all the flexible displacement coordinates into a vector $\mathbf{s}$

$$[M]\ddot{\mathbf{s}} + ([K] - [M]\omega_z^2)\mathbf{s} = [L](\omega_z, \dot{\omega}_z) \tag{86}$$

using $[M]$ and $[K]$ to represent the mass and stiffness matrices of the system and $[L]$ to group the apparent accelerations due to the rotation of the body. In the present work, all matrices of equation (86) are diagonal; a generalization is presented in Section 5.1.3.

By inspection of equation (84), one can note:

- The usual mass and stiffness terms of a SDOF oscillator, m_i and k_i;
- A gyroscopic reduction of stiffness, due to the linear modeling of the elastic term;
- A centrifugal acceleration term, forcing the vibration of the SDOF system;
- A tangential (Euler) acceleration term, depending on the first time derivative of the angular velocity.

The rotational motion thus perturbs and excites the dynamics of the flexible components, through the described coupling term. It is interesting to analyze how the attitude dynamics is in turn affected by the structural vibrations; looking at equation (83):

- The first term (between square brackets) represents the overall inertia moment of the body, considering both the rigid and the flexible sections;
- The second term is a non-linear coupling term between angular velocity and the velocities of the flexible parts;
- The last expression is an equivalent torque, exerted on the spacecraft, due to the inertia forces of the vibrating parts.

Note that if no flexible appendages are present, equation (83) reduces to the rigid body Euler equation about the z_b axis (28).

5.1.3 Extension to complex cases

The formulation presented in Section 5.1 refers to a planar model of spacecraft, with non-chained flexible components. Each of these appendages is assumed to be attached directly to the rigid part of the spacecraft, and to be composed by SDOF systems. The resulting matrices of equation (86) are then diagonal, since each vibrational motion is decoupled from the other ones.

With no further detail on the mathematical formulation, one might assume to have a dynamical model of the spacecraft (e.g. from a finite element analysis) in the form

$$[M]\ddot{\mathbf{u}} + [K]\mathbf{u} = 0 \tag{87}$$

where $\mathbf{u}$ represents a set of coordinates that describes the state of the flexible components. An equation analogous to (86) might then be obtained, where the gyroscopic, centrifugal and tangential acceleration contributions are coupled with the flexible dynamics. The full formulation is beyond the scope of the present work; wide literature reviews are available in [52], [59], together with the references presented in Section 1.2.

The important feature of LSS in a CR3BP environment is that they might possess very low structural frequencies, and the dynamical spectrum of the orbital and attitude motion is much wider than in Earth orbits. The majority of literature and specific papers treat dynamics of flexible spacecrafts in circular orbits, where the fundamental excitation comes from the angular frequency of the orbital mean motion. In a complex multi-body gravitational scenario, a fundamental frequency may still be identified (i.e. the inverse of the orbital period), but higher harmonics might anyway supply a sufficient level of excitation. This investigation focuses on providing preliminary results of such effects; it is thus preferred to proceed with the presented simplified model, and draw introductory conclusions to pave the way for future refined analyses.

5.2 HIGH STRUCTURAL FREQUENCIES

Apart from the vision of future extremely large structures, where natural frequencies might be in the same range of those relative to attitude and

orbital motion, it is usually reasonable to assume that such structural frequencies are always higher than the latter ones, i.e.

$$\Omega_i \gg \omega_z, \omega_{orb} \qquad \forall i \tag{88}$$

where $\omega_{orb} = 2\pi/T$ indicates the orbital angular frequency. For DROs, the order of magnitude of both pulsations is in the neighborhood of some non-dimensional unit (as deduced from the various results of the previous Chapters).

Under such assumptions, it is possible to draw some conclusion on the flexible response and the attitude motion, coupling their dynamics. Approximate analytical model are obtained and exploited to predict the perturbed spacecraft behavior. The subscript i is dropped throughout this Section unless necessary, to lighten the notation.

5.2.1 Flexible parts response

With the assumption (88), the gyroscopic contribution to the stiffness in equation (84) may be neglected, leading to

$$\ddot{s} + \Omega_i^2 s = \omega_z^2 L - \dot{\omega}_z A \tag{89}$$

It is further assumed that the flexible vibrations do not significantly perturb the attitude motion, and thus the time history of ω_z may be obtained by integration of the rigid body motion along the orbit with gravity gradient torque. Having ω_z a periodic behavior, equation (89) describes a SDOF, periodically forced system. Calling $f(t)$ the right hand term, it may be expanded in Fourier series, with the usual expression

$$f(t) = a_0 + \sum_{n=1}^{N_f} a_n \cos\left(\frac{2n\pi}{T}t\right) + b_n \sin\left(\frac{2n\pi}{T}t\right) \tag{90}$$

The dynamical response of the flexible parts will then be composed by a series of harmonics, multiple of the orbital frequency, plus a fundamental component due to the natural frequency of the SDOF system at hand. The solution will be made up by a series of terms:

- The static term a_0 will yield the well-known response

$$s_0(t) = \frac{a_0}{\Omega^2}\left[1 - \cos(\Omega t)\right] \tag{91}$$

- The cosine loads produce a cosinusoidal response

$$s_{cos}(t) = a_n \frac{\cos\left(\frac{2n\pi}{T}t\right) - \cos(\Omega t)}{\Omega^2 - \left(\frac{2n\pi}{T}\right)^2} \tag{92}$$

  which may be simplified, under the assumption (88), in

$$s_{cos}(t) = \frac{a_n}{\Omega^2}\left[\cos\left(\frac{2n\pi}{T}t\right) - \cos(\Omega t)\right] \tag{93}$$

- The sinusoidal term will contribute with an analogous response

$$s_{sin}(t) = b_n \frac{\frac{2n\pi}{T\Omega}\sin(\Omega t) - \sin\left(\frac{2n\pi}{T}t\right)}{\left(\frac{2n\pi}{T}\right)^2 - \Omega^2} \tag{94}$$

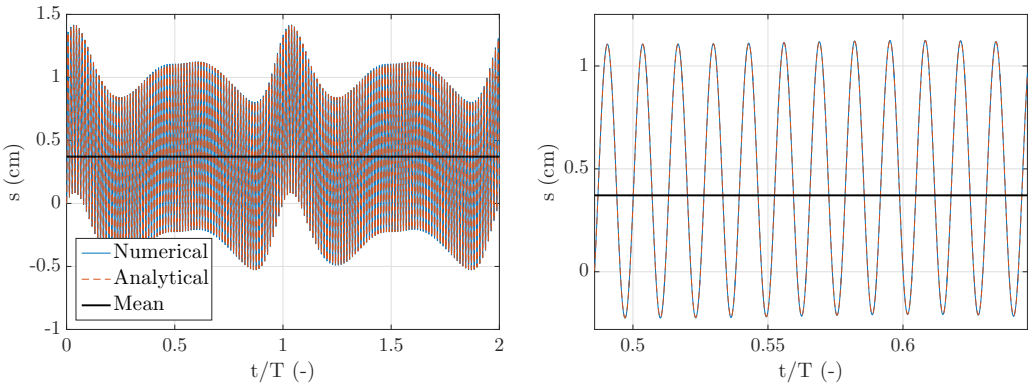
  simplified again in

$$s_{sin}(t) = \frac{b_n}{\Omega^2}\sin\left(\frac{2n\pi}{T}t\right) \tag{95}$$

Combining equations (91), (93) and (95) the response of each flexible coordinate s is obtained

$$\begin{aligned} s(t) = {} & \frac{a_0}{\Omega^2}\left[1 - \cos(\Omega t)\right] \\ & + \frac{1}{\Omega^2}\sum_{n=1}^{N_f} a_n\left[\cos\left(\frac{2n\pi}{T}t\right) - \cos(\Omega t)\right] + b_n \sin\left(\frac{2n\pi}{T}t\right) \end{aligned} \tag{96}$$

Equation (96) may be employed to investigate the dynamics and the harmonic content of the structural vibrations. The amplitude of such oscillations will depend both on the inverse square of Ω and on the coefficients A and L. The latter are a measure of how far from the barycenter is each flexible DOF, and thus how much it is affected by rotational motion. Note that, apart from the small periodic oscillations, each system will undergo a static deflection a_0/Ω^2. This consideration might help in structural design, taking into account that any flexible component will be affected by the rotational motion the farther is from the barycenter; if not compensated or considered,



(a) Time history **(b)** Detail

Figure 44: Sample flexible coordinate analytical solution

such deflection may lead to pointing errors or bias of some instruments (e.g. antennas, laser ranging sensors).

Figure 44 shows the good accordance between numerical integration and the analytical solution for s, assuming a rectangular 100×35 meters spacecraft, having a flexible component at one of the tips (e.g. a solar array) with a natural frequency of 6×10^{-5} Hz and a mass of 200 kg; the DRO has a period of 14.75 days, i.e. a frequency of $\simeq 8 \times 10^{-7}$ Hz. The considered flexible part frequency is few orders of magnitude lower than usual spacecraft structural frequencies, thus leading to a somewhat considerable static deflection ($\simeq 4$ mm); in linear elastic field, stiffer components would undergo much lower displacements.

5.2.2 Attitude motion perturbation

Once the dynamics of the flexible components is assessed, it is possible to analyze how they affect the attitude motion. The object of the analysis are the small perturbations manifested as equivalent torque, since the overall attitude motion is assumed to remain nominal, consistently with the procedure used to obtain the flexible response.

A first grasp on such perturbations may be obtained putting equation (96) into (83), noting that:

- As long as the assumption (88) is valid, the displacements s are small, and their contribution in the equivalent inertia moment is negligible with respect to the position coordinates $\bar{x}, \bar{y}$ and to the rigid inertia $\bar{I}_z$;

- The second term $(\dot{s}s + \dot{s}L)$ is negligible too, containing infinitesimal quantities;
- The gravity gradient torque should be included in the term T_z (alongside with other perturbations, if considered), integrating equations (30);
- The acceleration $\ddot{s}$, after some simplifications deriving from (88), results in

$$\ddot{s}(t) = a_0 \cos(\Omega t) + \sum_{n=1}^{N_f} a_n \cos(\Omega t) \tag{97}$$

The approximate rotational behavior of a flexible spacecraft may then be obtained using equations (97) and (98)

$$\dot{\omega}_z = K_z \left(3\frac{1-\mu}{r_1^3} e_2 e_1 + 3\frac{\mu}{r_2^3} l_2 l_1 \right) - \frac{1}{I_z} \sum_{i=1}^{M} m_i A_i \ddot{s}_i \tag{98}$$

where I_z is the overall inertia moment of the spacecraft at rest. The advantage of such simplified equation is the possibility to estimate the amplitude and the spectrum of the perturbation exerted by the small vibrations of flexible parts.

As expected, the frequency contribution comes from the natural structural frequencies of the spacecraft, while the amplitude depends on:

- The topology of the flexible parts, through the coefficients A_i and L_i;
- The rigid body periodic orbit-attitude solution , used as reference to compute the spacecraft rotation;
- The equivalent mass m_i of each flexible component.

Some of these term appear explicitly in equation (98), while others are naturally included into the Fourier coefficients that approximate $\ddot{s}_i$.

5.2.3 Highlights and wrap-up

The numerical integration of the complete problem, composed by equations (83) and (86), yields a detailed solution to describe the behavior of the flexible spacecraft, but might be time-consuming; the analytical formulation is able in turn to provide approximate, preliminary results, suitable for early stages of analysis and to dictate requirements for ACS. The basic step for the analysis are here recollected, in order to clarify the assumptions and the procedure:

1. With the methods described in Chapter 3, a periodic orbit-attitude solution is selected, obtaining the time history of the angular velocity ω_z with a rigid spacecraft;
2. The right-hand term of equation (89) is computed using the nominal ω_z profile, and its Fourier series approximation is computed;
3. The displacement of the flexible parts is obtained using equation (96);
4. From the time response it is possible to foresee the maximum and the mean displacement, which might be useful to check if structural requirements are met with the given orbital and attitude behavior. This may also indicate if the selected operational orbit is suitable for the spacecraft at hand, or vice versa to design a spacecraft suitable for a given orbit;
5. Eventually, the equivalent torque (or angular acceleration) exerted by the small vibrations is computed using equation (98), assessing its effect on the overall motion.

This analysis is able to yield results based on assumption (88), which is generally true for space structures.

5.3 LOW STRUCTURAL FREQUENCIES

When structural frequencies are very low, in the neighborhood of the attitude and orbital frequencies, strong couplings may arise between rotational motion, orbital trajectory and vibrations of flexible parts. The present

Section shows some results, keeping in mind the strong abstraction of the analysis, since this case is unlikely to happen in modern or future spacecrafts. The orbital motion is not considered, in analogy with the previous Section; it may be investigated in future studies. Section 5.4 will provide further remarks on the analysis.

5.3.1 Flexible parts motion

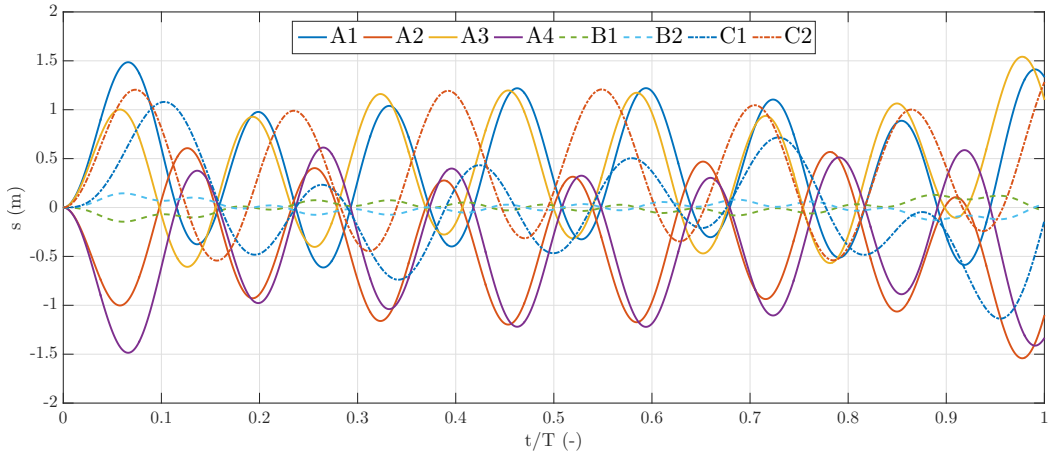
When the assumption that the structural frequencies are much higher than the body angular velocity, the set of equations (86) cannot be simplified, and should be numerically integrated together with the attitude motion (83) with gravity gradient as external torque. Other perturbing torques might be added as well in later investigations.

Figure 45 portrays the displacements of the flexible components of the reference spacecraft model, using lowered values of natural structural frequencies. The selected orbit is a DRO with $T = 14.75$ days, corresponding to a frequency of 7.85×10^{-7} Hz. The analyses are run reducing the natural frequencies Ω_i up to the orders of magnitude of 10^{-6}, 10^{-7} and 10^{-8} Hz respectively. Note that the time span on the horizontal axis are different, in order to catch the full dynamics of each response, while avoiding excessive superposition of the curves.

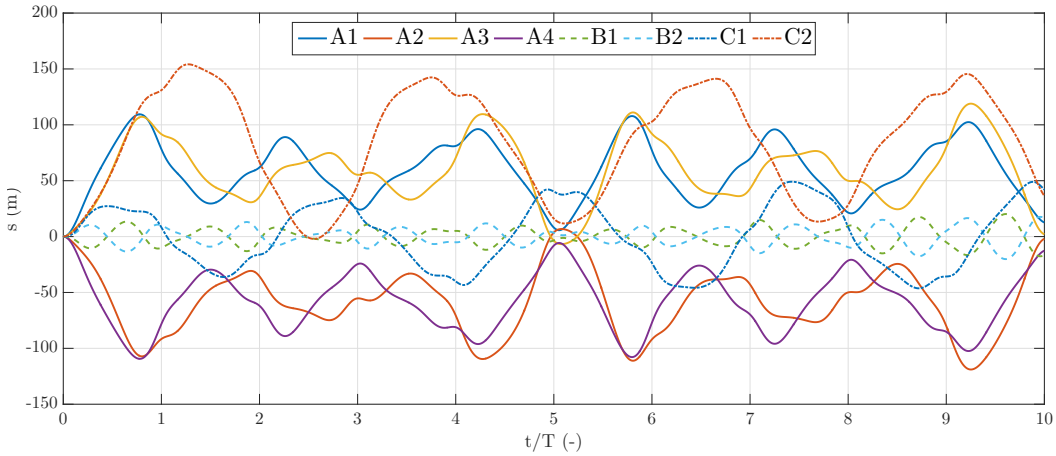
5.3.2 Attitude motion

Dropping assumption (88), the attitude motion too needs to be numerically integrated. The perturbation arising from the vibrations of the flexible components may no longer be considered as an external torque, since the non-linear coupling with angular velocity, i.e. the second term in equation (83), might be significant in the description of the fully-coupled motion.

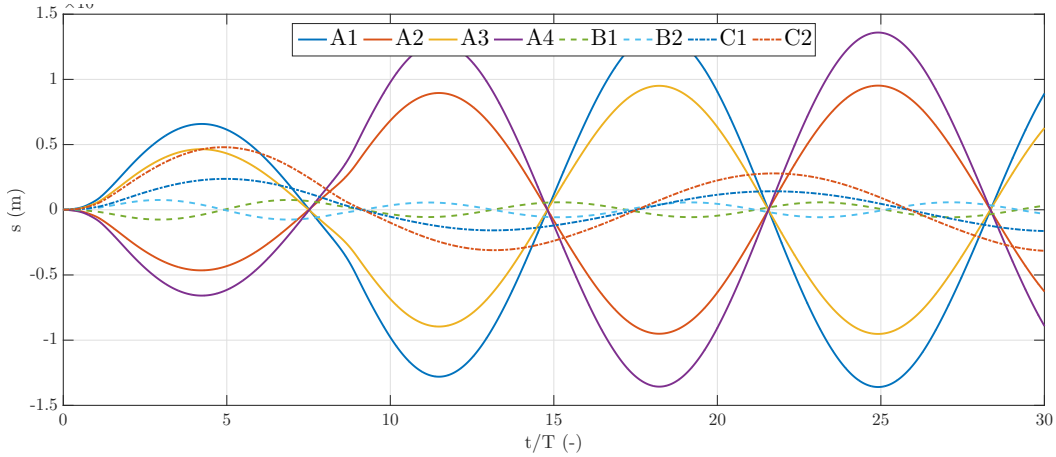
Figure 46 portrays the angular velocity time history with lowered structural frequencies; the test cases are the same used for Figure 45. The perturbed attitude profile is displayed together with the nominal one, obtained using a rigid body periodic orbit-attitude solution.



(a) Natural frequencies $\mathcal{O}(10^{-6})$ Hz

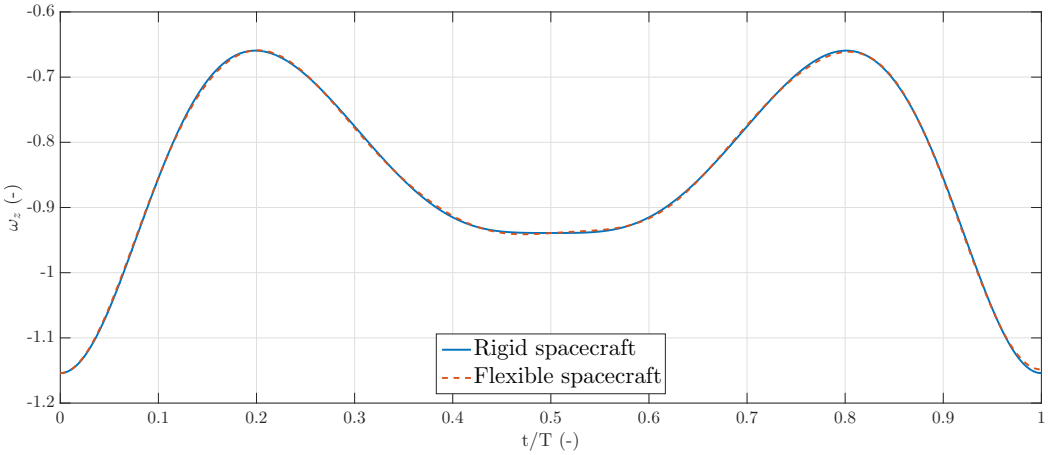


(b) Natural frequencies $\mathcal{O}(10^{-7})$ Hz

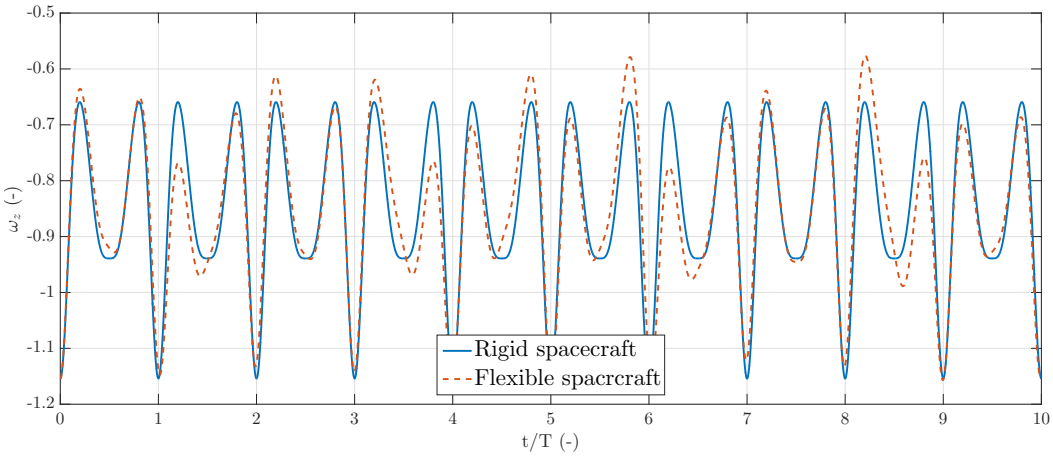


(c) Natural frequencies $\mathcal{O}(10^{-8})$ Hz

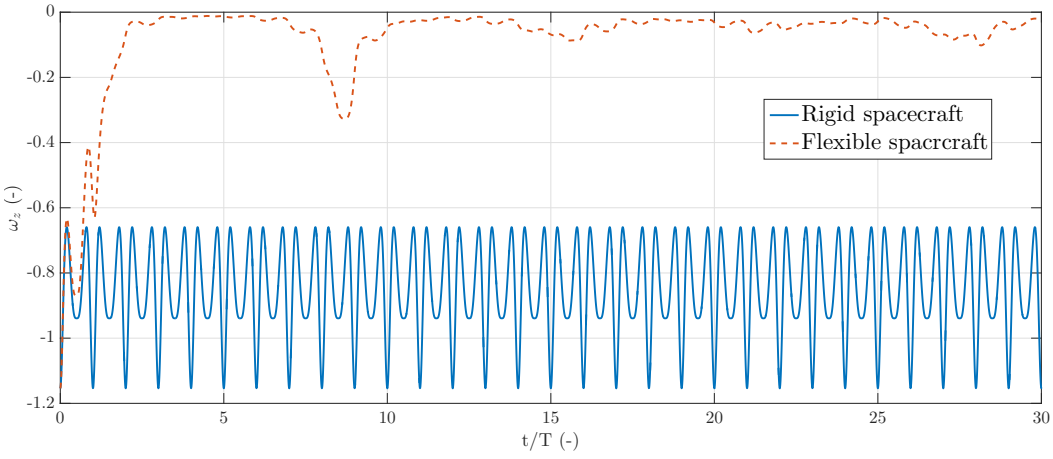
Figure 45: Structural response with lowered frequencies Ω_i



(a) Natural frequencies $\mathcal{O}(10^{-6})$ Hz



(b) Natural frequencies $\mathcal{O}(10^{-7})$ Hz



(c) Natural frequencies $\mathcal{O}(10^{-8})$ Hz

Figure 46: Body angular velocity with lowered frequencies Ω_i

5.3.3 Analysis of the results

According to the magnitude of the structural frequencies with respect to the orbital and attitude motion fundamental frequencies, different responses are observed:

A. When structural angular frequencies are low (Figures 45a and 46a), but at least one order of magnitude higher than the fundamental orbital pulsation, the flexible part response is again sinusoidal in shape, even though the analytical approximation of Section 5.2 is no longer valid. The obtained displacements are bounded, although non-negligible in magnitude. The attitude motion encounters small short-period perturbations, which do not hinder the overall behavior; the flexibility of the spacecraft may thus be considered as a perturbation of the rigid body attitude solution, and treated accordingly.

B. If structural frequencies are in the neighborhood of the orbital frequency, a strong coupling arises between attitude motion and vibrations. The displacements time history (Figure 45b) shows a greatly non-linear behavior, due to the interaction and mutual excitation between elastic and rotational motions. The angular velocity as well (Figure 46b) manifests such non-linear coupling; its periodicity is no longer dominated by the rigid body solution, since large oscillations due to the flexible structure excitation are present.

C. Eventually, when structural frequencies are much lower than those of orbital and attitude motion, the elastic components prevail on the spacecraft behavior. The body angular velocity (Figure 46c) rapidly deviates from the nominal behavior, settling in the neighborhood of zero; this means that the movement of the flexible parts is dominant, and their inertia forces are able to overcome the gravity gradient torque. The displacement of the lumped masses shows a non-linear oscillatory behavior, where the effect of the body rotation rapidly disappears (due to the disappearance of a body rotation itself); Figure 45c portrays such displacement coordinates, with an evident oscillatory motion with no contribution from the rotation of the body.

5.4 FINAL REMARKS

The effect of the spacecraft flexibility is assessed using a lumped-parameters linear elastic model. It is possible to identify four main typologies of behavior, according to the relationship between the structural frequencies Ω_i and the orbital $2\pi/T = \omega_{orb}$ and attitude motion ω_z angular velocities,

$\Omega_i \gg \omega_z, \omega_{orb}$ This case is, for present and near-future space mission, the most probable. In order to provide a numerical example, Figure 47 displays the first natural frequency for a free-free beam, 200 meters long and 50 meters wide, which might approximate the first frequency of a space station. The horizontal axis represents the speed of sound of the used material; some examples are provided. A full characterization of a flexible spacecraft requires in general a more complex model, but the free-free beam frequency yields a grasp on their order of magnitude.

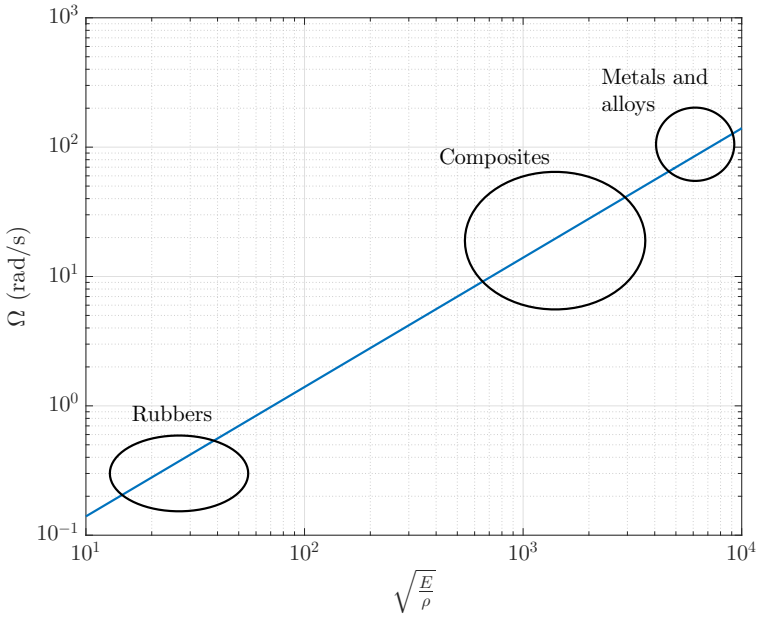


Figure 47: Free-free beam first natural frequency

Recalling the orbital periods of DROs (Figure 6) and the typical rigid body angular velocities that may be employed if a periodic motion is sought (Figure 31), one notes that assumption (88) is reasonably justified, since one non-dimensional unity of angular velocity corresponds roughly to 2×10^{-6} rad/s.

$\boldsymbol{\Omega_i > \omega_z, \omega_{orb}}$ When structural frequencies are moderately higher than the orbital and attitude ones, the displacement of the flexible components reaches non-negligible values, and the perturbation to the attitude motion is significant, although small and bounded. This case might be of interest for future applications, where large structures might have flexible components with very low natural frequencies, as well as if considering orbits with small period.

$\boldsymbol{\Omega_i \simeq \omega_z, \omega_{orb}}$ The case where structural, orbital and attitude frequencies have the same order of magnitude shows the strongest coupling between body angular velocity and elastic motion. The displacement of the flexible parts shows a greatly non-linear time history, covering a wide spectrum of frequencies in the neighborhood of the fundamental ones (i.e. Ω_is). The influence on the attitude motion can not be treated as a perturbation, but the fully coupled motion should be analyzed. Furthermore, it is underlined that the present formulation does not take into account trajectory deviations due to the structural vibration; while in the two previous cases this was a legit assumption, in this case the strong coupling suggests that also the orbital motion might be affected by the motion of the elastic components. The complete formulation, including orbital dynamics, may be investigated in future studies.

$\boldsymbol{\Omega_i < \omega_z, \omega_{orb}}$ The last case considers a spacecraft whose natural frequencies are lower than those if orbital and attitude motion. In this configuration, the flexible dynamics govern the overall motion, and the effect of gravity gradient (and thus the periodicity of the rigid body solution) is overwhelmed by the structural vibration; the natural periodic behavior is lost, and the spacecraft largely oscillates due to the displacement of the flexible component. It is underlined that in this case the orbital dynamics too might be greatly perturbed, suggesting investigations that include a more complete formulation.

The analysis relies on a lumped-parameters formulation, assuming that each flexible component is directly connected to the rigid base. Such model is suitable for a schematic representation of a spacecraft and its lower natural modes; more complex formulations (e.g. continuum mechanics, reduction to modal form) may yield more accurate results, and are recommended for later stage analyses. A modal form of equations seems particularly appealing, since it allows to have diagonal mass and stiffness matrices and develop a formulation analogous to that presented in Section 5.2.

A sensible coupling between structural flexibility and attitude motion is observed only for very flexible configurations, where the natural frequencies of the spacecraft match those of orbital and attitude dynamics. Such topology might represent very large future structures, with novel highly-elastic materials, or a formation flying set of vehicles, whose equivalent dynamics is described by very loose linear springs.

6 CONCLUSION

> It is far better to foresee even without certainty
> than not to foresee at all.
>
> HENRY POINCARÉ
> The Foundations of Science (1913)

Future deep-space and interplanetary missions will likely exploit the vast dynamical possibilities offered by a multi-body gravitational environment, and the Circular Restricted Three-Body Problem is a simple, yet very effective framework to investigate such opportunities. It is likely as well that large supporting infrastructures are to be placed in the vicinity of the Lagrangian points, to serve as a docking platform, a refueling outpost or an observation facility to ease long-term missions. The dynamical environment is highly non-linear regarding both orbital trajectories and attitude motion.

This work is focused on the investigation of coupled orbit-attitude behaviors of LSS, providing tools and techniques for preliminary analyses of missions that involve extended structures. The identification of periodic behaviors allows a deeper insight on the problem, fitting in the context of this novel research field. The mutual interaction between orbital and attitude dynamics is developed in a three-dimensional formulation; the analysis is focused on planar dynamics, with the advantage of a clearer visual representation of the results. The assumption of rigid spacecraft is first employed; effects of flexibility are eventually assessed and investigated with simple models.

6.1 ORBIT–ATTITUDE RIGID BODY DYNAMICS

The principal contribution of this investigation is the creation of periodicity maps, that depict visually the periodic orbit-attitude solutions along the

whole span of considered orbits. These maps provide the mission analyst a valuable tool for preliminary analyses, with an immediate grasp on the nature of the solution. A further contribution is the classification of the results into families of solutions, representing similar attitude behaviors; such families are evident in the maps, allowing an identification of the desired or undesired attitude behavior without the need of extensive numerical simulations.

The results are validated and compared to those existing in literature; it is remarked that such studies are very recent, underlining the novelty of the topic. The possible exploitations of the periodic orbit-attitude solutions are discussed, remarking the operational possibilities offered to large space stations and infrastructures; furthermore, the parametrization with respect to the inertia ratio allows to predict how a change in the topology of the spacecraft (e.g. after docking/undocking of modules) may affect the attitude behavior along the orbit.

6.2 COUPLED DYNAMICS WITH SOLAR RADIATION PRESSURE

The effect of Solar Radiation Pressure (SRP) is then investigated, focusing on the torque that is exerted on the spacecraft. This perturbation is able to produce a major disturbance in attitude motion of large structures, one that is able to overcome the effect of the gravity gradient torque. The analysis is, thus, devoted to introduce SRP as an integral part of the model, rather than treating it as a perturbations, opening novel operational possibilities.

Using a simplified representation of SRP torque, it is possible to obtain new periodicity maps, equivalent to those obtained with gravity gradient torque only; these maps portray a solution space where the effect of SRP contributes to the periodicity of the attitude motion, even overcoming the gravity gradient torque. A more realistic and refined model of SRP is then introduced, with the possibility to derive more spacecraft-specific solutions. The novelty of the study lays in the inclusion of SRP into the model, with larger possibilities to exploit its effect in a beneficial way, contributing to the periodicity of the solution.

6.3 EFFECTS OF SPACECRAFT FLEXIBILITY

The work eventually analyzes the dynamics of a flexible spacecraft in a CR3BP environment. Many papers investigated flexible spacecrafts in Earth orbit, focusing on the coupling between the orbital frequency and structural vibration. The advancement proposed by this study is to investigate such coupling along orbits with a richer frequency content; the CR3BP orbit-attitude dynamics, in fact, is characterized by a wide spectrum of multiples of the main orbital frequency, while circular and near-circular Earth orbits are dominated by a single angular frequency (i.e. the mean motion frequency).

The results show that the interaction between flexible and attitude motion is negligible if the structural frequencies are much higher (2-3 orders of magnitude) than the fundamental orbital frequency, as expected from previous studies. If the spacecraft natural frequencies fall in the range of the orbital and attitude frequencies, the rich harmonic spectrum of the latter excites a strong coupling, and the rotational motion itself is perturbed by the vibrational dynamics. The analysis employs linear lumped-parameters models, suggesting eventually possible improvements on the model and on the formulation.

6.4 FUTURE WORKS

The novelty of the problem and the few literature available on orbit-attitude coupled behaviors encourages future studies on the topic, in order to gain a deeper insight on the attitude dynamics of LSS in a CR3BP environment; furthermore, many results deserve a more thorough analysis and a larger variety of study cases. Some guidelines and suggestions are here provided to foster future investigations.

6.4.1 Analysis of other families of orbits

The present study included Distant Retrograde Orbits (DRO) exclusively; recent papers investigated also Lyapunov orbits, although a full map of the solution space was not treated. The creation of periodicity maps parametrized with respect to the inertia ratio, for other families of orbits may open new operational possibilities and lead towards a wider understanding of the problem.

6.4.2 Extension to spatial dynamics

Three-dimensional dynamics might be exploited for future space missions (e.g. considering halo orbits), and its analysis may yield novel interesting result. Furthermore, the spatial attitude dynamics needs to be investigated also in planar solutions, to assess the actual stability and real behavior of an extended rigid body.

6.4.3 Inclusion of Sun gravitational perturbation and Earth-Moon orbit eccentricity

In the Earth-Moon system, the gravitational pull of the Sun yields a considerable acceleration, which might deviate the spacecraft from the nominal trajectory; this deviation may affect rotational motion too, since the gravity gradient torque of the primaries might strongly differ from the nominal values that guarantee periodic behaviors. The Sun-Earth-Moon four-body problem might offer novel and interesting behaviors, being also a further step in a more realistic representation of the overall system. Furthermore, the eccentricity of the relative orbits of the Earth and the Moon ($e \simeq 0.05$) might be included as well to improve the reliability and validity of the model, going beyond the assumptions of the CR3BP.

6.4.4 Improvement of the elastic formulation

The presented lumped-parameters model allows a preliminary assessment of the flexible spacecraft behavior, but more refined models are necessary for a realistic representation of a large flexible structure. Finite elements and modal formulations are suggested to have an accurate representation of the spacecraft. Linear and non-linear elasticity models might be employed, extending the analysis to peculiar materials which may compose future spacecraft (e.g. visco-elastic composites, expandable and inflatable components). The usage of such refined flexible models might lead to novel results in the coupled attitude-structure problem, showing behaviors that are missed with the simple linear model.

SYMBOLS AND ABBREVIATIONS

Symbol	Description
a	Orbital semi-major axis
a_n, b_n	Fourier series coefficients
A	Spacecraft surface
$[A]$	Rotation matrix
$[\tilde{A}]$	Linearized state matrix
c_0	Speed of light in vacuum
C_s, C_d, C_a	Reflection and absorption coefficients
C_r	Generalized reflection coefficient
d	Distance between the two primary bodies
$\mathbf{d}_c$	Distance between center of pressure and barycenter
e	Orbital eccentricity
e_1, e_2	Earth-spacecraft vector direction cosines
E	Total mechanical energy
E_k, E_p	Kinetic and potential energy
$\mathbf{F}$	Force vector
G	Universal gravitational constant
h	Auxiliary parameter for linearized motion
$\bar{I}_z$	Inertia moment of the rigid spacecraft part
$[I]$	Principal inertia tensor
k_i	flexible system stiffness
K_z	Inertia ratio coefficient
$[K]$	Stiffness matrix
l_1, l_2	Moon-spacecraft vector direction cosines
L_1, L_2, L_3	Collinear Lagrangian points
L_4, L_5	Equilateral Lagrangian points
L_i, A_i	Auxiliary coefficients for flexibility analysis
$\mathcal{L}$	Lagrangian function
$[M]$	Mass matrix
m_i	Flexible system mass
m_1, m_2	Masses of the two primary bodies

Continues on next page

Continued from previous page

Symbol	Description
m_3	Mass of the third body
M	Number of flexible components
$\hat{n}$	Surface normal direction
N	Number of body rotations per orbital revolution
N_f	Order of the Fourier series
N_{sun}	Ratio between orbital and apparent Sun periods
P_i	Position of the flexible system
q_1, q_2, q_3, q_4	Quaternion components
r_p	Perigee radius
$\mathbf{r}$	Position of the third body with respect to a primary
s_i	Displacement of the flexible system
$\hat{s}$	Sun direction
t	Time
t_0	Initial instant
t_c	Vertical crossing instant
T	Orbital period
T_{sun}	Period of the apparent Sun motion
$\mathbf{T}$	Torque vector
$\mathbf{u}$	Generalized coordinate vector
U	Potential function
$[U]_{\mathbf{xx}}$	Matrix of second derivatives of U
W_0	Sun radiation flux
$\bar{x}_i, \bar{y}_i$	Coordinates of the flexible system
$x_b y_b z_b$	Principal body frame axes
XYZ	Reference frame
$X_i Y_i Z_i$	Inertial reference frame axes
$X_s Y_s Z_s$	Synodic frame axes
$\mathbf{x}$	Position vector
$\mathbf{x}_0$	Initial position vector
α	Angle between Sun direction and surface normal
α_i	Orientation of the flexible system
$\boldsymbol{\eta}$	State vector
θ, ψ	Roll and yaw rotation angles
Λ_z	Solar radiation pressure torque parameter
μ	Mass ratio of the CR3BP
ϕ	Pitch rotation angle in planar motion

Continues on next page

Continued from previous page

Symbol	Description
$[\Phi]$	State transition matrix
$\boldsymbol{\omega}$	Angular velocity vector
ω_{orb}	Orbital angular velocity
ω_z	Angular velocity in planar motion
Ω	Synodic frame angular velocity
Ω_i	Natural frequency of the flexible system
Ω_s	Sun apparent motion angular velocity
$[\Omega]$	Matrix of Coriolis acceleration terms
ACS	Attitude Control System
CR3BP	Circular Restricted Three-Body Problem
DOF	Degree Of Freedom
DRO	Distant Retrograde Orbit
ECI	Earth-Centered Inertial
GG	Gravity Gradient
JC	Jacobian Constant
LSS	Large Space Structures
LU	Length Unit
MU	Mass Unit
SDOF	Single Degree Of Freedom
SRP	Solar Radiation Pressure
STM	State Transition Matrix
TU	Time Unit

Ends from previous page

BIBLIOGRAPHY

[1] J.-L. Lagrange, *Théorie de la libration de la Lune*. 1780.

[2] J. P. Moran, "Effects of plane librations on the orbital motion of a dumbbell satellite," *ARS Journal*, Vol. 31, No. 8, 1961, pp. 1089–1096.

[3] E. Y. Yu, "Long-term coupling effects between librational and orbital motions of a satellite," *AIAA journal*, Vol. 2, No. 3, 1964, pp. 553–555.

[4] S. N. Mohan, J. V. Lange, and B. O. Lange, "Interaction Between Attitude Libration and Orbital Motion of a Rigid Body in a Near Keplerian Orbit of Low Eccentricity," *Celestial Mechanics*, Vol. 5, No. 2, 1972, pp. 157–173.

[5] G. B. Sincarsin and P. C. Hughes, "Gravitational orbit-attitude coupling for very large spacecraft," *Celestial Mechanics*, Vol. 31, No. 2, 1983, pp. 143–161.

[6] T. R. Kane, P. W. Likins, and D. A. Levinson, *Spacecraft dynamics*. 1983.

[7] E. A. Belbruno and J. K. Miller, "Sun-perturbed Earth-to-Moon transfers with ballistic capture," *Journal of Guidance, Control, and Dynamics*, Vol. 16, No. 4, 1993, pp. 770–775.

[8] D. C. Folta, N. Bosanac, D. Guzzetti, and K. C. Howell, "An Earth–Moon system trajectory design reference catalog," *Acta Astronautica*, Vol. 110, 2015, pp. 341–353.

[9] T. R. Kane and E. L. Marsh, "Attitude Stability of a Symmetric Satellite at the Equilibrium Points in the Restricted Three-Body Problem," *Celestial Mechanics*, Vol. 4, No. 1, 1971, pp. 78–90.

[10] W. J. Robinson, "The Restricted Problem of Three Bodies with Rigid Dumb-Bell Satellite," *Celestial Mechanics*, Vol. 8, No. 2, 1973, pp. 323–330.

[11] W. J. Robinson, "Attitude Stability of a Rigid Body Placed at an Equilibrium Point in the Restricted Problem of Three Bodies," *Celestial Mechanics*, Vol. 10, No. 1, 1974, pp. 17–33.

[12] A. Abad, M. Arribas, and A. Elipe, "On the attitude of a spacecraft near a Lagrangian point," *Bulletin of the Astronomical Institutes of Czechoslovakia*, Vol. 40, 1989, pp. 302–307.

[13] E. Brucker and P. Gurfil, "Analysis of Gravity-Gradient-Perturbed Rotational Dynamics at the Collinear Lagrange Points," *The Journal of the Astronautical Sciences*, Vol. 55, No. 3, 2007, pp. 271–291.

[14] B. Wong, R. Patil, and A. Misra, "Attitude Dynamics of Rigid Bodies in the Vicinity of the Lagrangian Points," *Journal of Guidance, Control, and Dynamics*, Vol. 31, No. 1, 2008, pp. 252–256.

[15] A. J. Knutson, *Application of Kane's Method to Incorporate Attitude Dynamics into the Circular Restricted Three-Body Problem*. PhD thesis, Purdue University, 2012.

[16] A. J. Knutson and K. C. Howell, "Coupled Orbit and Attitude Dynamics for Spacecraft Comprised of Multiple Bodies in Earth-Moon Halo Orbits," *63rd International Astronautical Congress (IAC)*, 2012.

[17] D. Guzzetti, R. Armellin, and M. Lavagna, "Coupling attitude and orbital motion of extended bodies in the restricted circular 3-body problem: a novel study on effects and possible exploitations," *63rd International Astronautical Congress (IAC)*, 2012.

[18] D. Guzzetti, "Large Space Structures Dynamics in a Multi-Body Gravitational Environment," Master's thesis, Politecnico di Milano, July 2012.

[19] D. Guzzetti and K. C. Howell, "Coupled Orbit-Attitude Dynamics in the Three-Body Problem: a Family of Orbit-Attitude Periodic Solutions," *AIAA/AAS Astrodynamics Specialist Conference*, 2014.

[20] D. Guzzetti and K. C. Howell, "Natural periodic orbit-attitude behaviors for rigid bodies in three-body periodic orbits," *66th International Astronautical Congress (IAC)*, 2015.

[21] S. F. Rafano Carnà, L. Bucci, and M. Lavagna, "Earth–Moon multipurpose orbiting infrastructure," *26th AAS/AIAA Space Flight Mechanics Meeting*, 2016.

[22] J. P. Álvarez, C. Bombardelli, M. Lara, F. R. Lucas, M. S. Rivo, D. Curreli, E. C. Lorenzini, and D. Scheeres, "Dynamic stabilization of L2 periodic orbits using attitude-orbit coupling effects," *Journal of Aerospace Engineering*, Vol. 4, No. 1, 2012, pp. 73–81.

[23] Y. Meng, R. Hao, and Q. Chen, "Attitude stability analysis of a dual-spin spacecraft in halo orbits," *Acta Astronautica*, Vol. 99, 2014, pp. 318 – 329.

[24] A. K. Misra and V. J. Modi, "The influence of satellite flexibility on orbital motion," *Celestial Mechanics*, Vol. 17, No. 2, 1978, pp. 145–165.

[25] W. Hooker and G. Margulies, "The dynamical attitude equations for n-body satellite," *Journal of the Astronautical Sciences*, Vol. 12, 1965, p. 123.

[26] P. W. Likins, "Dynamic analysis of a system of hinge-connected rigid bodies with nonrigid appendages," *International Journal of Solids and Structures*, Vol. 9, No. 12, 1973, pp. 1473–1487.

[27] W. Hooker, "Equations of motion for interconnected rigid and elastic bodies: A derivation independent of angular momentum," *Celestial Mechanics*, Vol. 11, No. 3, 1975, pp. 337–359.

[28] P. Hughes, "Dynamics of a chain of flexible bodies," *Journal of the Astronautical Sciences*, Vol. 27, 1979, pp. 359–380.

[29] H. Ashley, "Observations on the dynamic behavior of large flexible bodies in orbit.," *AIAA Journal*, Vol. 5, No. 3, 1967, pp. 460–469.

[30] V. K. Kumar and P. M. Bainum, "Dynamics of a flexible body in orbit," *Journal of Guidance, Control, and Dynamics*, Vol. 3, No. 1, 1980, pp. 90–92.

[31] A. Colagrossi, M. Lavagna, and S. F. Rafano Carnà, "Dynamical analysis of rendezvous and docking with very large space infrastructures in non-keplerian orbits," *6th International Conference on Astrodynamics Tools and Techniques*, 2016.

[32] R. H. Battin, *An introduction to the mathematics and methods of astrodynamics*. AIAA, 1999.

[33] H. Curtis, *Orbital mechanics for engineering students*. Butterworth-Heinemann, 2013.

[34] W. S. Koon, M. W. Lo, J. E. Marsden, and S. D. Ross, *Dynamical systems, the three-body problem and space mission design*. World Scientific, 2006.

[35] V. Szebehely, *Theory of orbits: The restricted problem of three bodies*. Academic Press, 1967.

[36] J.-L. Lagrange, "Essai sur le problème des trois corps," *Académie royale des Sciences de Paris*, Vol. 9, 1772, p. 292.

[37] C. G. J. Jacobi, "Sur le mouvement d'un point et sur un cas particulier du problème des trois corps," *Compt. rend*, Vol. 3, 1836, pp. 59–61.

[38] H. Poincaré, *Les méthodes nouvelles de la méchanique céleste*, Vol. 1. 1899.

[39] R. A. Broucke, *Periodic Orbits in the Restricted Three-Body Problem with Earth-Moon Masses*. Jet Propulsion Laboratory, 1968. Technical Report.

[40] M. Hénon, "Numerical exploration of the restricted problem. V," *Astronomy and Astrophysics*, Vol. 1, 1969, pp. 223–238.

[41] T. Lam and G. J. Whiffen, "Exploration of distant retrograde orbits around Europa," *15th AAS/AIAA Space Flight Mechanics Conference*, 2005.

[42] "Asteroid Redirect Robotic Mission (ARRM) Reference Mission Concept Study Public Information Package V1," 2013.

[43] O. C. Winter, "The stability evolution of a family of simply periodic lunar orbits," *Planetary and Space Science*, Vol. 48, No. 1, 2000, pp. 23–28.

[44] C. Douskos, V. Kalantonis, and P. Markellos, "Effects of resonances on the stability of retrograde satellites," *Astrophysics and Space Science*, Vol. 310, No. 3-4, 2007, pp. 245–249.

[45] L. Capdevila, D. Guzzetti, and K. C. Howell, "Various Transfer Options from Earth into Distant Retrograde Orbits in the Vicinity of the Moon," *24th AAS/AIAA Space Flight Mechanics Meeting*, 2014.

[46] X. Ming and X. Shijie, "Exploration of distant retrograde orbits around Moon," *Acta Astronautica*, Vol. 65, No. 5, 2009, pp. 853–860.

[47] M. Vaquero and K. C. Howell, "Leveraging Resonant Orbit Manifolds to Design Transfers between Libration Point Orbits in Multi-body Regimes," *23rd AAS/AIAA Space Flight Mechanics Meeting*, 2013.

[48] M. Vaquero and K. C. Howell, "Leveraging Resonant-Orbit Manifolds to Design Transfers Between Libration-Point Orbits," *Journal of Guidance, Control, and Dynamics*, Vol. 37, No. 4, 2014, pp. 1143–1157.

[49] A. N. Hirani and R. P. Russell, "Approximations of distant retrograde orbits for mission design," *16th AAS/AIAA Space Flight Mechanics Meeting*, 2006.

[50] J. V. Breakwell and J. V. Brown, "The 'Halo' Family of 3-Dimensional Periodic Orbits in the Earth-Moon Restricted 3-Body Problem," *Celestial Mechanics*, Vol. 20, No. 4, 1979, pp. 389–404.

[51] K. C. Howell, "Three-Dimensional, Periodic, 'Halo' Orbits," *Celestial Mechanics*, Vol. 32, No. 1, 1984, pp. 53–71.

[52] J. R. Wertz, *Spacecraft attitude determination and control*. Kluwer Academic Publishers, 1990.

[53] M. H. Kaplan, *Modern spacecraft dynamics and control*. John Wiley and Sons, 1976.

[54] D. B. DeBra and R. H. Delp, "Rigid body attitude stability and natural frequencies in a circular orbit," *Journal of Astronautical Sciences*, Vol. 8, No. 1, 1961, pp. 14–17.

[55] M. T. Aygün and U. Daybelge, "Attitude stability of DeBra-Delp satellites in circular orbit," *Journal of guidance, control, and dynamics*, Vol. 21, No. 6, 1998, pp. 965–970.

[56] M. Harris and R. Lyle, *Spacecraft radiation torque*, Vol. SP-8027 of *NASA space vehicle design criteria*. 1969.

[57] J. R. Wertz and W. J. Larson, *Space Mission Analysis and Design*. Microcosm, 2012.

[58] L. Bucci and M. Lavagna, "Coupled Dynamics of Large Space Structures in Lagrangian Points," *6th International Conference on Astrodynamics Tools and Techniques*, 2016.

[59] V. Modi, "Attitude dynamics of satellites with flexible appendages-a brief review," *Journal of Spacecraft and Rockets*, Vol. 11, No. 11, 1974, pp. 743–751.